Final Draft Report

Investigation of Hydrodynamic approach of flood inundation mapping along with assessment of changes in river planforms using a cloud-based Google Earth Engine (GEE) computing platform in data-scarce Western Himalayan River basin

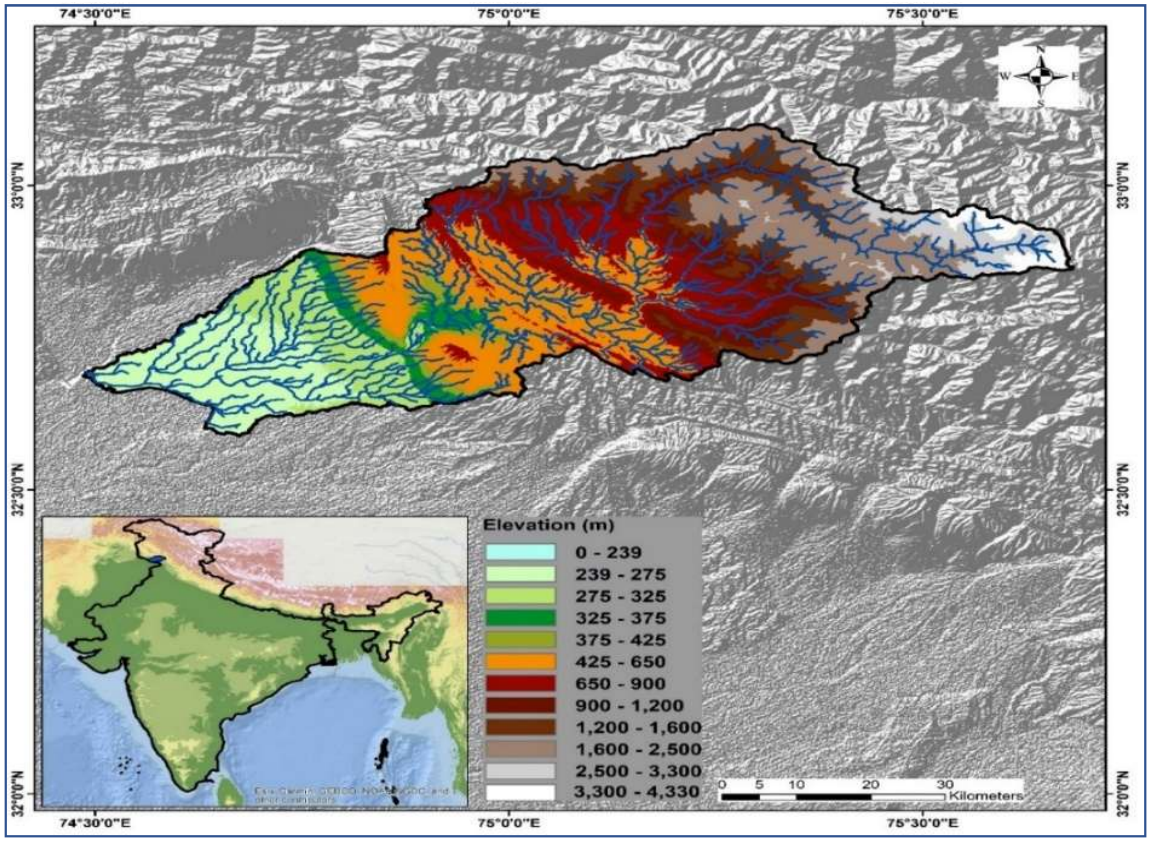

NATIONAL INSTITUTE OF HYDROLOGY

Surface Water Hydrology Division

October 2024

Final Draft Report

Investigation of Hydrodynamic approach of flood inundation mapping along with assessment of changes in river planforms using a cloud-based Google Earth Engine (GEE) computing platform in data-scarce Western Himalayan River basin

NATIONAL INSTITUTE OF HYDROLOGY

Surface Water Hydrology Division

October 2024

PREFACE

The fluvial geomorphological study is crucial for understanding watershed scale surface processes, including those in steep mountainous terrain and flat lowlands, especially if the mid- and downstream regions are densely inhabited and hazard evaluations are crucial. In other words, our capacity to estimate the effects of hydro-climatic risks depends on the understanding of fluvial geomorphological processes. The geomorphology of rivers and stream is the outcome of the interaction between streamflow and sediment transport within the context of the surrounding geology, as well as impacts from the climate, vegetation, and human activities. Human actions have directly impacted channel form (e.g., channelization, dredging) and the independent factors that govern river channel shape (flow and sediment load). Particularly, the Tawi River basin is continuously subjected to hydro-climatic disaster such as heavy torrential rainstorms, frequent cloud bursts, landslides and catastrophic floods.

However, our knowledge about such surface processes has relatively been limited Therefore, the need of hour is to come with promising scientific tools to assist in planning of efficient water-related disasters management and reduction strategies. In this context, the present study entitled as "Investigation of Hydrodynamic approach of flood inundation mapping along with assessment of changes in river planforms using a cloud-based Google Earth Engine (GEE) computing platform in data-scarce Western Himalayan River basin" which attempt to assess the fluvial geomorphology and its relation to flood hazards in the of the Tawi river basin is very essential as well as important.

This report has been prepared by Dr. Ravindra V. Kale, Scientist E, SWHD, NIH Roorkee, Dr. A. K. Lohani, Scientist G & Head, SWHD, NIH Roorkee, and Er. J. P. Patra, Scientist E, SWHD, NIH Roorkee.

(Dr. Manmohan Kumar Goel)

DIRECTOR

ABSTRACT

The physical properties and features of a river or stream and its surroundings are referred to as fluvial morphology. It includes research on the size, cross-sectional profile, channel patterns, movement of sediment, and interactions between the river and its surroundings. Fluvial morphology must be understood for a variety of applications, such as managing flood risks. Flood hazard is the risk that a river or stream would overrun its banks and inundate nearby regions, causing property damage, fatalities, and environmental harm. Fluvial morphology, hydrology (the study of water flow and distribution), land use, climate, and human activities are some of the variables that affect flood hazards. Understanding these intricate relationships and putting policies in place to lower the risks associated with floods are necessary for effective flood hazard assessment and management.

In line with these points, the Tawi River basin which is continuously subjected to water related disaster such as heavy torrential rainstorms, frequent cloud bursts along with its high precipitous relief is selected in this study. The major event that prompted government and civil organisations to plan better flood assessment and management as well as reduction strategies to fight water-related disasters in the Tawi River basin under ominous future climate change scenarios was the historic high rainfall event that occurred in September 2014. In view of this challenges, this study aims to undertake detailed fluvial geomorphological analysis of the Tawi basin in Jammu and Kashmir, India, using advanced geospatial tools and datasets. In order to prepare geomorphological map of the Tawi river basin, the Copernicus 30 Digital Surface Model (DSM) data is processed in QGIS to derive Digital Elevation Model (DEM) derivatives and the manual mapping identify various landform is carried out using Sentinel-2 satellite data. The integration of DEM derivatives and Sentinel-2 data enriches the characterization of the basin's terrain. In order to quantify and detect changes in the riverscape (i.e., water, sediment, and vegetation) at an unprecedented spatiotemporal resolution and to support flood risk and river management applications, this study makes use of the Google Earth Engine (GEE), a cloud-based computing platform for geospatial analyses. Accordingly, the annual active river channels were extracted from composite Landsat imagery using GEE platform to identify and analyse the changes in the Tawi River planform over 34 years (1988-2022). Overall, the findings are able to provide valuable insights into the basin's geomorphological features, processes, and the river's response to flood events, aiding in effective flood management and conservation strategies. Further, this study will attempts to evaluate the predictive capabilities of two dimensional Rainfall-Runoff-Inundation (RRI) model and it comparison with HEC-RAS/HEC-HMS model results in development of flood inundation mapping.

Table of Contents

Table of Figures

List of Tables

1.1 General

According to Kondolf and Piégay (2003), fluvial geomorphology is a discipline of synthesis at the intersection of the geosciences, geography, and applied engineering. It offers information beyond what can be learned from other disciplines (ecology, chemistry, hydrology, human and environmental sciences), and it enables the study of the river system in all temporal dimensions, from the channel to the floodplain, from the mountainous reaches to the estuarine or deltaic river mouths (Brierley and Fryirs, 2005). The fluvial geomorphology and the flood hazards in river basin are interlinked. However, knowledge of river geomorphology is essential for better understanding the region's landscape and river dynamics, supporting sustainable land use planning and environmental management efforts. In other words, our capacity to calculate the effects of hydroclimatic risks depends on the understanding fluvial geomorphology of the river basin.

1.2 Background and Problem Definition

The River Tawi, which passes through the heart of the Jammu city, is an important tributary of the Chenab River in the Western Himalayan region. The catchment area of the Tawi river basin is bounded by latitude 32° 35' 20"-33° 6' 6" N and longitude 74° 29' 8"-75° 40' 54" E which varies between 239 and 4331 m. The total catchment area up to its confluence with the Chenab River is around 2964 km. Location of the Tawi catchment is shown in Fig. 1.1. The average height of the catchment is about 2200 m above mean sea level (msl). Being a mountainous river Tawi has more than 2000 numbers of tributaries and sub-tributaries. However, there are nine numbers of predominant tributaries of the river Tawi. The Tawi River is comprised of streams of 1-6 orders.

The water-related disasters particularly flood hazard is on rise all over the world particularly in the western Himalayan region in its frequency, magnitude and damage caused to property and society. Therefore, there is very high societal demand to cope with flood hazards and incurred damages. The present study likely to attempt to utilize power of a cloud-based GEE to analyses the planforms changes. Further, this study attempts to evaluate the predictive capabilities of two dimensional Rainfall-Runoff-Inundation (RRI) model and it comparison with HEC-RAS/HEC-HMS model results in development of flood inundation mapping.

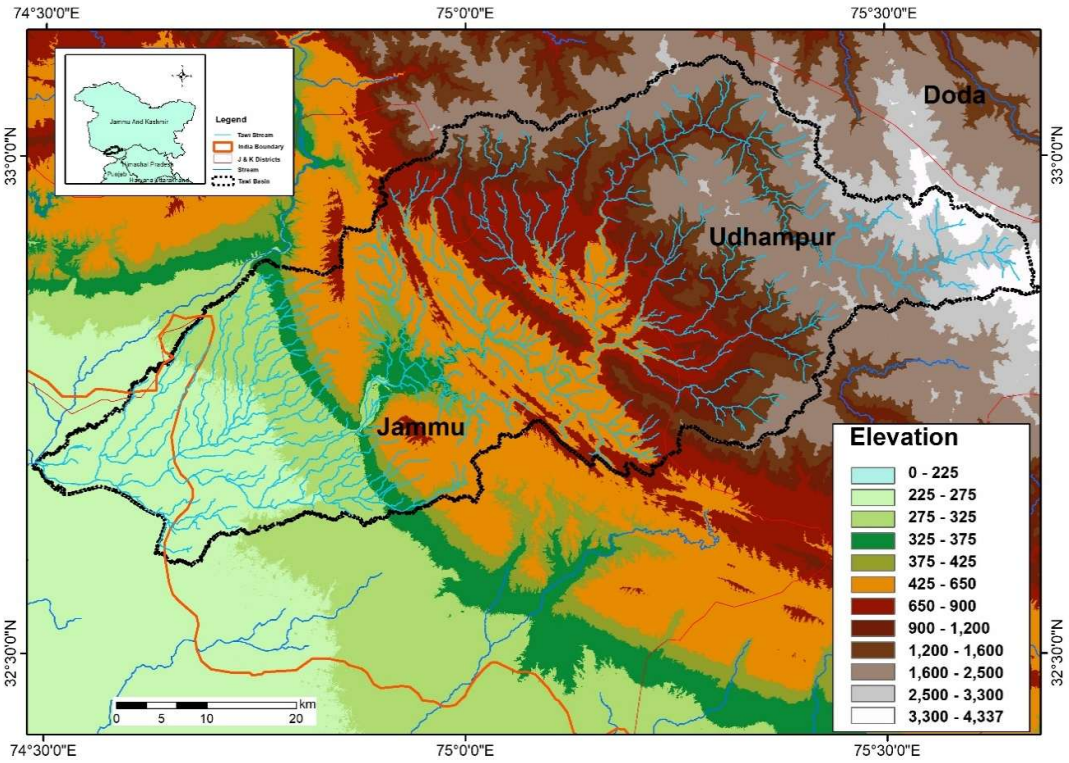

Figure. 1.1. Location map of Tawi River basin.

1.3 Fluvial geomorphology and flood hazard

Rivers play a crucial role in providing freshwater, transportation, and supporting natural habitats worldwide. However, they can also pose risks due to the dynamic nature of their geometry, known as the river planform, which undergoes various changes over time. These changes include channel migration, avulsion (the creation of new channels), and the formation of bars and islands. Understanding these processes is essential for successful river management, particularly in mitigating risks to infrastructure, flood safety, and shipping.

Geomorphological mapping plays a pivotal role in understanding the dynamic processes that shape the Earth's surface. It provides valuable insights into the landforms, geological structures, and evolution of landscapes within a specific region. In this context, the geomorphological mapping of the Tawi basin, located in the state of Jammu and Kashmir, India, holds significant importance. The Tawi basin, with its diverse topography and geological settings, offers an intriguing opportunity to explore the interplay of natural forces that have shaped its geomorphological features. The Tawi river, the lifeline of the Jammu and other cities in the region, meanders through a complex terrain, giving rise to various landform units such as highly rugged mountains, moderately rugged hills, intermontane basins, piedmonts, and alluvial plains. Each landform unit bears distinct characteristics,

influenced by factors like tectonic activity, erosion, sedimentation, and climate over geological time scales. Geomorphological mapping of the Tawi basin aims to decipher the spatial distribution and relationships of these landforms, revealing the underlying geological processes and the influence of past and present environmental conditions.

The utilization of modern technologies, such as remote sensing data, geographic information systems (GIS), and digital elevation models (DEMs), has revolutionized the approach to geomorphological mapping. These tools facilitate the creation of accurate and detailed representations of the basin's terrain, allowing for the identification of subtle geomorphic features and patterns that might have been overlooked in traditional mapping methods. By conducting a comprehensive geomorphological mapping of the Tawi basin we can gain a deeper understanding of the basin's landscape dynamics. The identification of fault lines, drainage patterns, erosional and depositional landforms, and the morphometric analysis of river channels can aid in assessing the basin's vulnerability to natural hazards, understanding the hydrological processes, and guiding land-use planning and resource management.

River planforms refer to the characteristic geometric patterns or shapes that river channels exhibit as they flow through a landscape. To classify and understand different river planforms geometry (or channel patterns), various schemes have been proposed. The well-known classification includes straight, meandering, braided, and anabranching channels (Leopold & Wolman, 1957). Two types of alterations to channel planform were observed by Lewin (1977). The channel's lateral migration occurs naturally as part of autogenic changes, which are part of the river regime. Contrarily, allogenic changes take place in reaction to exogenous factors like climatic change or human activities. Brewer and Lewin (1998) referred to these modifications as intrinsic and extrinsic, respectively, and both terminology were used by Hooke (2007). Straight Planform rivers have a relatively linear or gently curving pattern without significant meanders. They typically occur in areas with a relatively uniform slope and a balance between sediment transport and channel morphology. Straight planforms are commonly found in low-gradient plains or alluvial settings (Knighton, A.D. 1998).

Meandering rivers have a sinuous, curved pattern with loops or meanders. They exhibit a single channel that migrates within a floodplain, creating curves, cutbanks (outer river bends), and point bars (inner river bends). Meandering planforms are influenced by the flow dynamics and sediment transport within the river system. Braided rivers have multiple interconnected channels that divide and rejoin, creating a braided pattern. These rivers often carry high sediment loads and exhibit variable flow paths. The channels are typically separated by sandbars or gravel bars. Braided planforms are common in areas with significant sediment supply and steep gradients (Brice, J.C. 1982). Anabranching refers to a river channel pattern where the main channel splits into multiple

smaller channels that flow in parallel and then rejoin further downstream. These smaller channels often have stable vegetated islands between them. Anabranching rivers are characterized by their multithreaded nature (Knighton, D. 1998).

On the other hand, anastomosing refers to a river channel pattern where the main channel divides into several smaller channels, but instead of re-joining, these channels create a network of interconnected channels. These interconnected channels may enclose islands or landforms within them. Anastomosing rivers typically have a complex and braided network of channels (Kleinhans, M. G., & van den Berg, J. H. 2011).

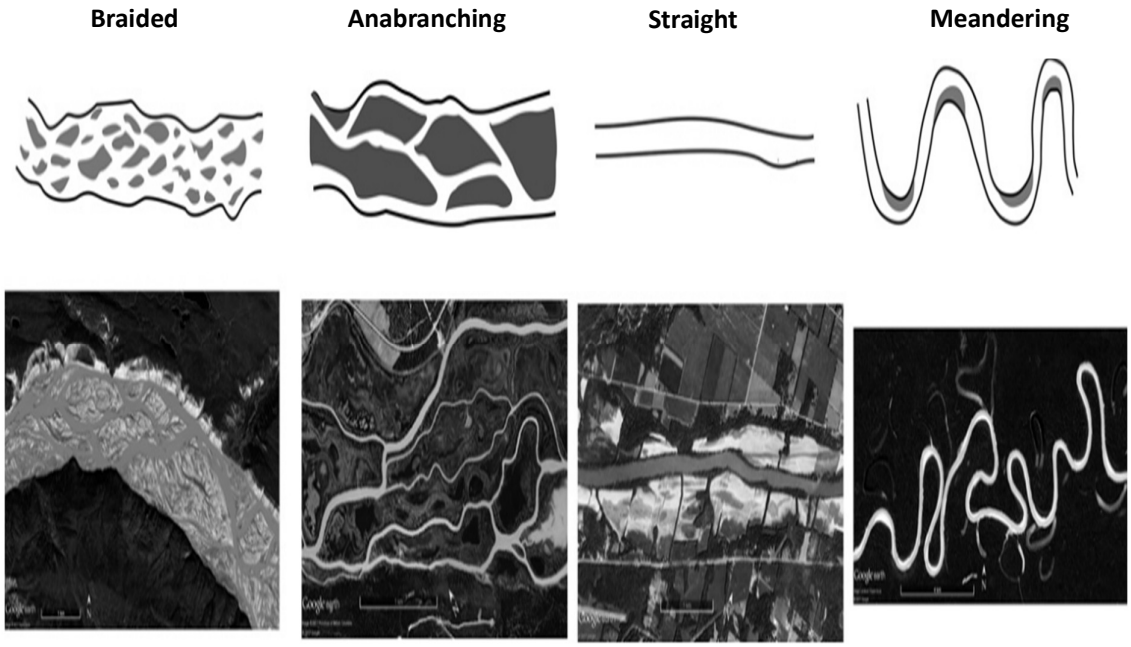

Figure 1.2. Major categories of channel patterns. [Source: Images from left to right are: Chitina River, Alaska, USA; upper Columbia River, British Columbia, Canada; Wabash River, Indiana, USA; Jurua River, Brazil. https://doi.org/10.1017/9781108164108.008].

Satellite imagery plays a crucial role in the analysis of geomorphological features of rivers, allowing for spatial and temporal assessments that would be difficult or even impossible to achieve solely through field observations. Fortunately, there are several sources of freely available remote sensing data that can be utilized to study morphological variations in rivers. However, the process of downloading, storing, and processing remote sensing information poses significant challenges for users, as it often demands high computational performance and storage capabilities. To address these challenges, Google developed the Google Earth Engine (GEE), which has proven to be a valuable solution for remote sensing data processing. GEE provides users with access to powerful computational resources that facilitate the efficient processing of satellite images. Moreover, it offers an extensive collection of up-to-date remote sensing databases, enabling scientists and academics to

leverage these resources for their research and analysis purposes (Gorelick et al., 2017). One of the notable advantages of GEE is its capacity to foster the sharing of knowledge and developed codes among users, particularly within the geoscience's community (Hansen et al., 2013; Global Forest Watch, 2014; Sturrock et al., 2014; Lobell et al., 2015; Zhang et al., 2015; Patel et al., 2015; Coltin et al., 2016; Climate Engine, 2016; Collect Earth, 2016; Map of Life, 2016; Mutanga and Kumar, 2019). The Tawi River, a significant waterway in the study area, has experienced diverse geomorphic changes over the years. Understanding the dynamics of its active channel is essential for effective river management and conservation efforts. By unraveling the interactions between climate variations, human activities, and geomorphic processes on the Tawi River's channel, this study contributes to a deeper understanding of its dynamics and supports informed decision-making for river management and conservation efforts.

1.4 Study Objectives

The following are the study objectives of this study:

- To use a cloud-based Google Earth Engine (GEE) computing platform to systematically identify inter-annual changes in river planform morphology
- Interpret changes in channel conveyance that are relevant for flood risk assessment
- To evaluate predictive capabilities of Rainfall-Runoff-Inundation (RRI) modeI in development of flood inundation map
- To carry out comparison of the RRI model based flood inundation maps with those obtained by using HEC-RAS and HEC-HMS models.

CHAPTER - 2
REVIEW AND LITERATURE

2.1 General

Flooding is caused when high water levels inundate the nearby floodplain and is managed by a number of distinct mechanisms that operate at local and watershed sizes. The river channel morphology of the river basin reflects local hydraulic and sedimentary controls. The relationship between fluvial morphology and flood hazard is given herewith for brevity:

Channel Morphology: The shape and dimensions of a river channel greatly influence its ability to convey water. Wide, shallow channels with a gentle slope may have a higher capacity to carry water without flooding, while narrow, steep channels are more prone to flooding.

Bank Erosion: Fluvial processes can lead to erosion of the riverbanks, potentially widening the channel and increasing flood risk. Erosion can compromise infrastructure, like bridges and buildings, located along the riverbanks.

Sediment Transport: Sediments carried by the river can accumulate within the channel, altering its capacity to carry water. Excessive sediment deposition can lead to reduced flow capacity and increased flood risk.

Floodplain Characteristics: The floodplain, the area adjacent to the river channel, plays a significant role in flood hazard. Its elevation, land use, and natural features like vegetation and wetlands influence the extent and impact of flooding.

Channel Patterns: The way a river meanders or braids affects its flood behavior. Meandering rivers have a larger floodplain and may reduce the speed of floodwaters, while braided rivers can experience rapid changes in flow paths during floods.

Urbanization and Infrastructure: Human activities such as urban development can alter fluvial morphology and exacerbate flood hazards. Pavement and buildings reduce natural absorption and increase runoff, potentially leading to flash flooding.

Flood Modeling and Mapping: Scientists and engineers use fluvial morphology data to create flood models and hazard maps. These tools help predict potential flood extents, depths, and impacts under different scenarios.

Flood Mitigation: Understanding fluvial morphology is essential for designing effective flood mitigation strategies. These can include constructing levees, floodwalls, and other flood control structures, as well as implementing land-use planning and natural floodplain management approaches.

Fluvial morphology and flood risk have a complicated and multifaceted connection. We can better understand and reduce the hazards associated with floods by studying and controlling river morphology, protecting populations and ecosystems in flood-prone areas.

2.2 Role of Remote sensing and GIS in Fluvial geomorphology

Remote sensing is transforming what we map, measure, and analyse in fluvial geomorphology (Marcus & Fonstad, 2010), helping transform the field from a data poor to a data-rich science (Church, 2010). River channel mapping and the analysis of planimetric change have long been key foci of fluvial geomorphology research (Gilvear & Bryant, 2016). The acquisition of satellite imagery at predictable time intervals is a major advantage for this purpose (Carbonneau & Piégay, 2012) and, for very large river systems, aerial or satellite remote systems can be the only way to observe and quantify planimetric morphology (Gilvear & Bryant, 2016). Sensor advances have refined spatial and temporal resolutions, increasing the analytical space within which remote sensing geomorphic analysis can be undertaken (Smith & Pain, 2009). With increased availability of remotely sensed data, the methods used in fluvial geomorphology applications are changing (Piégay, Kondolf, Minear, & Vaudor, 2015), allowing us to see temporal change at wider spatial scales. Furthermore, multispectral satellite imagery is being used to reveal fluvial dynamics and support bio-geomorphological applications in large rivers (Henshaw, Gurnell, Bertoldi, & Drake, 2013). However, information derived from these remote sensing applications has largely been used to test existing concepts in fluvial geomorphology, rather than for generating new concepts or theories (Piégay et al., 2020).

Multitemporal analysis of multispectral satellite imagery has provided fundamental geomorphic insights into fluvial systems across a range of settings. Satellite imagery analysis has often been complemented by analyses of other data sets, including historical mapping, aerial photography, topography, and field survey (e.g., Surian et al., 2016). Combined, these data have improved the understanding of river planform classification, planform evolution, bar morphodynamics, and planimetric form/process interactions over various spatiotemporal scales (e.g., Dixon et al., 2018; A. Gupta et al., 2002; Thorne et al., 1993). However, analyses have often been restricted in their spatial scale (i.e., analysis scales <500 km), focused on single "case study" river systems, and the temporal resolution between discrete analyses has been limited to Interannual to decadal timescales. A spatiotemporal limit has therefore been imposed on fluvial geomorphology analyses through traditional approaches (i.e., desktop computing).

Traditional approaches whereby remotely sensed data are downloaded and stored on personal devices, before analysis tasks can be undertaken, are time-consuming and inefficient when dealing with large data sets (Sudmanns et al., 2020). Commercial software and/or licences are often required as part of processing workflows, alongside considerable computational resources, especially for

multitemporal analyses over large spatial areas. Furthermore, suboptimal satellite imagery (e.g., obstructions from cloud or vegetation cover) may prevent observation and limit geomorphic interpretation (Kondolf & Piégay, 2016). The above factors combine to pose considerable challenges and limit the scale of inquiry for multitemporal analyses of large river reaches. Technological advances in digital infrastructure, increased computing power, and data storage capabilities have given rise to cloud-based computing platforms, providing on-demand access to high-performance computing facilities without the need to own and maintain physical hardware (Sudmanns et al., 2020). This could potentially revolutionize remote sensing applications in geomorphology. The platforms can support massive data storage, helping to resolve data intensity problems associated with the large volumes of Earth observation data (C. Yang et al., 2011). An example of such a platform is Google Earth Engine (GEE), a cloud-based computing platform, accessible through a web-based interface, for planetary-scale geospatial analysis (Gorelick et al., 2017). GEE holds a data catalog of publicly available freely accessible remotely sensed imagery (including Landsat and Sentinel collections), geospatial and other environmental data sets. The cloud-based computing platform aligns with the concept of virtualization, freeing users from resource management and concerns around their physical implementation (Lee, Gasster, Plaza, Chang, & Huang, 2011), meaning that users can bring their own algorithms to the data (Wulder & Coops, 2014). Virtualization allows users to interact with Earth observation data without investing in computing and data management infrastructure (Giuliani, Chatenoux, Piller, Moser, & Lacroix, 2020), removing logistical and know-how constraints from resource-poor researchers (Mutanga & Kumar, 2019). As such, cloud-based computing platforms have been described as a democratizing force (Sultan, 2013), especially as more platforms become available in the future. A key distinction is made here between Google Earth, a virtual globe for viewing digital imagery of the Earth's surface (Tooth, 2013) and GEE, a planetary-scale platform for analyzing geospatial information (Google, 2020). GEE is not the only cloud-based computing platform available, Earth on Amazon Web Services also provides on-demand cloud-based computing resources, though the registry of Earth observation and geospatial data is currently (in 2020) smaller than that of GEE.

GEE has been leveraged for global analyses, including terrestrial and mangrove forest inventories and change detection (Hansen et al., 2013; Thomas et al., 2017); surface water occurrence mapping (Donchyts et al., 2016; Pekel, Cottam, Gorelick, & Belward, 2016); coastal erosion and accretion estimates (Mentaschi, Vousdoukas, Pekel, Voukouvalas, & Feyen, 2018); tidal flat distributions (Murray et al., 2019); and delta morphologies (Nienhuis et al., 2020). For smaller areas, multitemporal analyses of morphological change in river and tidal zones (Khoi et al., 2020), semi-automated landslide detection from time series (Deijns et al., 2020) and the mapping of sediment

transport regimes in arid and semiarid landscapes (Olen & Bookhagen, 2020) have been successfully demonstrated.

2.3 Applications of GEE In Fluvial Geomorphology

Given the potential benefits of using GEE for spatiotemporal analyses, relatively few published studies have utilized this application. GEE has been applied in a fluvial geomorphology context and for river channel change analyses. The first common theme is that GEE has been used as a tool for mining the satellite imagery data archive (particularly Landsat collections), cloud-masking images and then generating multitemporal image composites (e.g., Aadland & Helland-Hansen, 2019). The examples also demonstrate the variety of temporal resolutions over which GEE has been applied, enabling the analysis of shorter-term (e.g., monthly median surface sediment concentrations; Markert, Schmidt, et al., 2018) and longer-term river responses (e.g., median suspended sediment concentrations between 1999 and 2013; Overeem et al., 2017). The utility of multispectral indices for classification purposes is demonstrated (e.g., X. Yang, Pavelsky, Allen, & Donchyts, 2020) and application of transformations to fingerprint specific geomorphic processes (e.g., Tasseled cap transformation; Valenza et al., 2020). The second common theme is that many applications have provided accessible methods (e.g., shareable links to the GEE or source code) and accessible results (e.g., data repositories), promoting transparent and open science. For river channel change analysis, the algorithms can be tested across geodiversity settings and shared between researcher and practitioner communities. The final common theme is that cartographic, graphical, and statistical analyses are almost always completed outside of the GEE environment. Although GEE has the functionality to complete some of these tasks, and additional packages are available to analyse and visualize data sets interactively within Jupyter-based environments (e.g., Wu, 2020), some users choose to export their data to environments or tools with which they have greater familiarity. Reporting this important methodological information would improve the future transparency, methods reproducibility, and completeness of analytic reporting (Goodman, Fanelli, & Ioannidis, 2016).

2.4 Preparation of Fluvial Geomorphological Map

One of the initial attempts to create a geomorphological map of the Gangetic basin was carriedout by Geddes (1960) using traditional survey techniques. Geddes mapped a series of alluvial cones and the areas between them along the Himalayan front. He established a correlation between sediment load, discharge, and the size of the alluvial fans. Subsequently, satellite data and topographic maps were utilized by researchers like Bajpai (1989) and Bajpai and Gokhale(1986) to identify major geomorphic features such as uplands, ravines, floodplains, and paleo channels.

In a study by Sinha et al. (2005), seven distinct mega-geomorphic units were identified to characterize the Gangetic plains, including the active channel belt, active floodplain, minor channels and floodplains, inactive floodplains, slightly dissected surface, highly dissected surface, and piedmont plain. Friend and Sinha (1993) developed parameters for meandering and braiding in order to understand the morphology of channels within the channel belt at the reach scale. Sinuosity (P) and the braid channel ratio (B) were used to assess the spatial variability and morphology of channels in different rivers. Parua (2002) and Thakur et al. (2012) employed remote sensing and GIS data to observe the morphological changes in the Lower Ganga River before and after the construction of the Farakka Barrage. Sinha and Ghosh (2012) also noted significant dynamics in the river both upstream and downstream of the Farakka Barrage. The meandering or braiding nature of the river depends on factors such as sediment load, slope of the basin, bank material, and vegetation (Sinha and Ghosh, 2012). According to Sinha and Friend (1994), the presence of braided or meandering characteristics in rivers is determined by their sediment load. Rivers originating in the Himalayas, with their high sediment load, tend to exhibit a braided pattern, whereas rivers originating in plains, with lower sediment load, typically meander. While it is commonly believed that slope and discharge play a role in shaping the sinuosity and braiding of rivers, Sinha and Friend (1994) found that the availability of bed load sediment compared to suspended load sediments has a more significant influence on these characteristics.

According to Brook and Luft (1987), the planform of a channel is influenced by the interactionbetween erosional forces exerted by the flowing water and the resistance to erosion provided by the channel bed and banks. This interplay of erosional and depositional processes can result in the formation of meandering or braided channels, as well as channel cut-offs and avulsions,where the channel position shifts. The balance between these processes is determined by various factors including the slope of the channel bed, discharge of the channel, sediment load, size of bed material, and composition of bank material (Richards, 1982b; Robert, 2014). Any changes in these variables disrupt the equilibrium and can lead to either aggradation or degradation of the channel. The changes in channel pattern correspond to various alterations in other morphological characteristics of the channel. This includes an increase in both gradient and width-depth ratio, as well as a probable increase in peak discharge, sedimentsize, and sediment load. These geomorphic and hydrologic changes consequently result in hydraulic differences, with flow velocity, tractive force, and stream power increasing from pattern 1 to 5. Consequently, the stability of a graded stream decreases as the channel pattern progresses from 1 to 5, with patterns 4 and 5 representing the least stable conditions (Brook and Luft, 1987). The movement

and shifting of rivers is a natural occurrence, although human activities can often trigger or intensify this process. Evaluating the migration behaviour of rivers is crucial for urban planning and the development of river management strategies. It also aids in studying river bank erosion, flood hazards, and slope failures such as avulsions. Traditional methods forstudying changes in channel patterns involve ground surveys using techniques like Plane tableand Theodolite survey. However, these methods are laborious, time-consuming, and require frequent field visits. Therefore, the utilization of satellite imagery for mapping and monitoringplanform changes has gained popularity due to its high temporal resolution and easy accessibility (Philip et al., 1989).

Satellite image-based planform mapping provides valuable insights into the spatial and temporal variations of river channels. It enables the reconstruction and delineation of stream changes over time. Researchers have made significant efforts to reconstruct and understand the migration of channel planforms and the dynamic processes shaping them (e.g., Gupta et al., 2013; Leopold and Wolman, 1957; Sinha et al., 2014; Stølum, 1998). These studies contribute to a better understanding of river dynamics and support the development of effective management strategies for rivers and their surrounding areas.

Friend and Sinha (1993) introduced modifications to the parameters used to characterize braiding and meandering in rivers. They proposed the use of sinuosity (P) as a measure of channel curvature, defined as $P = L_{cmax}/L_R$, where L_{cmax} is the length of the midline of the channel (in single-channel rivers), or the widest channel (in multi-channel rivers), and L_R is theoverall length of the reach. They also introduced the "braid-channel ratio" (B) as a measure ofthe multiple channels' lengths compared to the main channel, where $B= L_{ctot}/L_{cmax}$, where L_{ctot},is the total of the mid-channel lengths of all the channels in a reach. Surian (1999) conducted a study on the Piave River in the eastern Alps, Italy, to examine the impact of human interventions on channel changes. Using historical maps and aerial photographs, the author analysed how the dynamics of the river were influenced by bank protection structures and hydroelectric dams. The study found that the presence of the dam resulted in reduced flow and sediment supply, leading to a decrease in channel width to only 35 percent of its initial value. Additionally, the braiding index, which indicates the degree of channel braiding, decreased from 3 to 1.5. Surian predicted that this trend would continue untilthe channel reaches an equilibrium state. Hudson and Kesel (2000) investigated channel migration and meander-bend curvature in the Lower Mississippi River from 1877 to 1924. They established a relationship between meanderbend curvature and migration rates. The study revealed that the highest migration rates were observed in channels where the meander bend radius to channel width ratio ranged between 1and 2. Kummu et al. (2008) conducted a study on the Mekong River in China, specifically the stretch between Vientiane and Nong Khai, to examine bank erosion and deposition rates as well as

changes in alluvial islands over a period of 44 years from 1961 to 2005. The study found that the average annual erosion rates were higher on the left banks compared to the right banks. Theimplementation of bank protection measures on the right bank (Thailand side) resulted in decreased erosion rates. The authors also highlighted the impact of the presence of a dam on the river, which led to reduced sediment transport downstream, making the river "hungry" forsediments. This resulted in increased river bank erosion, with higher erosion rates observed inthe islands compared to the river banks. Rutherfurd et al. (1996) conducted a similar study in the Vientiane-Nong Khai reach of the Mekong River, using hydrographic atlases from 1961 and 1992. Their study aimed to estimate bank erosion and accretion rates.

2.5 River Planform Changes

Gupta et al., (2013) conducted a study, utilized the Landsat archive to analyse and characterize the dynamic behaviour of the river Ganga, shedding light on the cyclic processes and morphological evolution taking place within the system. The findings reveal that the river displays a self-organizing behaviour, periodically reaching a critical sinuosity value that triggers one or more chute cut-offs. Interestingly, this repeating pattern is locally fixed by geological features and the Farakka Barrage, indicating its likely persistence in the short-term. The insights gained from this research enhance our understanding not only of the Ganga River but also of mega-rivers in general. Furthermore, these findings have practical implications for local planners and decision-makers. Contrary to concerns about lateral migration and land erosion, this study demonstrates that the river follows a periodic pattern, reworking existing materials rather than causing significant changes. This information provides reassurance and guidance for addressing the challenges and opportunities associated with the river Ganga. Sinha et al., (2014) explored the avulsion of the Kosi River in August 2008, investigating the causes of this event, such as sediment build-up, shifts in planform dynamics, and the absence of a reliable monitoring system. This study aimed to validate avulsion simulation models proposed by previous researchers through field-scale observations. To assess the potential for future avulsions, the study introduced an avulsion threshold index (ATI) that considers both topography-driven factors (e.g., slope ratios) and process-related factors (e.g., planform dynamics). The analysis identified several areas at risk of future avulsions, apart from the location where the 2008 avulsion occurred, namely Kusaha. While the Kosi River has been restored within the embankments since the breach was repaired in January 2009, certain sections, including Kusaha along the eastern embankment, remain vulnerable due to unchanged causal factors. To prevent a similar disaster, continuous monitoring of these sites, regular surveys of cross sections and planform, and monitoring of seepage channels are recommended. Petropoulos et al., (2015) showcased the efficacy of Earth Observation (EO) technology and Geographic Information System (GIS) methods in analyzing the spatio-temporal changes of coastlines in the river deltas of Axios and Aliakmonas, located in the

Thermaikos Gulf, northern Greece. This research employed both direct photo-interpretation and a semi-automatic classification technique based on Support Vector Machines (SVMs) to evaluate the morphological changes in the dynamic coastline. The findings indicated extensive erosion and shoreline retreat in both river deltas between 1984 and 2009, primarily attributed to decreased discharges and disrupted sediment dynamics caused by river regulation and irrigation. The SVMs-based coastline changes mapping showed similar trends to the photo-interpretation but with slight differences in magnitude. This study highlights the potential of using SVMs in synergy with freely distributed EO data, such as Landsat, for cost-effective and accurate coastline changes management. The research contributes to the understanding of Mediterranean river deltas dynamics and underscores the importance of integrating EO data with ancillary information for comprehensive coastline interpretation and management, particularly in the face of climate extremes, human activities, and land-use practices.

Schwenk et al., (2017) proposed a framework to precisely map and quantify planform changes in expansive, dynamic meandering rivers, achieving high spatiotemporal resolutions. By mapping annual planforms at a 30-meter scale using Landsat imagery, the research offers insights into the factors influencing local planform changes and their broader context within the river reach. It emphasizes the importance of capturing key processes such as cut-offs that drive nonlocal morpho-dynamic changes, which can be missed with insufficient temporal resolution. This study also introduces the RivMAP toolbox, a MATLAB-based toolkit that allows for intuitive and customizable analysis of meandering river masks derived from various data sources. The RivMAP tools efficiently calculate widths, centerlines, banklines, migrations, and erosion/deposition rates over large spatial domains using a personal computer. The tools are designed to handle complex river systems, including multithreaded channels, and can be parallelized for application to larger datasets. The framework and tools contribute to a better understanding of how rivers shape their geometries in response to both internal (autogenic) and external (allogenic) forces, such as cut-offs and climate. Singh et al. (2018) aimed to comprehend the Ganga River's behavior by analyzing recent changes in its planform and dynamic fluvial characteristics. The study focused on the Mirapur Khadar to Narora region in Uttar Pradesh, measuring meandering indices and the braiding index to gain insights into the river's course. This study utilized satellite images spanning from 1975 to 2015, obtained from the United States Geological Survey site, to analyze the morphological changes of the Ganga River over a 40-year period. The images, with a spatial resolution of 30 meters, were processed using ArcGIS software. Topographic maps and Landsat images were georeferenced and resampled to a common resolution. The deviation of the river's bank line was determined by overlaying the maps, and the planform changes were assessed by digitizing the Ganga River in GIS. Meandering indices and

braiding index were then calculated to identify these changes. In this study, researchers found that after the construction of the barrage, there was a notable increase in the braiding index from 0.17 to 0.41 between 1975 and 2015. Similarly, the meandering indices also showed an increase from 1.26 to 1.36 during the same period. This suggests that the river exhibited both braiding and meandering patterns. The construction of the Bijnor and Narora barrages had an impact on the overall shape of the Ganga River. The study findings indicate that both natural factors and human activities contribute to the fluctuating nature of the river. Additionally, the researchers discovered that Landsat images were effective in identifying changes in meandering indices, braiding index, and the river's overall shape. Dixon et al. (2018) conducted a preliminary analysis of confluence mobility patterns in the Amazon and Ganges-Brahmaputra-Meghna rivers. The study findings indicated that confluences with high sediment loads tend to be more mobile, whereas those with low sediment loads, particularly in stable geological settings, are more likely to be fixed. Confluences with braided tributaries are also prone to high mobility, driven by changes in the dominant flow position within the braid belt(s). In meandering channels with high sediment loads, the location of the confluence depends on the cut off of meander necks in the tributary channels. When tributaries have low sediment loads, low discharge variability, or erosion-resistant banks, confluences are more likely to be fixed or migrate slowly. These findings have implications for interpreting scour surfaces in the geological record and reconstructing past environmental changes. Mobile confluences can create scour areas much wider than the junction's channel width, resulting in larger and more complex erosional surfaces than previously assumed. This study emphasizes the need for further research on scouring and sediment deposition in large river confluences to improve the criteria for distinguishing these features from depositional signatures driven by larger-scale processes.

Gutierrez et al. (2018) highlighted the scarcity of computer programs available for analyzing bed forms in fluvial and marine environments. The study pointed out that most of these programs are either inaccessible or discontinued, indicating a need for more accessible and up-to-date tools for researchers in this field. To address this gap, they presented Bedforms Analysis Toolkit for Multidimensional Modelling (Bedforms-ATM) as a potential solution. They applied the software to fluvial and synthetic bed form fields and observed promising results. Bedforms-ATM offers a standardized framework for analysing bed form dimensionality and discriminating scales, providing valuable insights into the dynamics of bed form systems and their relationship with hydrodynamic characteristics. This open-source software is designed to facilitate expandability through user collaboration. However, future enhancements, such as MATLAB code for parallel computing and GPU, are necessary to further improve its capabilities. Johnston et al. (2019) conducted a study with the aim of investigating the formation of levees. The researchers sought to understand whether levees

grow and develop through sediment transfer from the adjacent channel or are influenced by flood basin dynamics. By analysing empirical data and conducting modelling experiments, the researchers found no conclusive evidence that levee presence or size is genetically linked to the planform morphology of the adjacent channel. While a sinuous channel was expected to transfer more sediment to the channel margins during floods, it did not show a direct relationship with levee formation. The modelling experiments revealed that in fine-grained systems, levee initiation is related to the channel planform, but as levees grow taller relative to flood-wave height, their sediment supply diminishes, causing the deposition maximum to shift towards the levee toe. This transition results in progradation down-valley and genetically disconnects the levees from the channel. Therefore, on narrow floodplains of fine-grained rivers, levee size and shape are influenced by flood-basin hydrology and the interaction of factors such as inundation frequency, flood wave propagation, and suspended sediment transport pathways.

Yang et al. (2020) Introduced RivWidthCloud, an automated algorithm for extracting river width using the cloud computing services provided by Google Earth Engine (GEE). Through validation against same-day in-situ width measurements, they demonstrate the algorithm's accurate performance in deriving river widths from Landsat images. It should be noted that the error assessment conducted in this study may be conservative, as it does not account for errors in in-situ measurements or discrepancies between in-situ and satellite measurement locations in rapidly changing width areas. RivWidthCloud offers two notable advantages over previous river width measurement algorithms. Firstly, it leverages the user-friendly cloud computing environment of GEE, making it easy to use without the need to download, store, and process remote sensing data locally. Secondly, it incorporates a flagging capability that automatically mitigates the impact of features like clouds and shadows. This enables users to extract width statistics and time series efficiently. The algorithm also allows for the generation of spatially continuous multitemporal width data, which can serve as a valuable dataset for future satellite missions like SWOT or for estimating river discharge using the Adaptive Moving Horizon-based Gridding (AMHG) method alone or in combination with other remote sensing data products. Although RivWidthCloud currently utilizes Landsat data due to its extensive mission history and wide application, the algorithm can easily be expanded to incorporate other remote sensing data products such as Sentinel 2 or Moderate Resolution Imaging Spectroradiometer (MODIS) data.

Kong et al. (2020) conducted a study that examined the changes in the shape and characteristics of the Lower Yellow River (LYR) over a period from 1987 to 2017. The upper section of the river showed more significant alterations in anabranching, braid-channel ratio, sinuosity (curviness), and lateral migration rate compared to the lower section. However, the number and area of sandbars

decreased in the upper reaches (R1-R3) after the Xiaolangdi Dam began operating, while they increased in the lower reaches (R6-R7). The overlap between the current and 1987 channel masks gradually decreased, indicating substantial channel migration. Most planform parameters, except sinuosity and sandbar area, decreased after the dam's operation. The Xiaolangdi Dam prevented the river from drying up and protected it from floods, while also prolonging the duration of low and medium water flow stages. Although the effective discharge magnitude did not change significantly after the dam's operation, it became more compressed within a narrower range of annual variability, with larger low-level discharges and shorter rising-flood stages. This study highlights that the LYR is still adjusting differently along its course due to the changes in water and sediment patterns caused by the Xiaolangdi Dam and the Water-Sediment Regulation Scheme (WSRS). It was crucial to address sedimentation issues in the lower LYR. In the medium term (decades ahead), the WSRS should consider the LYR's response time to the Xiaolangdi Dam operation plan, as well as other factors like climate change, changes in floodplain land use, and future river engineering projects, which are not covered in this research.

Sivanpillai et al. (2021) focused on flood mapping and proposed the use of inundation maps derived from the differencing of Modified Normalized Difference Water Index (MNDWI) values. The study highlighted that this approach provides a valuable tool for identifying flooded areas that remain unaffected by cloud cover, improving the accuracy of flood assessment. By comparing MNDWI values from pre- and post-satellite imagery, analysts can generate accurate maps of newly inundated regions within a reasonable timeframe. These maps are then superimposed onto post-flood satellite images to assist response personnel in navigating the affected landscape. However, the accuracy of inundation maps derived from differencing Normalized Difference Water Index (NDWI) values is lower due to limitations in satellite data collection. To expedite the generation process, it is beneficial to access derived products through agencies like the USGS and explore implementation on platforms such as Google Earth Engine. Analysts must also consider the impact of water extent in the pre-flood imagery, as it significantly influences the accuracy of the resulting flood map. It is important to address minor errors, such as misclassified pixels, either by removing them based on a minimum mapping unit or by alerting emergency response agencies for exclusion during rescue mission planning. Tobón-Marín and Cañón Barriga (2020) developed algorithms in Google Earth Engine (GEE) for river delineation, utilizing the NDWI, MNDWI, and AWEI indices. The study found that the AWEI index offered an intermediate delimitation of surface water, the MNDWI tended to overestimate it, and the NDWI sometimes underestimated it. Refinement of surface water delimitations using the GSW dataset greatly improved planform accuracy, particularly for MNDWI. The Zhang and Suen method generally yielded good results for centreline delimitation, although

braided reaches posed challenges due to errors in surface water delineation. Calculations of mean width, connectivity, and sinuosity served as a basis for analysing planform variations over time, allowing for correlation with macroclimatic events. Their GEE tool facilitated spatiotemporal analysis and geomorphological parameter analysis in an efficient manner without requiring large data volumes. By analysing eight Colombian rivers, they observed changes in different regimes and configurations. The tool successfully identified stable sections and detected new branches in braided reaches. Annual variations and their relationship to ENSO were analysed, with results varying across river types. The advantages of using GEE were evident in terms of time and computational resources compared to conventional GIS platforms. However, image quality issues, such as scan-line error stripes, affected planform parameter estimation and required additional treatment. Regular inspection of images during analysis was recommended to ensure accuracy.

Rowland et al. (2016) discuss the evolution of remotely sensed imagery usage in characterizing river properties and detecting plan view changes. The increasing availability of satellite imagery and processing tools in the last decade has expanded the potential to enhance the spatial and temporal understanding of river morphology and dynamics. While existing GIS and automated analyses mainly focus on single-threaded meandering river systems, Rowland introduces a set of analysis algorithms collectively known as Spatially Continuous Riverbank Erosion and Accretion Measurements (SCREAM). These algorithms are designed to analyze plan view river metrics regardless of river morphology, offering a versatile approach for complex multi-channel planforms. SCREAM quantifies erosion and accretion rates, changes in river channel and floodplain areas, and island dynamics using binary masks of channels from imagery acquired at two different periods. The program also assesses variations in erosion rates about local channel attributes, enabling comparisons across rivers of varying sizes and morphologies. Rowland emphasizes that SCREAM, validated against manual measurements, has the potential to provide accurate data for quantitative examinations of erosion rate controls and comparisons across diverse river systems.

Boothroyd et al., (2021a) focused on a specific section of Po River in Italy and analyzed satellite images from Landsat 5, 7, and 8, covering the period from 1988 to 2018, using Google Earth Engine (GEE). The objective of this study, was to examine changes in the river planforms morphology and the dynamics of vegetation in relation to the temporary or short-term variations and dynamics of water within a hydrological system. Their goal was to better understand the relationship between river morphology, vegetation, and water flow, which can help in managing sediment transport and vegetation growth to reduce the risk of flooding. The study focused on two indices: the Modified Normalized Difference Water Index (MNDWI) and the Normalized Difference Vegetation Index (NDVI). The MNDWI was used to track changes in the wetted area of the river, providing

information about sediment movement. The NDVI was used to assess changes in vegetation coverage along the river. The results of the analysis showed that changes in the shape of the river were mostly localized, with the majority of the river reach remaining stable. By using the occurrence frequency of the wetted channel as a measure of stability, the researchers found that almost two-thirds of the wetted channel extent (covering a total area of 86.4 km2) had a frequency of occurrence greater than 90%, indicating stability. They also observed a loss of complexity in the river shape, particularly in areas where secondary channels used to exist or where the main channel had narrowed. A time series analysis of vegetation dynamics using the NDVI was also conducted and found that the highest values of NDVI, indicating greater vegetation coverage, were recorded in May/June. These peaks in vegetation coincided with the first peak in the hydrological regime, which occurred in late spring and was associated with snowmelt. Based on findings, this study concluded that remote sensing data, such as satellite imagery, can provide valuable insights for river scientists and contribute to the management of heavily modified rivers. By understanding the relationship between river morphology, vegetation, and water flow, scientists and policymakers can make informed decisions to mitigate flood risks in anthropized watercourses, which are rivers heavily influenced by human activities. Boothroyd et al. (2021) This study contributes to the quantification of dynamism patterns in tropical river systems and highlights the effectiveness of Google Earth Engine (GEE) in fluvial geomorphology applications. This research demonstrates significant planimetric changes in the wandering/braided section of the Bislak River and measures the migration rates along the Cagayan River, which vary over time. The utilization of tools like GEE allows for the acquisition of multi-temporal data across large river reaches, facilitating the testing of theories related to geomorphic change and the re-evaluation of fundamental concepts such as river channel pattern classification in fluvial geomorphology. The ability to conduct multi-temporal analyses at relevant temporal resolutions enables the monitoring of both gradual and abrupt changes in river systems, aligning with the timescales of geomorphic processes of interest.

Dey et al. (2022) addressed the persistent challenges of riverbank erosion and recurrent flooding along the Ganges in eastern India, focusing on the state of West Bengal. Analyzing Landsat imagery from 1987 to 2019 using ArcGIS and the RivMAP toolbox, the study aimed to understand the annual to decadal-scale changes in the Ganges' path and their impact on sediment reworking in the floodplain. Over the past three decades, the Ganges in the Malda district exhibited variable mean reach-averaged migration rates ranging from 200 to 600 m/yr, resulting in a net land loss of approximately 140 km^2 and an average annual loss of 4.5 km^2. The research highlighted a positive correlation between riverbank erosion and peak annual discharge, emphasizing the significant influence of climate on river migration and bank erosion. The findings pointed to specific threats in

the northern and southern parts of the district, indicating increased meandering and an eastward shift of the channel, respectively. Despite a recent slowdown in net land loss, the study suggested potential rejuvenation with another phase of higher discharge. Over the last three decades, the total land loss amounted to 140 km^2, contributing to an erosion rate of 4.4 km^2/yr and an annual sediment yield of approximately 26-29 Mt, constituting 10-15% of the total sediment load downstream.

Khan et al. (2022) conducted a comprehensive study on the morphological changes near the confluence of the Ganges, Jamuna, and Padma rivers spanning a 25-year period from 1990 to 2015. Through meticulous analysis of satellite imagery and precise digitization techniques, they quantified the shifting patterns of riverbanks and channel widths. The study revealed significant erosion along the riverbanks, with discernible trends in bank line displacement and river width fluctuations. Notably, the maximum width observations across various segments were documented, alongside staggering rates of bank line shifting at specific locations and timeframes. Utilizing Landsat satellite data, the study provided invaluable insights into the planform dynamics of the Ganga–Jamuna confluence, emphasizing the urgent need for proactive measures to address riverbank erosion and its cascading impacts on the socioeconomic fabric of the region. Moreover, the study highlighted the interconnectedness of anthropogenic activities and structural interventions with morphological changes in the river, underscoring the necessity for integrated management strategies to safeguard the region's ecological integrity and community well-being.

Abebe and Mulat (2021) aimed to investigate the planform changes in the lower reach of the Gilgel Abay River, specifically focusing on the 56-kilometer stretch from the river mouth to Lake Tana. The study analyzed the river's evolution over a three-decade period. To achieve this, the researchers utilized advanced techniques such as GIS and remote sensing, along with field observations. The various data sources, including topographic maps, Landsat images, and recent Spot images of 2016 were employed to identify and map the planform change features within the study area over the past 35 years. The study identified, quantified and mapped different planform changes, including river bank migration, length, valley length, sinuosity, width, lateral migration, and lake shoreline variation, specifically around the river mouth where it enters Lake Tana, from 1984 to 2019. One significant planform change observed was the bifurcation of the river channel, occurring 5 kilometres upstream from its current mouth. The sinuosity of the study reach, representing the level of meandering, was categorized as low sinuous, with values ranging between 1 and 1.32. The study found a general decrease in sinuosity by approximately 4.31% over the analyzed period. On average, the river migrated laterally by 39.79 meters, with a yearly migration rate of 1.99 meters to the left between 1996 and 2016. Since 1984, the average yearly migration rate had been 1.05 meters to the left. Considering the identified planform changes and their potential impacts, the researchers

suggested that it was crucial to develop planning and management policies for the lower reach of the river and these policies should aim to minimize river planform change, including issues such as channel shifting, delta and island expansion and alteration, and their effects on the lake level and the overall balance of the surrounding ecosystem. Vercruysse and Grabowski (2021) conducted a study that focused on assessing the influence of human activities on the morphological changes of rivers in the Himalayan Sutlej-Beas River system. The study examined both short-term and long-term dynamics to better understand the impact of human interventions on river shape and behavior in the region. The findings revealed significant variations in river characteristics at different timescales, including centuries, years, seasons, and months. These changes were observed both between and within the rivers, showing spatial and temporal complexities. The researchers categorized the geomorphic dynamics into different evolutionary trajectories, namely ramp, press, and pulse, drawing analogies from ecological concepts. This study highlighted the persistent influence of human impacts on river systems, as indicated by the dominance of press-ramp trajectories. However, it also emphasized that the impact of a single human activity can lead to different trajectories depending on the scale and metrics considered. This approach of understanding timescale-dependent evolutionary trajectories in river systems can be applied to various metrics in catchments with different geographical and human-environment interactions. The insights gained from this research contribute to a better comprehension of the diverse temporal dimensions of human impact on river shape, which can inform the development of comprehensive river management strategies.

Z. Li et al. (2021) investigated the Layue Basin, located near the Eastern Himalayan Syntaxis, which has undergone substantial geomorphological changes leading to the formation of multiple knickpoints. This study categorizes the knickpoints into two groups: movable 4 k knickpoints and fixed damming-type knickpoints. Using slope area analysis and χ analysis, the study reveals that most knickpoints in the Layue Basin are primarily located at 4000 m elevation, while the pattern of damming-type knickpoints is less evident. The research examines the geomorphic characteristics of three natural damming events investigated in the field, namely the Jiaobunong and Delun landslides and the Baimu deposit. The Jiaobunong and Delun landslides show distinct knickpoints and abrupt changes in the normalized steepness index (k_{sn}), indicating their impact on the longitudinal profile of the river. However, the Baimu deposit has a negligible effect on the river's profile, suggesting it may not be a large-volume landslide dam or moraine dam. The study reconstructs paleo profiles using fifteen selected channels and finds that the average relief of the basin has increased by approximately 104% since the knickpoint entered the basin, indicating significant uplift and erosion. The celerity model successfully replicates the observed knickpoints, demonstrating the mobility and homogeneity of the 4 k knickpoint group. Furthermore, a paleo profile reconstruction is conducted for the

intermediate reach associated with the JBN-KP, confirming the significant influence of large landslides on the river profile over short time periods.

Sebastianelli et al. (2021) present a research paper that introduces a novel tool designed to automate the generation of appropriate datasets for artificial intelligence (AI) applications within the context of Earth Observation (EO). The paper presents two versions of the tool's architecture, both of which are accessible on Git-Hub and include a user-friendly graphical user interface (GUI) for non-expert users. Currently, the tool supports data from the Google Earth Engine catalogue and has undergone extensive testing using Sentinel-1 and Sentinel-2 data. Future testing will involve incorporating other data sources available in the Google Earth Engine catalogue and integrating new data sources. The tool holds significant value for researchers applying machine learning (ML) techniques to EO and remote sensing (RS) data, providing them with a powerful resource for generating datasets tailored to their AI applications. Zhou et al. (2021) utilized TopoToolbox in their research to extract and analyze the longitudinal profile, knickpoints, and ksn values of the Indus River basin. These parameters were then compared with the types and locations of dams identified through remote sensing interpretation. They identified a total of 178 dams and 102 knickpoints, with 55 of the knickpoints being associated with dams. The results revealed a notable spatial correlation between dams, high steepness index (k_{sn}), and river knickpoints within the Indus basin. Furthermore, they observed that debris flow dams had a more significant impact on the river's longitudinal profile compared to landslide and glacial dams in the upper Indus River. Knickpoints formed by debris flow dams exhibited maximum heights exceeding 900 meters. Their study highlights the significant role that dams play in shaping the evolution of river longitudinal profiles. Consequently, when using river knickpoints to derive information on tectonic activity, it is crucial to consider the potential influence of dams.

Hasenhündl and Blanckaert (2022) present a research paper that introduces a new MATLAB script designed to quantify morphometric characteristics in rivers, channels, and canyons across diverse environments. The script effectively determines planform metrics such as bankfull width (B), centreline radius of curvature (R), and sinuosity (SI), while also identifying cross-section orientation, bend apices, and crossovers. Additionally, it incorporates bathymetric or topographic digital elevation data to provide further morphometric details like thalweg, slope(S), bankfull depth (H_B), cross-sectional area (A), channel aspect ratio (B/H_B), and levee slope (α). The application example using Lake Constance demonstrates the script's user-friendly nature and computational efficiency, allowing inexperienced users to acquire relevant metrics in just two hours. With default parameters ensuring robust performance, the script also offers customizable options for enhanced flexibility and optimization. This MATLAB tool serves as a valuable resource for efficiently analysing

morphometric characteristics in a wide range of research and engineering applications involving bathymetric and topographic data. Aziz et al. (2022) conducted a study that addresses the challenges faced by researchers worldwide in processing and preparing Sentinel-1 data for generating flood maps. In situations with dense cloud cover during natural hazards like floods, the active SAR sensor becomes the only viable option. However, the large data size and the need for high-end computing facilities often limit routine research. Cloud computing methods, such as Google Earth Engine (GEE), offer significant benefits in terms of time and resources. In 2020, Bangladesh experienced severe flooding in various regions. This study utilizes freely available satellite datasets and GEE to simplify the complex and time-consuming data processing steps. The study introduces a cost-effective and time-saving approach for mapping floods and calculating affected areas, which is particularly valuable for developing countries. The timely availability of empirical evidence aids in implementing mitigation and disaster management strategies. Furthermore, this study opens avenues for future research, integrating digital elevation models (DEMs) to enhance water flow analysis and vulnerability assessment. Bengal et al. (n.d.) conducted a study that utilized a combination of LANDSAT image analysis and remote sensing of flow parameters to examine the Ganga River in the Malda district of West Bengal. The study draws several significant conclusions based on their findings. Firstly, it identifies land loss caused by channel migration, with the northern part of the district experiencing increased meandering and the southern part witnessing an eastward shift of the channel. Secondly, this study establishes a strong correlation between the annual bank erosion rate and the annual peak discharge from 1999 to 2018, highlighting the significant influence of climate on river-bank erosion. Lastly, it quantifies the extent of land loss over the past three decades, estimating a total loss of approximately 140 km², corresponding to an erosion rate of 4.4 km² per year. With an average bank height of around 3 meters, the study also estimates an annual sediment yield of approximately 26-29 million metric tons from this stretch of the Ganga River.

Basnayaka et al. (2022) conducted a study that focused on the Lower Mahaweli River in Sri Lanka. The researchers analyzed the planform changes of the river over a thirty-year period, using Landsat satellite images for their analysis. The river exhibited dynamic geomorphological characteristics, with noticeable river braiding at four locations. Although the planform of the Lower Mahaweli River remained relatively stable over the past three decades, downstream segments showed significant changes. The formation of an oxbow lake near Trincomalee was identified, leading to altered flow paths and sediment bar depositions. Migration rates of the river centrelines were calculated, revealing slower rates overall but higher rates at specific locations associated with oxbow lake formation. The study emphasizes the need for quantitative analyses, especially in the downstream areas. While medium-resolution satellite images are suitable for planform analysis when

field data is limited, cloud coverage poses limitations. The research serves as an introductory study, providing insights for future detailed mathematical analyses. The proposed methodology is applicable to narrow rivers and can contribute to water resource management, particularly in the downstream region with its renowned natural harbor near the sea outlet of the Mahaweli River. Bhatpuria et al. (2022) developed a comprehensive monitoring system for the Ayeyarwady River in Myanmar. The study utilized long-term Landsat remote sensing data within the Google Earth Engine (GEE) platform to establish this monitoring system. This system allowed for mapping seasonal erosion, accretion areas, and channel width changes along the river's 3882 km length. This study employed the Modified Normalized Difference Water Index (MNDWI) and thresholding techniques to differentiate the river channel from land pixels. The accuracy assessment revealed an overall accuracy of 89% when comparing satellite-based observations with field observations in 2019. The analysis identified six hotspots of active riverbank erosion, including areas near major cities and the river delta. Time series analysis highlighted changes in river width, with the largest change occurring in the Lower Ayeyarwady section following the confluence of the Upper Ayeyarwady and Chindwin rivers. This study demonstrated the potential of the monitoring system for hazard mapping, vulnerability assessment, and operational planning by the Department of Water Resources and Improvement of River Systems (DWIR) in Myanmar. Future enhancements include incorporating higher-resolution satellite data such as Sentinel-1 and Sentinel-2 to improve the detection of riverbank changes.

Tolentino et al. (2022) emphasized that understanding the character and behavior of rivers is essential for sustainable river management. In the Bislak Catchment, eight distinct River Styles have been identified, with Confined (57%) and Partly-confined (37%) River Styles being the most prevalent in terms of stream network length. When examining the downstream sequences of these River Styles, 11 out of 17 major tributaries displayed a similar pattern, indicating that they pass through catchments with similar characteristics such as steep slopes and homogeneous geology. However, it was found that the variation in channel slope alone is insufficient to determine the type of river in a given reach. To achieve sustainable river management, it is essential to adhere to the guiding principles of the River Styles Framework, which involve interpreting the landscape, working harmoniously with natural processes, and having a thorough understanding of the catchment's diversity and river patterns. By adopting a geomorphological perspective and developing catchment-scale visions, sustainable river management practices can be informed and implemented effectively. Abad et al. (2022) conducted a study on the Ucayali River, which is renowned for its active meandering in the Amazon Basin. The research revealed that the river experiences average migration rates of 60-80 meters per year. This study focused on analysing three bends of the river, with two

bends exhibiting cut-off processes during the study period, and the third bend, located near Jenaro Herrera town, showing signs of an impending cut-off. Examining the planform evolution between 1987 and 2020, it was found that the migration rate of the JH bend was 25 m/year, lower than the average migration rates observed in the Ucayali River. This reduced migration rate can be attributed to the presence of secondary channels and islands that modify flow patterns and sediment distribution, resembling processes observed in anabranching rivers. This study identified two potential mechanisms for cut-off occurrence in the region: Migration I, involving the reactivation of oxbow lakes, and Migration II, characterized by the collapse of two bends forming a typical neck cu-toff. Both mechanisms would result in significant changes to the configuration of the JH bend, triggering erosional and depositional processes upstream and downstream of the cut-off location. Long-term hydrogeomorphic monitoring is crucial to comprehend cut-off dynamics, plan socioeconomic development including town relocation, and assess the impact of extreme events, climate change, and human activities on river dynamics.

CHAPTER - 3
METHODOLOGY

3.1 Study Area

The Tawi river basin is a sub basin of the Chenab basin, and a major part of this basin falls in the State of Jammu and Kashmir, India, and nearly 5% falls in Pakistan. The Tawi river originates from Kali Kundi glacier and covers 141 km before its confluence with Chenab in Pakistan. The elevation of the entire basin varies between 189 m at confluence of Chenab and Tawi to 4295 meters near Kailash-Kund glacier from mean sea level (Figure 5.1). The upper portion of the river basin is characterized by rugged mountainous topography, the middle part consists of low hills followed by piedmonts and alluvial plains. Total basin area of the Tawi basin is about 2897 km2 out of which 1390 km2 and 1372 km2 area falls in Udhampur and Jammu districts respectively and the lower most portion with 135 km2 area in upstream of the confluence of Chenab and Tawi falls in Pakistan. The Udhampur district lies in the mighty Himalayan Range and it is situated in south eastern part of Jammu and Kashmir state. Physiographically, the district is characterized by mountain ranges trending NW-SE direction, the district is covered partly by Pir Panjal ranges and partly by Outer Himalayas. Major slope of the terrain is towards south and southwest. The gentle terrain occurs in southern and southwestern part while in northern part is covered by complex and high mountainous terrain. Majority of the district is occupied by the rocks belonging to Murree and Siwalik formations of tertiary period.

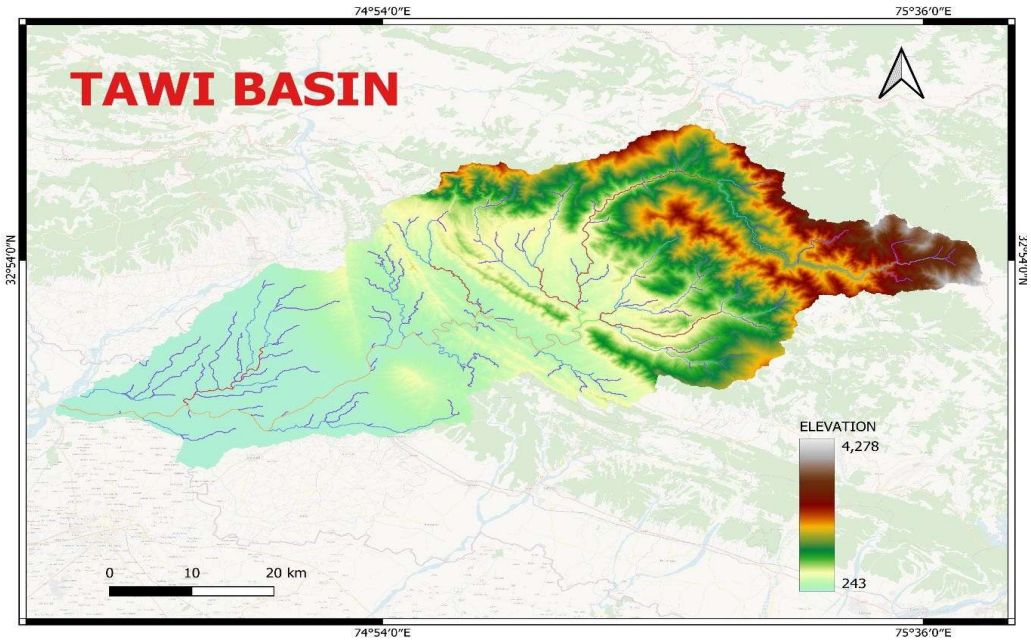

Figure 3.1. The geographical area of Tawi River Basin

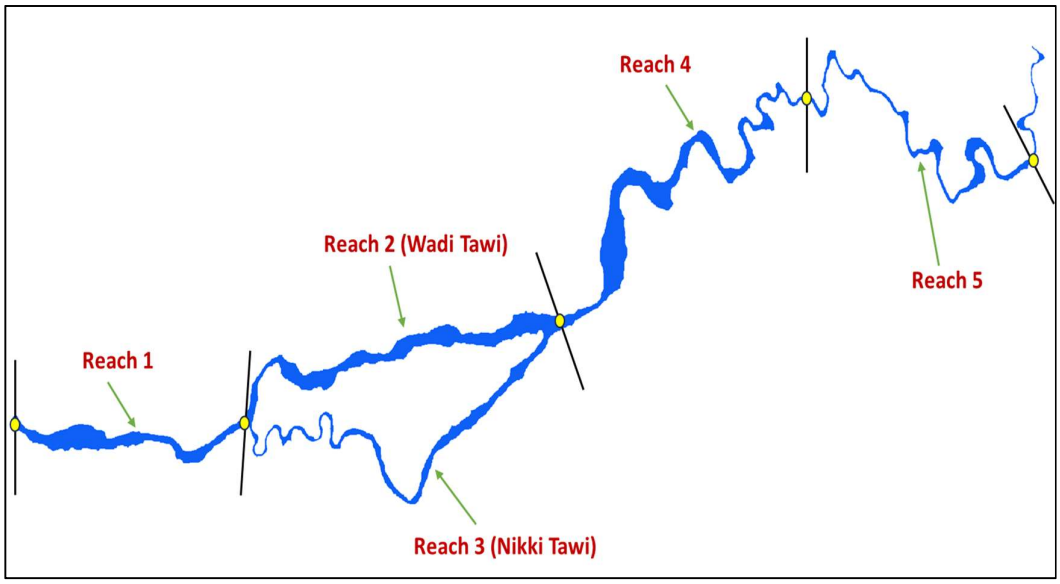

Figure 3.2 Tawi River with 5 reaches

3.2 Data Used

The Google Earth Engine (GEE) data catalog offers a comprehensive repository of such data, providing researchers with access to a wide range of spatial and temporal datasets relevant to fluvial geomorphology applications. The GEE catalog includes datasets with varying spatial resolutions, temporal revisit frequencies, temporal archives, and spatial coverages. One notable data set available in the catalog is the Landsat series, comprising Landsat 5 TM (Thematic Mapper), Landsat 7 ETM+ (Enhanced Thematic Mapper Plus), and Landsat 8 OLI/TIRS (Operational Land Imager/Thermal Infrared Sensor). These datasets offer spatial resolutions ranging from 30 m and temporal revisit frequencies of 16 days (Table 4.1), covering extensive temporal archives from as early as 1984 to the present day. Importantly, these data sets provide global coverage, making them valuable resources for fluvial geomorphology studies across different geographic regions.

Table 3.1 Available remote sensing datasets used in this study

Data Set	Spatial resolution	Temporal revisit	Temporal archive	Spatial coverage
Landsat 5 TM	30 m	16 days	1984–2012	Global
Landsat 7 ETM+	30 m	16 days	1999–now	Global
Landsat 8 OLI/TIRS	30 m	16 days	2013–now	Global

Notes: ETM = Enhanced Thematic Mapper, MSI = Multispectral Instrument, OLI = Operational Land Imager, TIRS = Thermal Infrared Sensor, TM = Thematic Mapper.

3.2.1 Extracting the Active River Channel within GEE

Step-1: In this study, Landsat imagery available in Google Earth Engine was utilized to analyze and classify the active channel, encompassing water and exposed sediment, over 34 years from 1988 to 2021. The Landsat satellites employed in this analysis included Landsat 5 (LT05), Landsat 7 (LE07), and Landsat 8 (LC08). Leveraging the multispectral data captured by these satellites, with a spatial resolution of 30 meters, enabled the characterization of diverse features within the riverscape. The region of interest (ROI) was defined by specifying a geometry or uploading a shapefile within Google Earth Engine.

Step-2: The start and end dates were set to cover the desired 34-year timeframe from October 1st to April 30th each year. The choice of October 1st to April 30th as the study period aligns with the dry season, often characterized by reduced water flow and lower water levels. This period provides a clearer view of the channel morphology and facilitates the identification of channel features, patterns, and exposed sediment. The reduced water flow during this period enhances the visibility and allows for a more accurate analysis of the active channel. Landsat 7 experienced a significant issue with its SLC (Scan Line Corrector) in May 2003, resulting in data loss in every alternate scan line. These missing scan lines caused diagonal gaps or stripes in the acquired images, reducing their overall quality and usability for specific applications. In the GEE code snippet, a filter was applied to exclude Landsat 7 images within the specified time range affected by the SLC failure.

Step-3: In this study, the modified normalized difference water index (MNDWI), proposed by Xu (2006), was chosen to map surface water and identify the wetted channel position. The MNDWI is computed as follows:

$$\text{MNDWI} = \frac{\text{G} - \text{SWIR1}}{\text{G} + \text{SWIR1}} \tag{4.1}$$

where G and SWIR1 represent the green and shortwave infrared bands, respectively, the resulting MNDWI values range from -1 to 1, with more positive values indicating the presence of water. This approach generated 30-meter resolution water maps by applying the constant threshold to annual temporal composite images, resulting in binary water masks.

In addition to MNDWI, the normalized difference vegetation index (NDVI), first introduced by Rouse et al. (1974), was used to produce proxy maps for live green vegetation (Fig.4.2d). NDVI is commonly employed for vegetation monitoring (Dzubáková et al., 2015) and is computed as follows:

$$\text{NDVI} = \frac{\text{NIR} - \text{R}}{\text{NIR} + \text{R}} \tag{4.2}$$

where NIR represents the near-infrared band, and R denotes the red band. Higher NDVI values indicate healthier and more abundant vegetation.

By utilizing both MNDWI and NDVI, the study was able to analyze surface water distribution and the presence of live green vegetation along the fluvial reach, enabling a comprehensive understanding of the dynamic interactions between water bodies and vegetation in the study area.

Step-4: The determination of water bodies through water indices involves the application of a threshold value, serving the purpose of the composition, as highlighted by Diniz et al. (2019). This methodology aligns with the wetted channel classification method employed by Zou et al. (2018), where multispectral indices such as the Modified Normalized Difference Water Index (MNDWI) and Normalized Difference Vegetation Index (NDVI) are utilized to create a binary water mask in the temporal composite image. The process involves setting threshold values for MNDWI and NDVI to differentiate between water bodies and other land cover types. Furthermore, this approach extends to the classification of alluvial deposits, where the same multispectral indices are utilized, and the active channel boundary is maintained by excluding vegetated pixels.

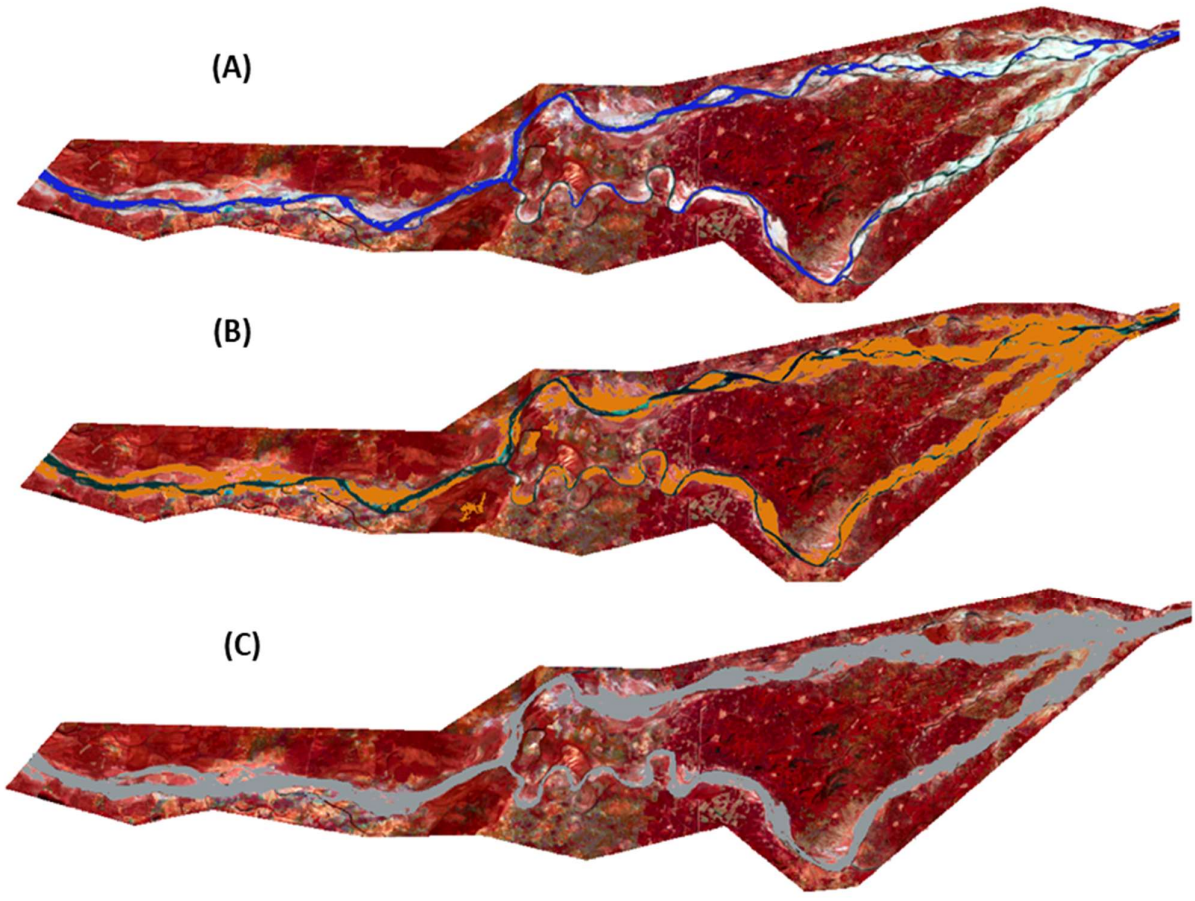

Figure 3.2. Delineated channel characteristics showing (a) Wetted Channel (blue color), (b) Alluvial channel (orange color), (c) Combined wetted channel and sediment deposits or Active Channel (Gray color).

Step-5: Binary wetted channel (Fig. 4.2a) and alluvial deposit (Fig. 4.2b) masks are combined (i.e., geometric union) to give an active channel river mask (Fig. 4.2c). An optional step for cleaning/noise removal was implemented here. Final binary masks are exported to Google Drive as a GeoTIFF file for subsequent analysis outside the GEE environment. Additionally, the Landsat image of the Brahmani-Baitarani River for 1998 was not available, so instead, an image from 2001 was used. It was important to not use an alternate year image otherwise the change would not show.

3.2.2 Manually Cleaning and Filling Gaps in Channel Masks Images

Each composite image underwent manual cleaning by using MATLAB image processing technique, where any connected components not hydraulically linked to the river, such as tributaries, cities, misclassified clouds, and cutoff remnants, were removed to maintain consistency across the imagery (Fig. 4.3b). Additionally, any gaps in the composite image were filled to ensure the continuity of the river features (Fig. 4.3c). To illustrate, when quantifying erosion and deposition, differences in composite-derived channel masks between different times were analyzed. For example, if a chute channel was present in one composite but not in another due to poor Landsat imagery, its absence might be mistakenly interpreted as deposition, while its reappearance might erroneously suggest erosion, even if no actual erosion or deposition occurred.

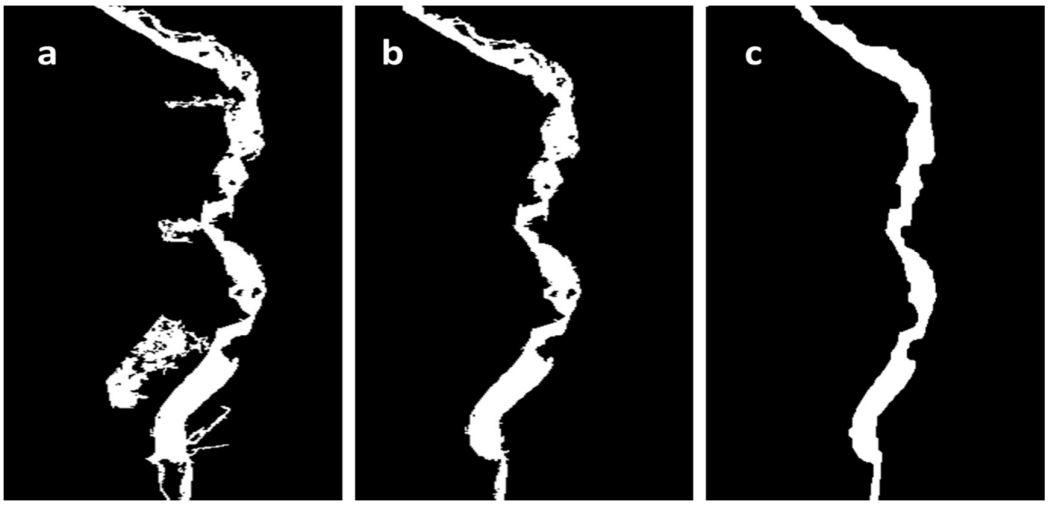

Figure 3.3. Manual Cleaning Process and Gap Filling in Composite Image. (a) Raw composite image, (b) Manually cleaned and (c) Gap Filled in Composite Image.

3.3.4. Planform Characteristics Extraction Using RivMap Toolbox

RivMAP was employed for a detailed analysis of the Brahmani and Baitarani River channels, leveraging its diverse toolkit to process binary active channel masks of these rivers. This approach facilitated an extensive examination of the rivers' planform geometries, allowing for the extraction of centerlines and banklines, as well as the measurement of various parameters such as widths, lengths, angles, and curvatures specific to each river system. By harnessing RivMAP's functionalities, temporal changes within the Brahmani and Baitarani rivers were effectively assessed. This included identifying areas of migration along the centerline and bankline. Through this targeted analysis, valuable insights into the distinctive geomorphological characteristics and dynamic alterations within these river systems were obtained. The application of RivMAP in river channel analysis demonstrated its efficacy in precisely processing channel masks derived from images, highlighting its utility in geomorphic studies.

3.3.5 Centreline and bankline extraction from channel mask

The process begins by preparing the input mask for the RivMAP tool, which involves filling any holes and removing areas not connected to the main channel, allowing for the efficient extraction of river features from a given channel mask and exit sides variable. Subsequently, skeletonization is applied to the mask, aimed at generating the centerline. However, this step encounters challenges, particularly at the ends of the channel mask, where the skeleton no longer accurately traces the centerline due to intersecting corners. To address this, the channel mask image is padded with mirrored versions of itself, ensuring smooth transitions beyond the original boundaries. Once the padded image is obtained, the centerline is extracted and cropped to remove any boundary effects resulting from the skeletonization process. Additionally, another issue encountered during skeletonization is the presence of unwanted spurs, which must be effectively removed. Rather than individually eliminating these spurs, the centerline is determined as the shortest path along the skeleton between its endpoints. This process ensures the removal of spurious elements while accurately capturing the centerline's path (Fig. 4.4). It's worth noting that the resulting centerline is resolved at single-pixel resolution, meaning that the spacing between centerline nodes is dependent on the resolution of the input mask.

This process makes efficient use of MATLAB's image-processing tools. Initially, the mask is cropped to the point where the river intersects the image edge, and any holes within the mask that border the image boundary are filled. Subsequently, the perimeter of the cropped image is identified and separated into left and right banks. This separation is achieved by retaining only the bankline pixels while removing all others at the image boundaries. Finally, the bankline coordinates are evaluated and arranged in an upstream-to-downstream order, providing a comprehensive representation of the channel's banks.

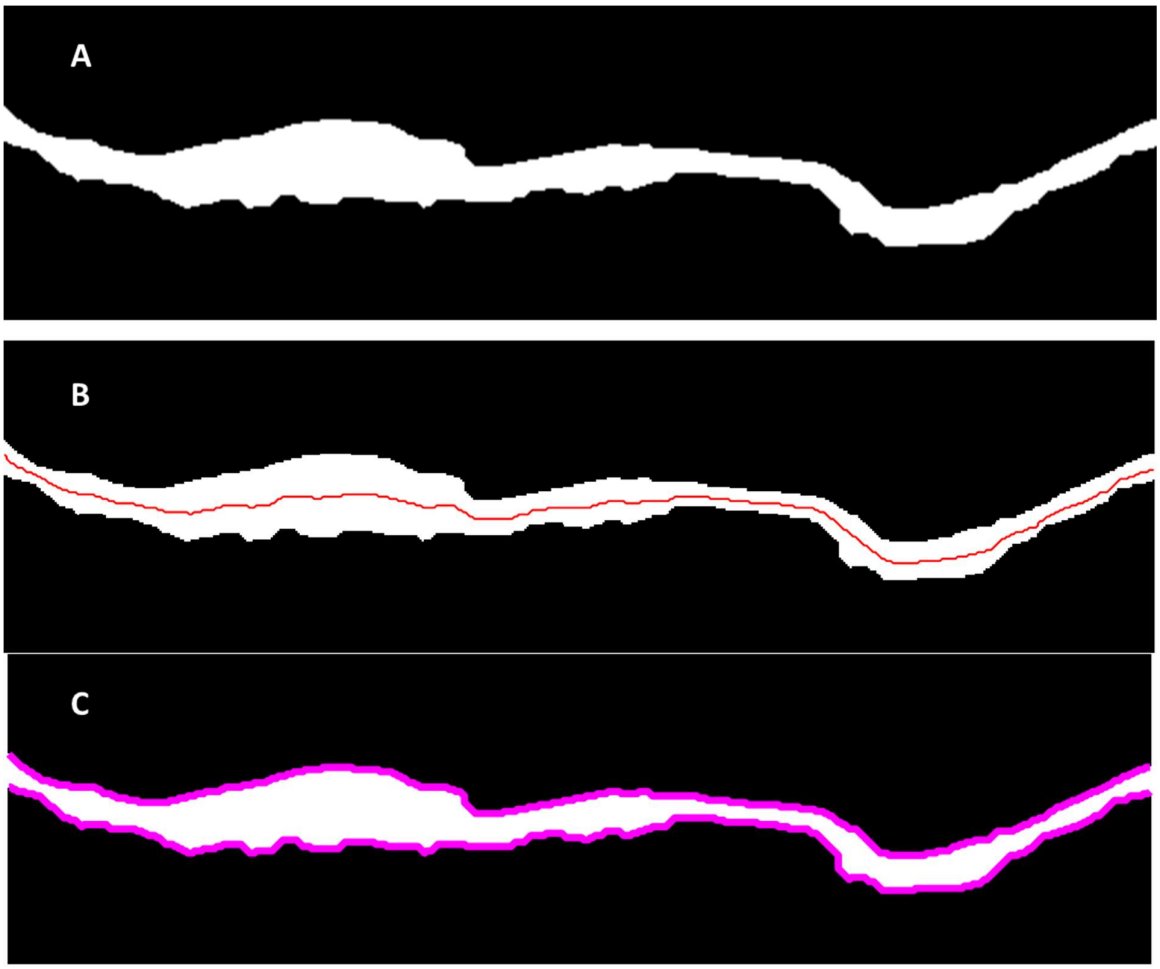

Figure 3.4. Extracted centerline and bankline image from binary image showing (a) Binary Channel Masks, (b) Centerline and (c) Bankline.

3.3.6 River width estimation

Over the years, the reach average width (Wra) and average width along the centerline (Wavg) of the river channel exhibit dynamic patterns. The computation of river width in the RivMAP toolbox involves a detailed process. The centerline is parameterized by calculating streamwise distances (dsi) between successive points (xi,yii). This is achieved using the formula:

$$ds_i = \sqrt{(x_{i+1} - x_i)^2 + (y_{i+1} - y_i)^2} \quad (4.1)$$

The reach-average width is computed by summing the streamwise distances and dividing by the number of pixels in the channel mask (P):

$$W_{ra} = \frac{P}{\sum ds_i} \quad (4.2)$$

where P is the number of pixels in the holes-filled channel mask, and the summation of dsi is over all centerline nodes in the channel mask. The centerline coordinates are smoothed to provide a stable estimate of the centerline direction at each node, computed as:

$$\theta_i = \arctan\left(\frac{y_{i+1} - y_i}{x_{i+1} - x_i}\right) \quad (4.3)$$

The centerline is broken into J equally spaced segments of user-selected length and a buffer polygon is created for each jth segment by constructing perpendicular vectors at the first and last nodes of the segment. The perpendicular vectors are connected by polylines defined from the centerline nodes within segment j for the left and right banks:

$$\left(x_{lb,i}, y_{lb,i}\right) = \left(x_i - (\sin(\pi - \theta_i))2W_{ra}, y_i - (\cos(\pi - \theta_i))2W_{ra}\right) \quad (4.4)$$

$$\left(x_{rb,i}, y_{rb,i}\right) = \left(x_i + (\sin(\pi - \theta_i))2W_{ra}, y_i + (\cos(\pi - \theta_i))2W_{ra}\right) \quad (4.5)$$

The intersection of buffer polygons with the channel mask determines the number of channel pixels within each buffer (Pj). The length of the centerline within each buffer is calculated by summing the streamwise distances for the corresponding segment:

$$l_j = \sum_{i(j)}^{i(j+1)} ds_i \quad (4.6)$$

where i(j) refers to the ith centerline node at the beginning of segment j. The average width for each segment is then computed as the ratio of the number of pixels in the buffer to its length:

$$W_{avg\ .j} = \frac{P_j}{l_j} \quad (4.7)$$

Unwanted blobs, potentially arising from buffer overlap, are removed based on the distance from the centroid of each blob to the midpoint of the centerline between the beginning and ending nodes of segment j. Blobs with a distance greater than 1.5· lj are excluded. This approach (Fig. 4.5) ensures conservative buffer calculations, minimizing errors associated with pixel-based line lengths, and provides a comprehensive assessment of river width dynamics.

To calculate channel widths between banklines at centerline nodes, perpendicular line segments are extended from each node, intersecting both left (LB) and right (RB) banks. This process involves identifying the intersections of these segments with the banks. The channel width (Wbl) is then calculated as the distance between these intersection points. If a perpendicular segment intersects more than two banks, only the two closest intersections are retained. This method utilizes a nominal reach width (Wra) to assist in the computation. However, it's worth noting that this approach may not accurately represent the wetted width for channels with multiple threads.

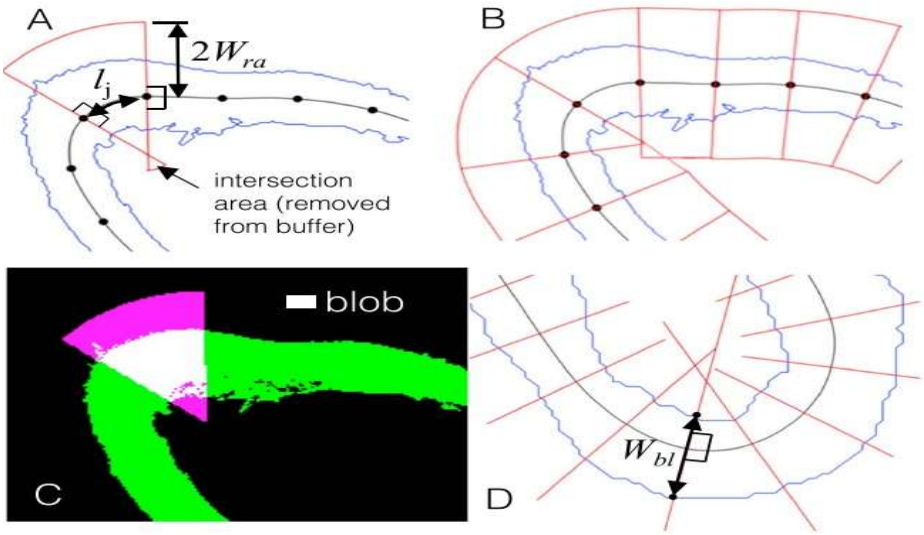

Figure 3.5. Procedure of channel width computation: (a) Average width (Wavg) for a river segment involves establishing buffer boundaries around the smooth centerline, with buffer spacings indicated by black dots. (b) Buffer polygons are generated based on these spacings. (c) These buffers are applied to the channel mask, resulting in a white area representing the intersection of the buffer and mask images. The average channel width is determined by dividing the number of white pixels in the intersection by the length of the segment (lj). (d) Channel width computation from banklines is illustrated in blue representing the channel banks and black denoting the smoothed centerline. Red perpendicular vectors are shown at every tenth pixel. (Schwenk et al. 2016)

3.3.7. Migrated areas and migration rate due to erosion and accretion

The quantification of channel migration within the RivMAP toolbox involves two distinct methods for analyzing planform areas, including centerline and bankline migration areas as well as erosional and depositional areas. These approaches also encompass routines for distinguishing cutoffs from migrated areas. Instead of relying on vector-based techniques, these methods employ image processing methodologies.

To conduct the migration analysis, input data such as coordinates of centerlines or banklines from different time instances, along with details about their exit sides, a nominal channel width (e.g., Wra), and the dimensions of the image used for coordinate extraction are necessary., Both smoothed and unsmoothed coordinate data can be utilized for the analysis. Binary masks are created for the centerlines (Fig. 4.5), with areas on one side of each image filled. This process generates two images, $I_{half,t1}$ and $I_{half,t2}$ The migrated area image (Fig. 4.6) is then computed by combining the forward and backward differences between the images captured at times t_1 and t_2:

$$I_{M,cl} = \left(I_{half,t2} - I_{half,t1}\right) \cup \left(I_{half,t1} - I_{half,t2}\right) \quad (4.8)$$

A verification process is implemented to ensure that the centerline at time t_1 contributes no area to IM,cl, while the centerline at time t_2 does, except for pixels where the centerline remains unchanged.

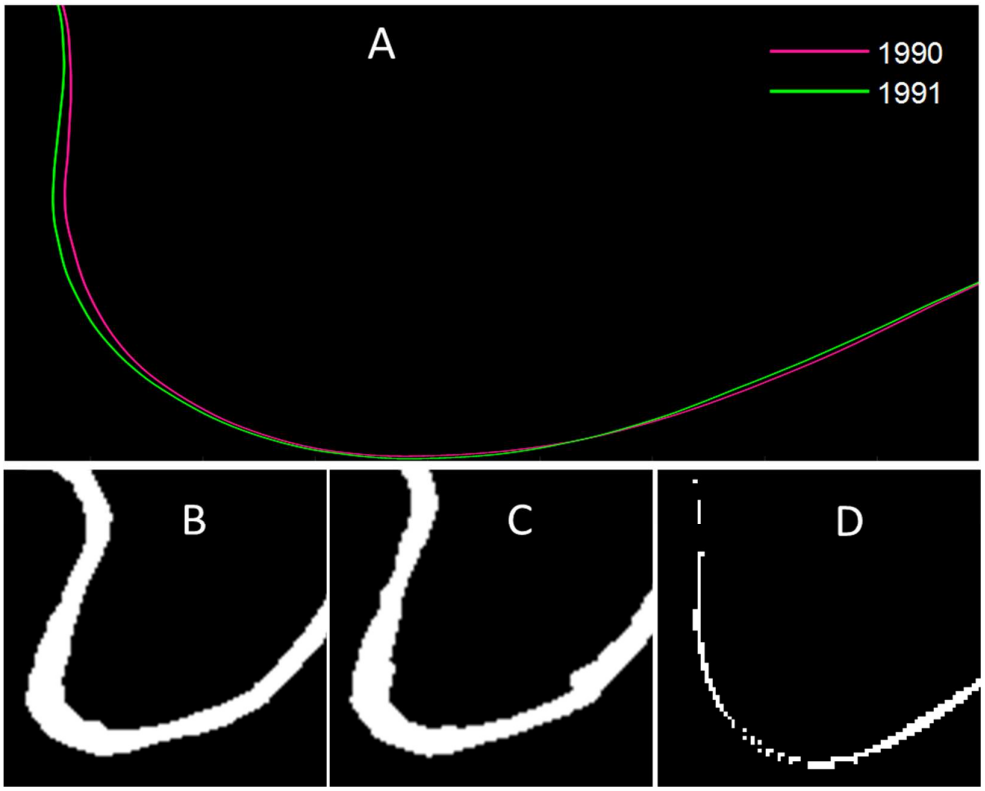

Figure 4.6. Procedure for computing migrated areas from centerline or bankline data. a) centerlines at both times are shown; filled image halves are displayed for 1990 (b) and 1991 (c); d) migrated area, obtained by the union of their differences, is depicted by the white pixels.

In cases where the centerline experiences cutoffs between t1 and t2, the areas of these cutoffs appear as migrated areas in IM,cl and require separation. Subsequently, the RivMAP function migration_cl identifies cutoffs by applying a threshold to the change in streamwise distance between centerline segments.Initially, all intersections between the centerline at times t1 and t2 are located and ordered from upstream to downstream. Each consecutive pair of intersections defines a segment. The centerline length of each segment is then determined for both the t1 and t2 centerlines as follows:

$$\text{seglen}_{j,t_1} = \sum_{i(j)}^{i(j+1)} ds_i \qquad (4.9)$$

where i(j) refers to the ith centerline node corresponding to the jth segment.

3.3.8 River Sinuosity Estimation

Sinuosity is commonly defined as the ratio of the river's centerline length to the straight-line distance between its start and endpoint. This ratio quantifies the degree of meandering or winding of the river channel (Ratzlaff et al., 1991). Mathematically, sinuosity (S) can be expressed as:

$$S = \frac{CL}{D} \tag{4.10}$$

where S = Sinuosity, CL = Actual length of the river channel, and D = Straight-line distance between the start and endpoint of the river.

Straight rivers are characterized by minimal meandering and follow relatively direct paths, resulting in a sinuosity close to 1.0. In contrast, meandering rivers, with their numerous bends and curves, have sinuosity values ranging from 1.1 to 1.5 or higher, depending on the degree of meandering, which can vary significantly. Braided rivers, on the other hand, consist of multiple interconnected channels separated by bars and islands of sediment and typically have lower sinuosity values, ranging from 0.5 to 1.0, due to their complex, braided channel patterns. Anastomosing rivers, with sinuosity ranging from 1.0 to 1.5 or higher, feature multiple channels that branch and rejoin, creating a network of interconnected channels separated by stable islands or bars, making their sinuosity comparable to or even higher than meandering rivers depending on the channel network's complexity. Lastly, the sinuosity of incised or entrenched rivers can vary widely, as these rivers, which have cut deeply into the landscape often forming canyons or gorges, may see a decrease in sinuosity due to the confinement of the channel within steep valley walls.

3.3.9 Average rate of migration

The average rate of migration for a river reach is calculated using the formula:

$$M_{\mathrm{Cl}} = \frac{A_{\mathrm{cl}}}{A_c(t_2 - t_1)} \times 100\%$$

In this equation, A_{cl} represents the total area migrated by the centerline, A_c is the area of the channel, and M is expressed in percentage per unit time. Normalizing by the channel area eliminates dependence on both width and length, but migration rates can also be normalized by the centerline length, as suggested by Larsen et al. [2006].

3.3 Geomorphological Analysis

Multispectral satellite images and digital elevation models (DEMs) have become essential tools for mapping landforms and gaining valuable insights into the morphology of an area. These data sources offer high-resolution spatial, temporal, spectral, and radiometric information, enabling the identification and analysis of landforms using various techniques. The methodology

followed to prepare geomorphological map of the Tawi River Basin is presented in Figure 3.2. In the context of the Tawi river basin, a geomorphic map has been created to depict the currentstate of the river and its surrounding landform units. This mapping involved the utilization of satellite images and DEM derivatives, such as profile, slope, hill shading, aspect, and 3-D flythrough visuals. These data sources provide a comprehensive understanding of the landforms and their characteristics within the basin. Geomorphic features in the channel belt and the active floodplain were delineated using satellite images and specific indices derived from them, such as the Normalized Difference Water Index (NDWI). These features were mapped to record the behaviour and characteristicsof the river, allowing for the identification of distinct physical processes at work in different sections. To analyse the topographic characteristics of the entire Tawi basin, available Sentinel-2 data with a resolution of 30 meters was utilized. Various DEM derivatives were derived from this data, which were then corrected and validated using recent Sentinel-2 and Copernicus DSM data. This integration of different datasets provides a comprehensive understanding of the topography and landforms present in the basin.

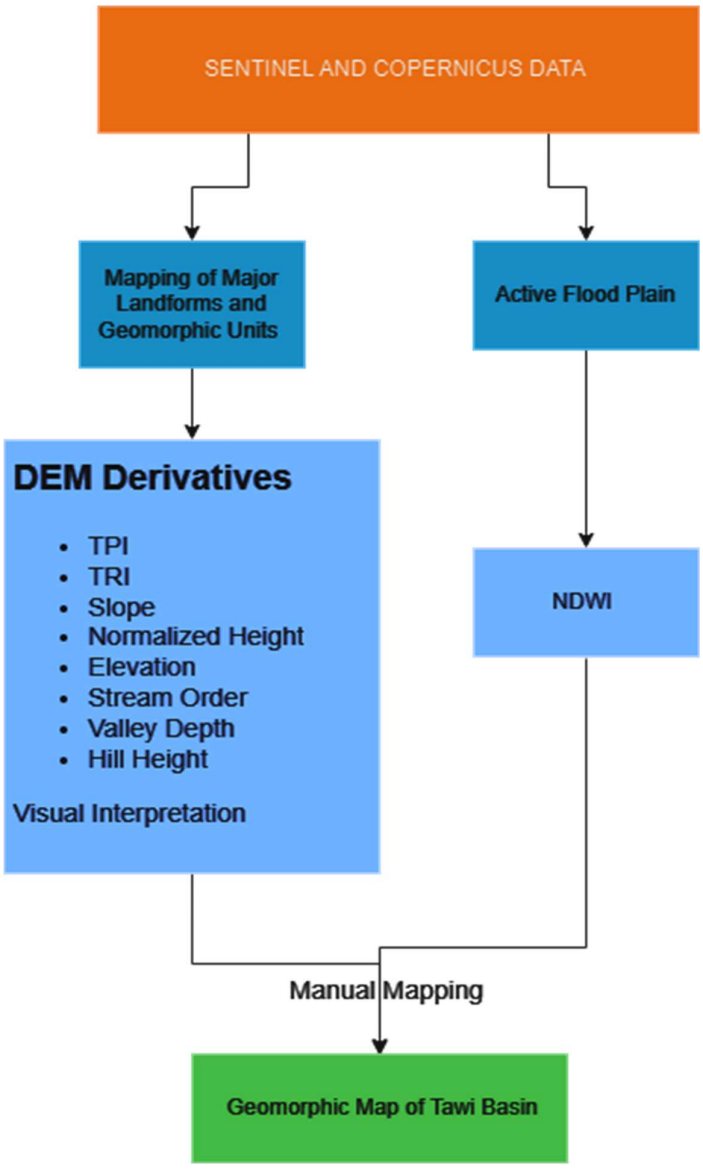

Figure 5. 2. Flow chart showing methodology used for geomorphological map generation.

Landform delineation in the study was conducted using on-screen image interpretation techniques. Geomorphic features were interpreted based on key elements of interpretation suchas shape, tone or colour, pattern, shadow, association, and texture. False colour composites (FCCs) were generated using different combinations of satellite data bands to aid in image interpretation and manual mapping. The visual representation of terrain played a crucial role inidentifying landforms, particularly in hilly areas where it can be particularly challenging. Digital Elevation Models (DEMs) were employed to capture the spatial variations of the surface and assist in the identification of landforms, especially in hilly regions. The study utilized SENTINEL -2 data to generate various topographic indices. Planform mapping was conducted in Q-GIS using a UTM projection and WGS-84 datum. Additionally, various DEMderivatives were calculated using

software tools such as SAGA-GIS and Q-GIS. By employing these techniques, we were able to visually interpret and map different landforms based on their distinct characteristics. The utilization of DEMs and derived indices provided valuable information about the topography and landform patterns within the study area. These findings contribute to a comprehensive understanding of the landforms present, especially in hilly areas where traditional mapping approaches may face limitations.

3.3.1 Dem derivatives

Terrain Ruggedness Index (TRI): it calculates the difference in elevation between each grid cell and the mean elevation of its 8-cell neighbourhood within a moving window. TRI values range from 0 m to higher values, where 0 represents the minimum roughness. By utilizing TRI,we were able to quantify the roughness of the terrain, identifying areas with higher variability and heterogeneity.

Topographic Position Index (TPI): it calculates the difference between the elevation of a celland the mean elevation of its surrounding neighbourhood. The neighbourhood is determined by a moving window centered on the cell of interest. Positive TPI values indicate that the cellis higher than its surrounding neighbourhood, while negative values indicate lower elevation. TPI is a scale-dependent index, sensitive to local variations compared to regional elevations. It is valuable for identifying landscape patterns associated with different rock types, geomorphicprocesses, soil characteristics, vegetation, or air drainage. By applying TPI, we were able to delineate ridges and depressions within the study area, providing insights into the spatial distribution of these landforms.

Normalized height: it is another morphometric index used in the study. It controls the way maximum slope values are incorporated into a cell's neighbourhood, considering local slope differences between cells. Smaller slopes result in more maximum values being included in thecell, leading to a smoother or generalized pattern. On the other hand, higher slopes result in fewer values being incorporated, leading to a more irregular pattern due to small changes in elevation between cells.

Stream Order: To map stream order within the study area, we utilized SENTINEL 30m data, which provided higher spatial resolution compared to SRTM 30/90 m data. Stream order delineation was carried out using SAGA-GIS tool within Q-GIS software. Stream order and the drainage pattern offer insights into the influence of slope, lithology, and structural controls on the drainage basin.

For a better understanding of the study area, 3D visualization was employed using high-resolution SENTINEL and Copernicus DSM data. This visualization technique enabled us to identify major landform units and gain a visual perspective on the terrain.

3.4 Detecting Changes in River Planform

To investigate spatial differences in river planform, the rivers will be classified into number of reaches defined by their physiographic setting and valley gradient. This study employed a semi-automated workflow in Google Earth Engine (GEE) Google Earth Engine to extract information on river planform morphology from multitemporal, multi-spectral satellite imagery. Landsat surface reflectance products (Landsat 5 Thematic Mapper, Landsat 7 Enhanced Thematic Mapper and Landsat 8 Operational Land Imager) and sentinel data products (Sentinel-1 SAR GRD and Sentinel-2 MSI) as the primary source of satellite imagery available from 1988 onwards and other imagery data may be used in the investigation. Various indices particularly Normalized Difference Water Index (NDWI), Modified Normalized Difference Water Index (MNDWI) and or Automated Water Extraction Index (AWEI) and other suitable approaches will be used to achieve active channel mapping at multi-temporal scale. The active channel, encompassing water and exposed sediment, is a dynamic zone critical for understanding river behavior, floodplain evolution, and ecological processes. Through GEE, annual image collections covering the entire 34-year duration (1988-2022) are constructed. Cloud masking procedures in GEE ensure the exclusion of cloudy pixels, enhancing the reliability of the analysis.The main steps followed to extract active channel are shown in Fig. 3.3 and are described as follows.

- **Time and ROI Filter:** Annual image collections were constructed by filtering the Landsat imagery based on the desired time-period and the region of interest (ROI).
- **Cloud Masking Procedure:** A cloud masking procedure was applied to mask out cloud and cloud shadow pixels from the image collections, ensuring reliable data for analysis.
- **Temporal Compositing:** Temporal compositing was performed using the median reducer, which aggregated overlapping cloud-masked images to generate annual images (temporal composites).
- **Classification:** Water and alluvial deposits were classified using well-established spectral indices, such as the Modified Normalized Difference Water Index (MNDWI) and (Normalized Difference Vegetation Index (NDVI).
- **Binarization:** The wetted channels and sediment deposits masks were combined into a single binary image through a union operation. The resulting binary image, representing the

active channel, was then exported as a GeoTIFF file to Google Drive for further analysis and visualization.

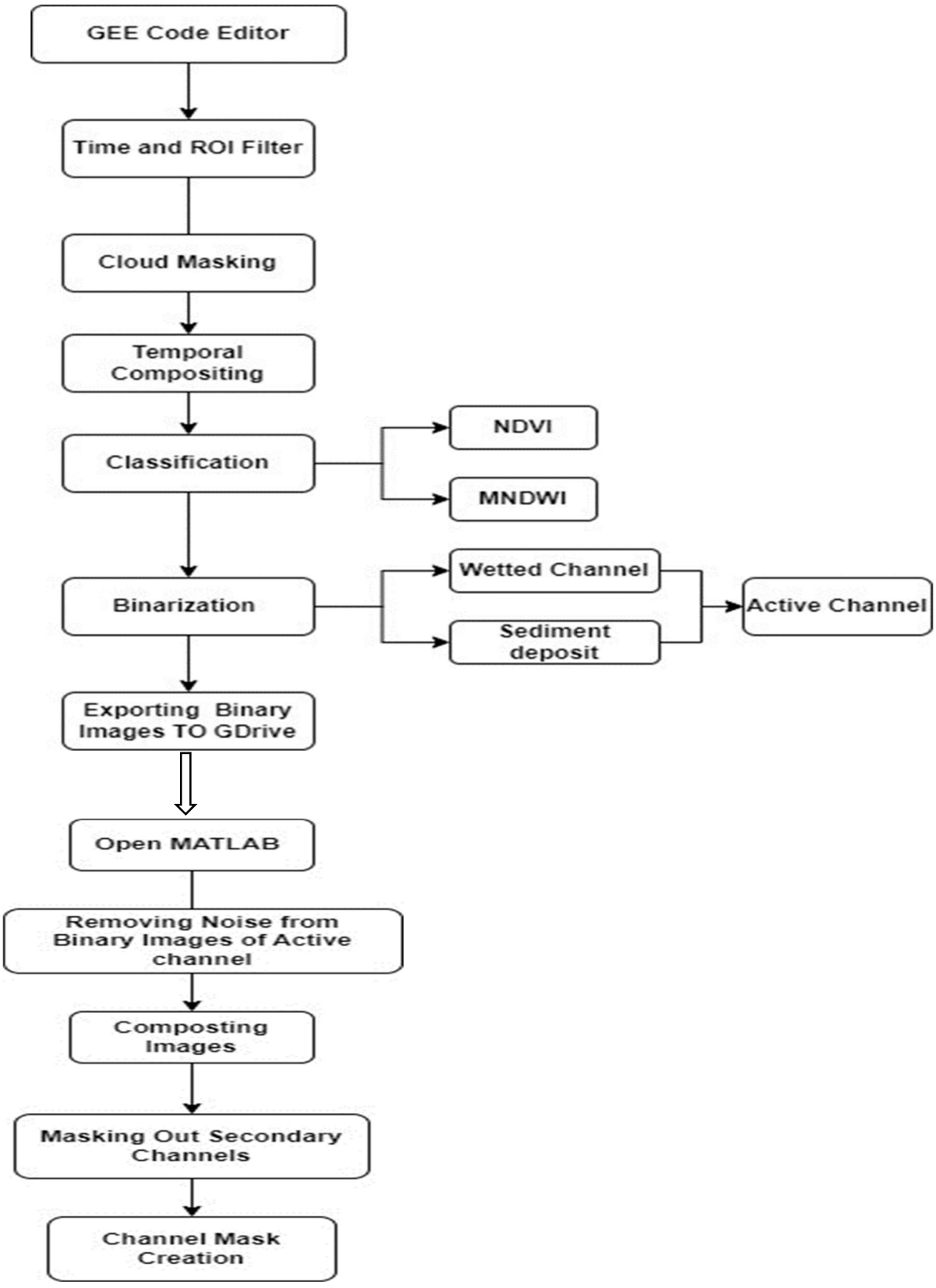

Figure 6. 3. Flow chart showing methodology used for generation of active channel masks in GEE.

Numerous automated and semi-automated tools in python or MATLAB programming languages for planform analysis exist, with the outputs from GEE ready to be used to derive planform statistics and quantify change. These tools will be used to derive planform statistics and quantify the changes. The developed active river channel masks for period 1988-2022 are processes in MATLAB to analyse river planform changes. In MATLAB, a semi-automated workflow is implemented to clean binary images of the active channel and mask out non-relevant features and secondary channels. The resulting hydraulically connected binary channel masks enable a focus solely on the primary channel for each annual composite. This approach provides a comprehensive view of the active channel's temporal changes and planform geometries. The steps followed are given below

- **Removing Noise from Binary Images of Active channel:** This involved the elimination of disconnected pixels that did not belong to the active channel.
- **Composting Images:**
- **Masking Out Secondary Channels:** The mean composite image was cleaned, and secondary channels, tributaries, and other non-relevant features were masked out from it.
- **Channel Mask Creation:** Hydraulically connected binary channel masks were generated from the cleaned composite images, focusing on the largest set of connected water and sediment pixels.

3.5 Flood Hazard Mapping

The Rainfall-Runoff-Inundation (RRI), a two-dimensional coupled hydrological and inundation model, which include three key components: a rainfall-runoff model, a river routing model, and a flood inundation model will be used develop the flood inundation map for the selected high flood events in the study as well as for 10-, 50- and 100-year return year flood at gauging site based on standard frequency analysis and unit hydrograph techniques. Further, the flood inundation results for the study area by RRI model will be compared with those obtained by the application of the HEC-RAS and HEC-HMS model. Brief methodology about modelling approach for flood inundation mapping is shown in Figure. 3.4.

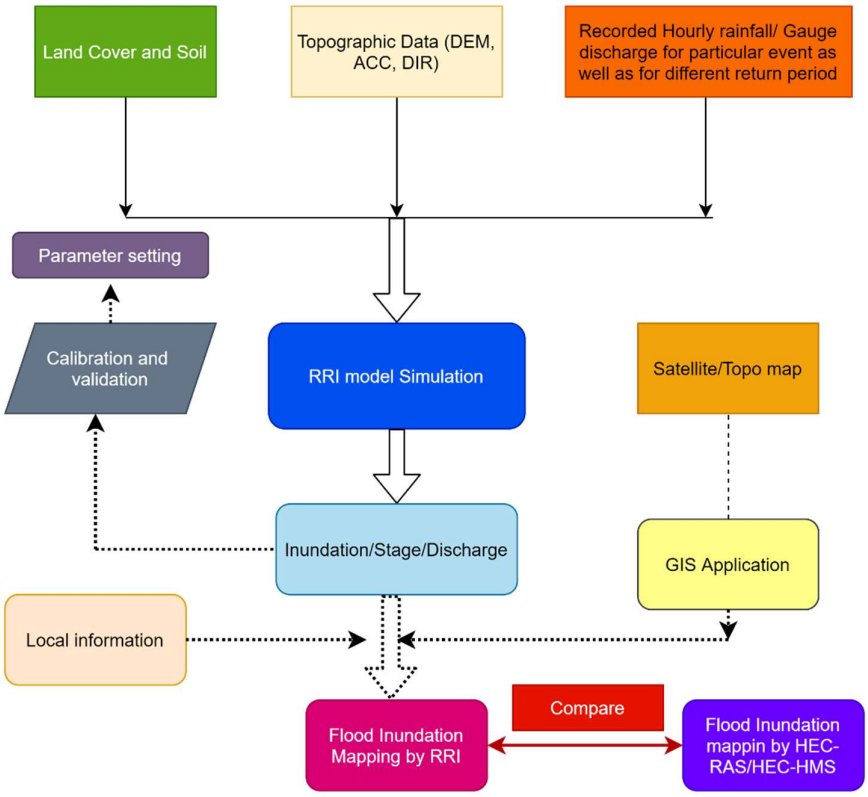

Figure 3.4. Schematic diagram of hydrodynamic modelling approach of flood inundation mapping

CHAPTER - 4
RESULTS AND DISCUSSIONS

4.1 Geomorphic Mapping of Tawi Basin

Based on the digital elevation model (Figure 3.1) and following the methodology presented in section 3.3 an attempt has been made to develop geomorphology map for the Tawi River Basin. In order to generate geomorphology map, the number of maps are produced which includes Topographic roughness index (TRI), Topographic position index (TPI), Normalized height, Hill height, Valley depth, Elevation, Slope map, Normalized Difference Water Index (NDWI) and Stream Order map. The detailed information about this produced maps is presented as follows:

a) **Topographic roughness index (TRI) map**: The TRI index measures how much elevation varies between various landform units. It aids in determining the terrain's heterogeneity or abrasiveness. The TRI map is presented in Figure 4.1 which emphasizing the elevation changes throughout the basin.

b) **Topographic position index (TPI) map**: TPI map helps to study area's ridges and depressions' spatial distribution. The proportional depth of depressions is not mentioned, only their location and that of these characteristics. Additionally, TPI aids in locating the drainage pattern within various landform units. The TPI map is presented in Figure 4.2, which shows locations where the ridges and depressions are distributed.

c) **Normalized height map**: This indicator helps to distinguish the alluvial plain itself from the outer edge of the piedmont alluvial plain. Additionally, it highlights the basin's peaks and valleys. The normalized height map, which emphasizes these features is presented in Figure 4.3.

d) **Hill height map**: The hill height index emphasizes the basin's ridges in particular. It makes it easier to spot elevated terrain and distinctive hill characteristics. The hill height map is presented in Figure 4.4, highlighting the ridges.

e) **Valley depth map**: This measure concentrates on the basin's main valleys. It aids in locating main valleys and emphasizing how deep these troughs are. The valley depth map presented in Figure 4.5 shows the main valleys that are existing in the basin.

f) **Elevation map**: The mountains and other landform units are clearly separated by the elevation. It aids in separating elevated mountainous regions from nearby landforms. This boundary is shown on the elevation map in Figure 4.6.

g) **Slope map**: The DEM was used to create a slope map (Figure 4.7), which shows the slope gradient throughout the basin. Each landform unit's mean slope was calculated.

h) **Normalized Difference Water Index (NDWI)**: The Sentinel-2 datasets was used to create a water index map. This map (Figure 4.8) is used to create the active flood plain of the basin.

i) **Stream Order** map: Stream order and the drainage pattern (Figure 4.9) offer insights into the influence of slope, lithology, and structural controls on the drainage basin.

With the use of these many DEM derivatives, it is possible to analyse and comprehend the Tawi river basin's landforms, terrain abrasiveness, drainage patterns, and other significant elements.

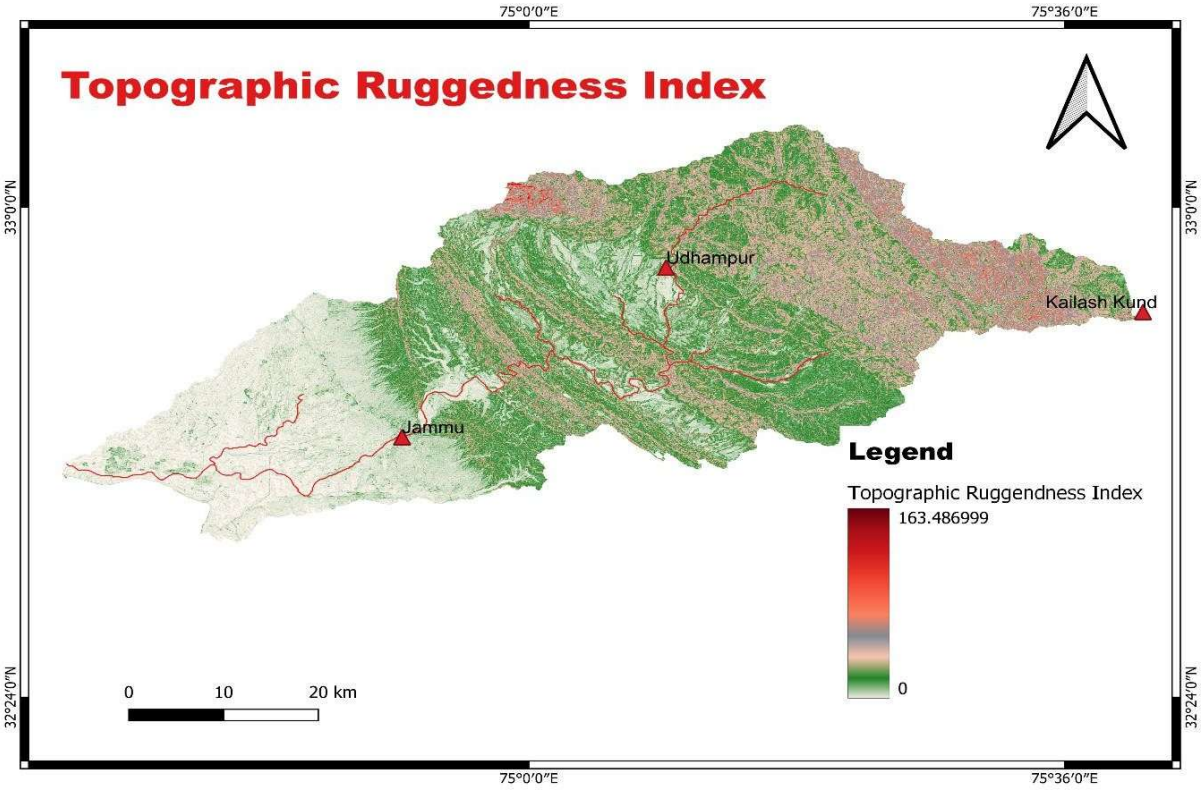

Figure 4.1. Topographic ruggedness index map of Tawi basin.

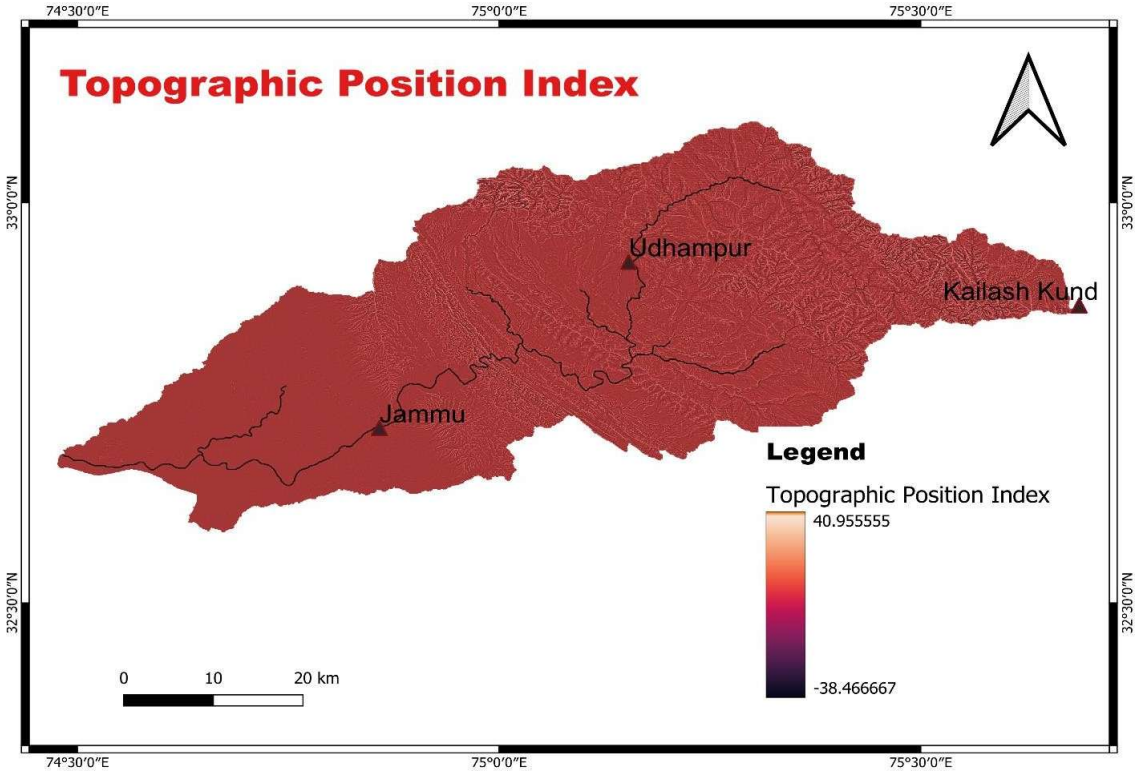

Figure 4.2. Topographic position index map of Tawi basin.

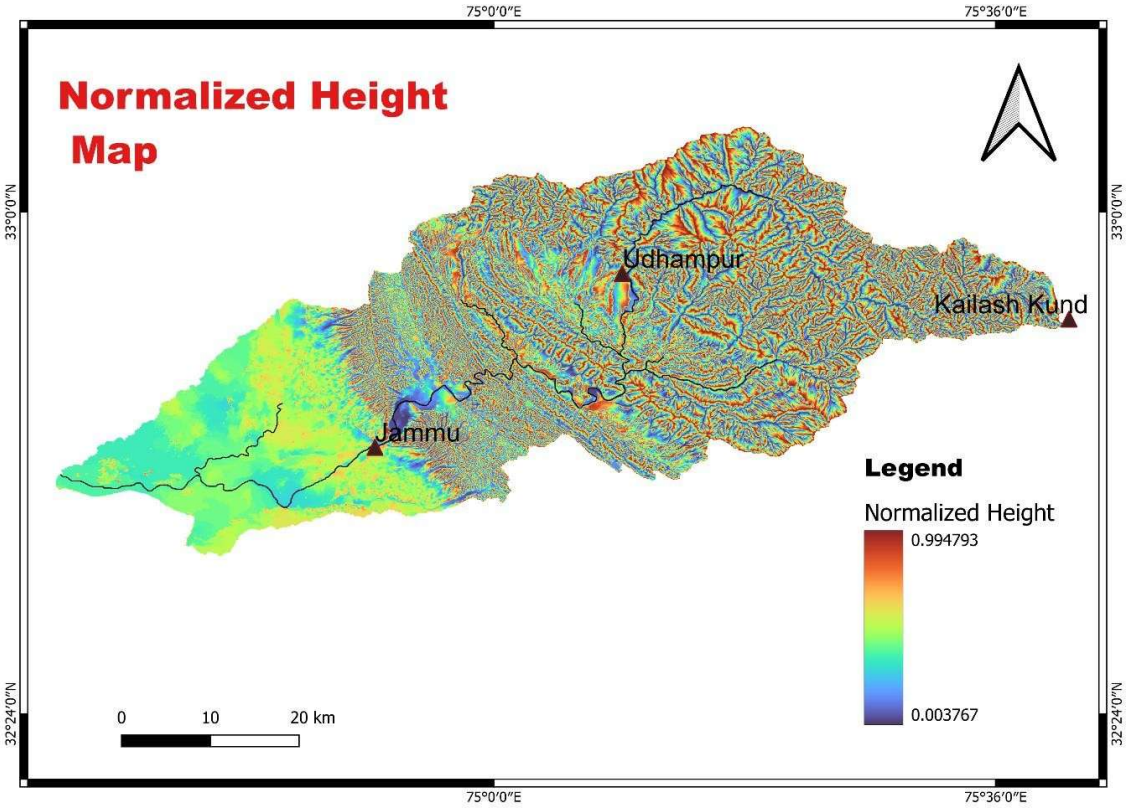

Figure 4.3. Normalized height map of Tawi basin.

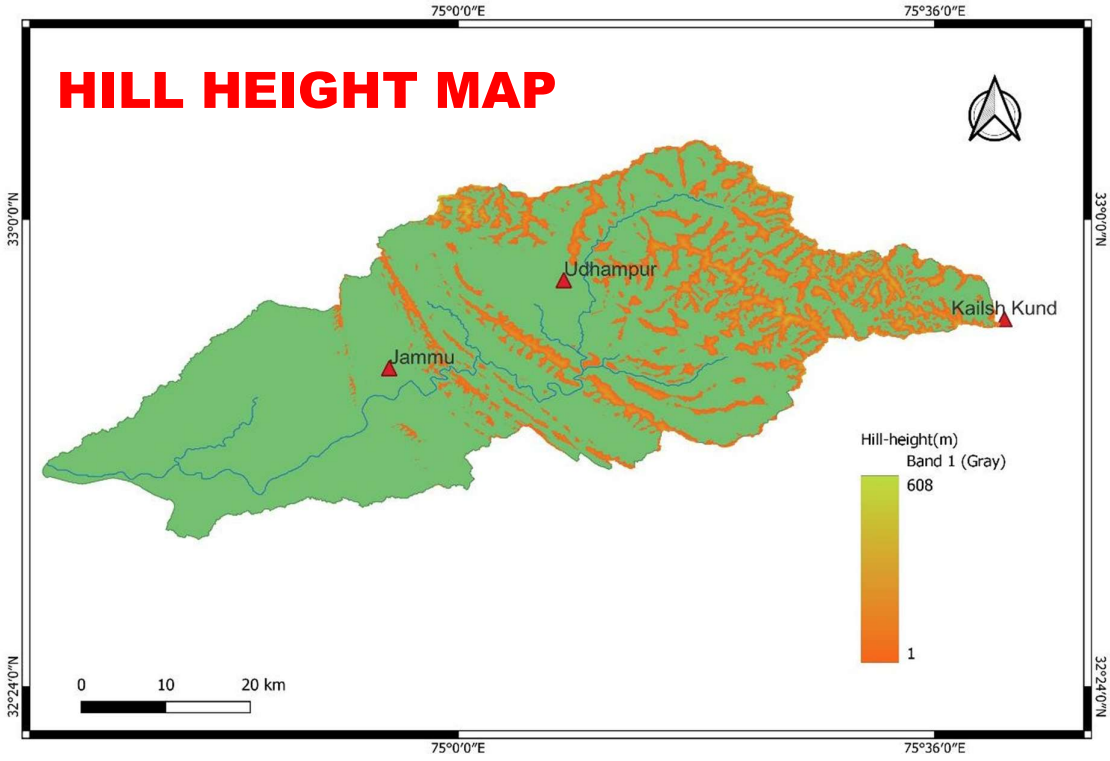

Figure 4.4. Hill height map of Tawi basin.

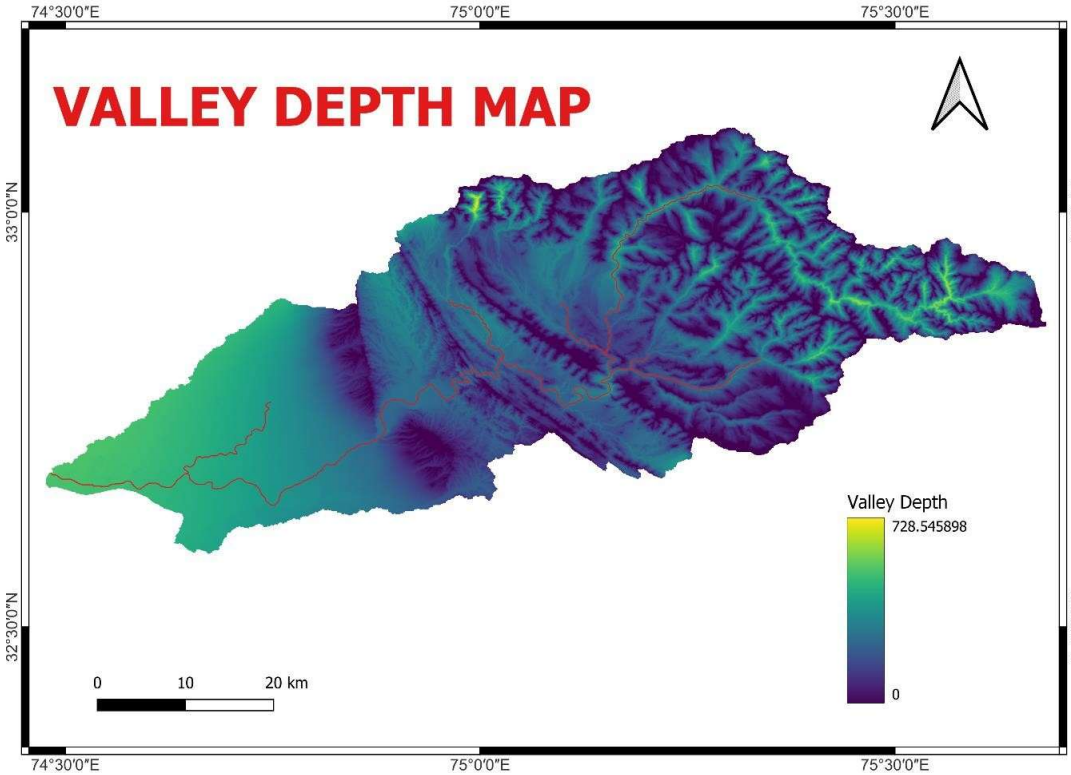

Figure 4.5. Valley depth map of Tawi basin.

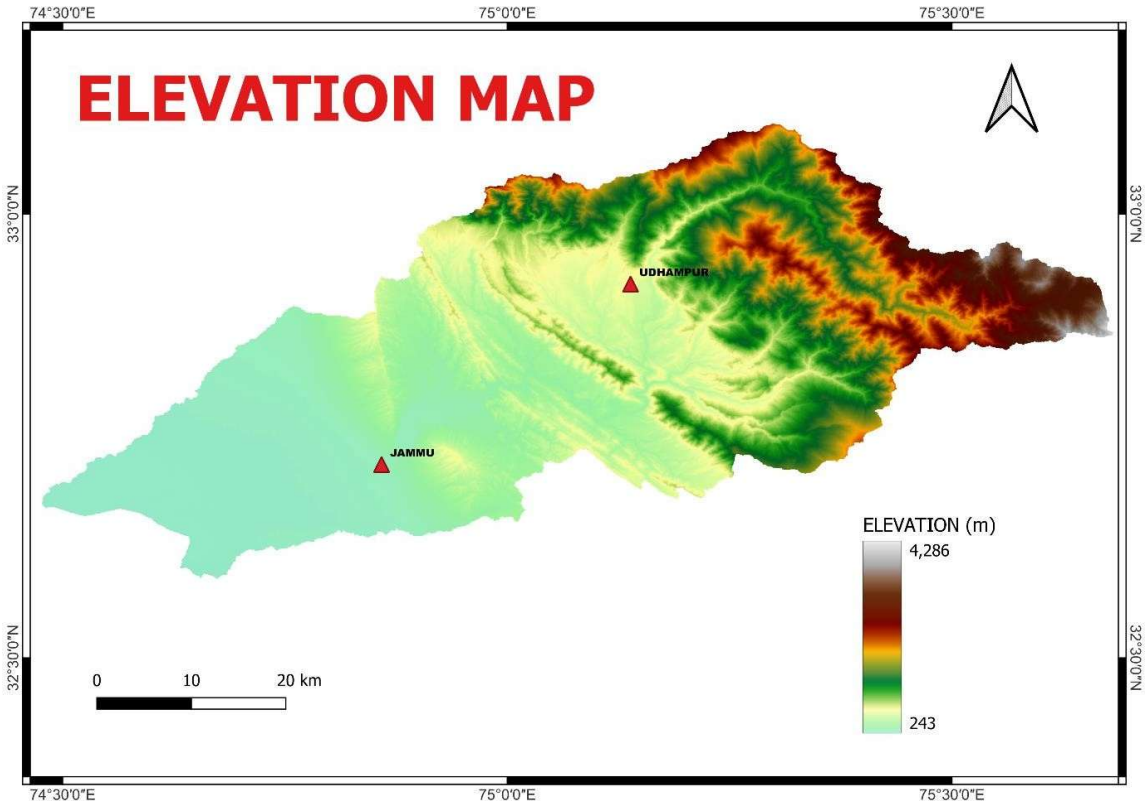

Figure 4.6. Elevation map of Tawi basin.

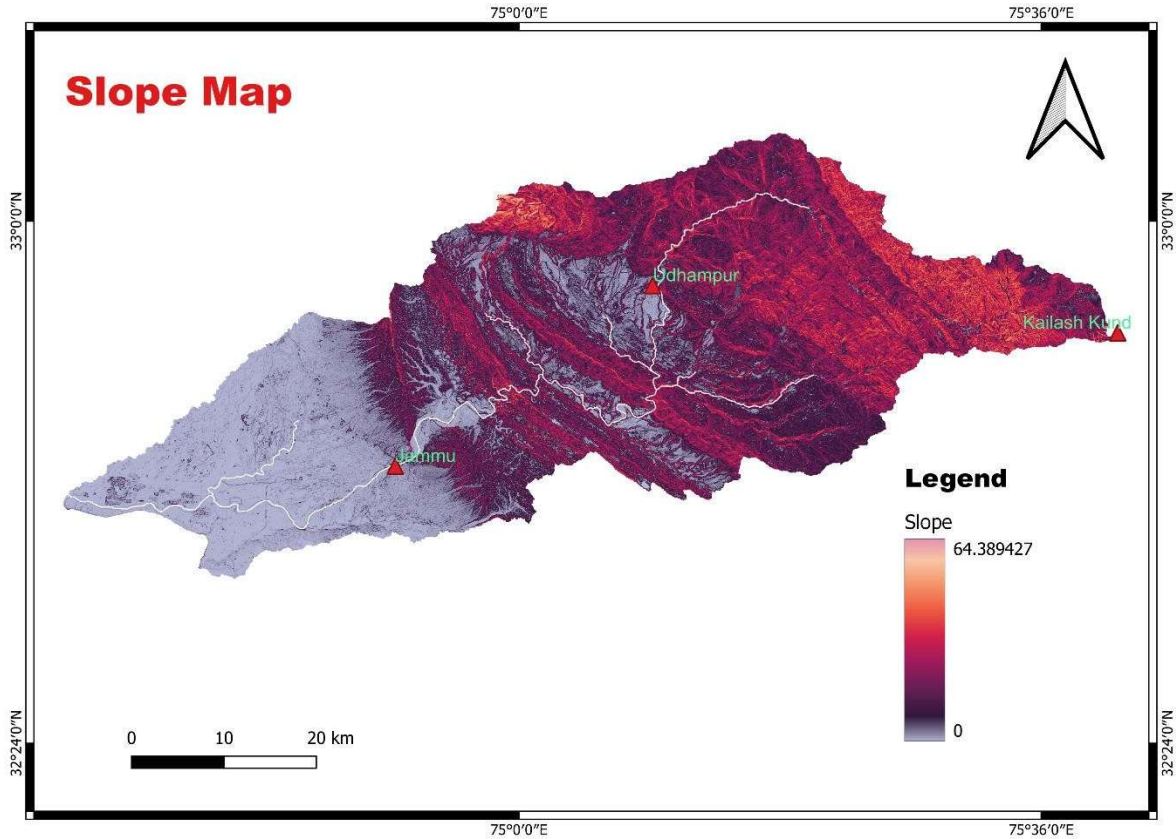

Figure 4.7. Slope map of Tawi basin.

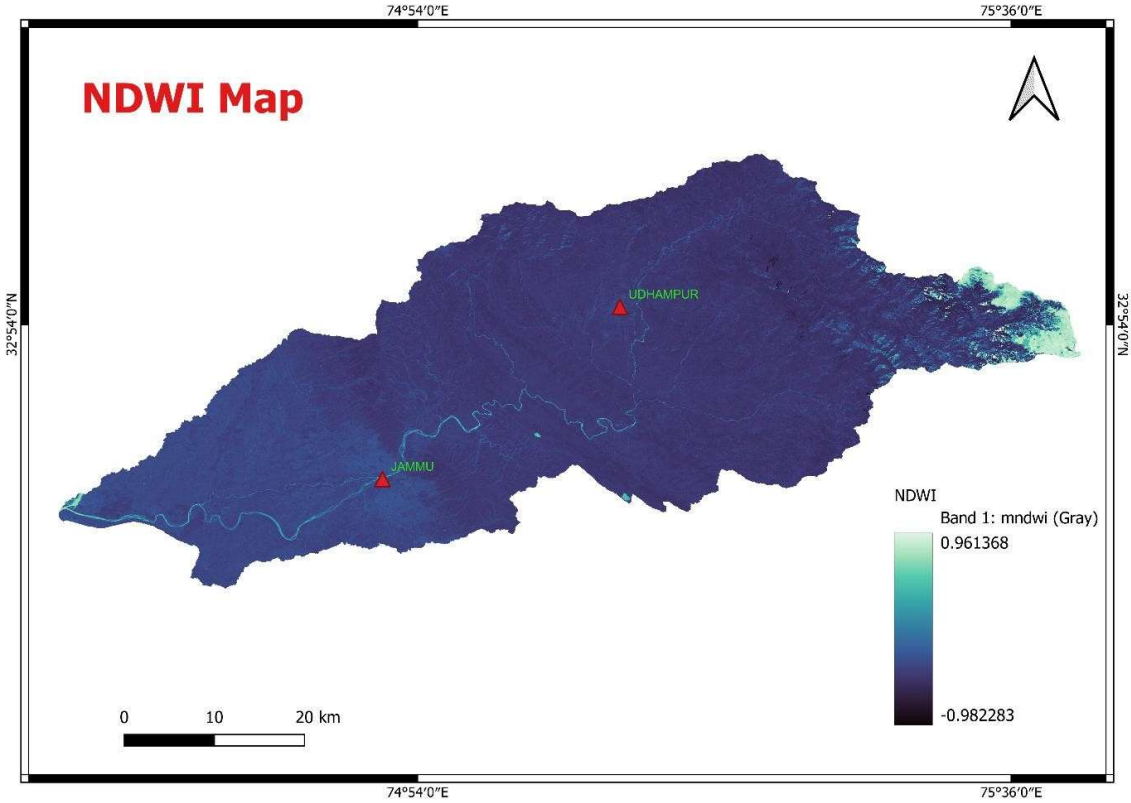

Figure 4.8. NDWI Map of Tawi basin.

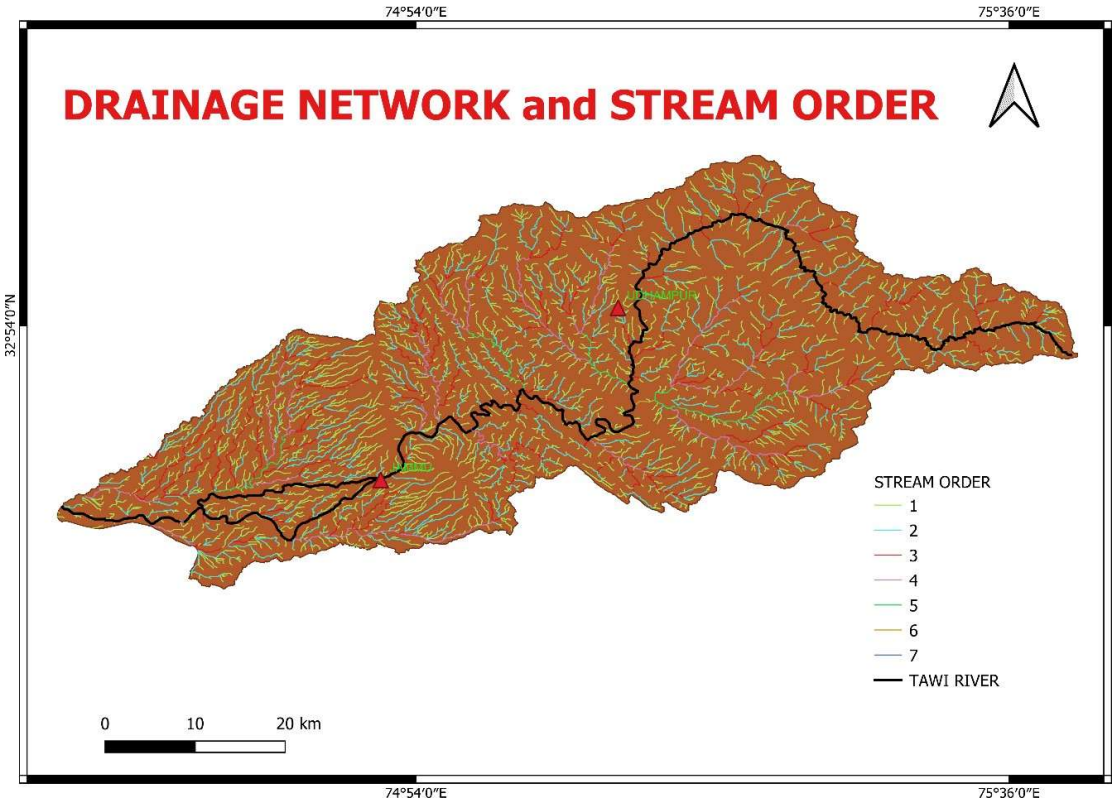

Figure 4.9. Drainage network and stream order of Tawi basin.

The maps presented in the above sections are used to generate the geomorphological map of the Tawi Basin. The generated geomorphological map of the Tawi basin is presented in the Figure 4.10.

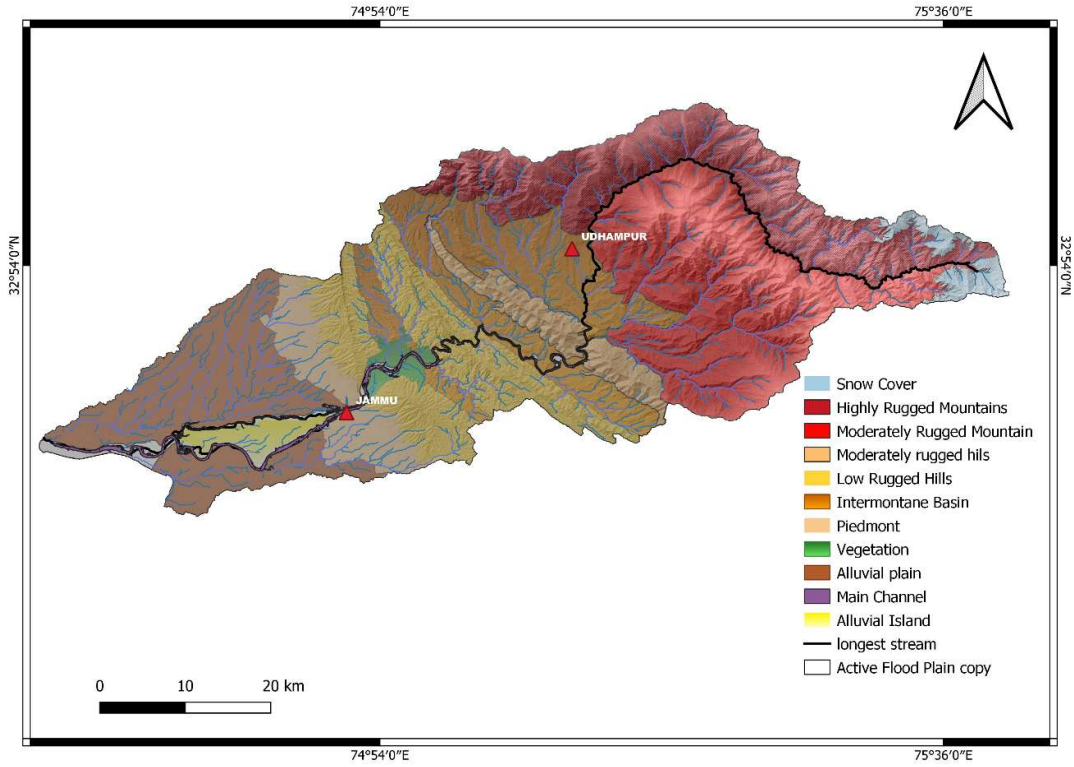

Figure 4.10. Geomorphological map of Tawi basin.

Based on the geomorphological map depicted in Figure 4.10, it can be seen that Tawi river basin exhibits seven major types of landforms units. Each landform units is characterized by distinct topographic and geomorphic features. The description of these landform units is presented as follows:

1. **Highly rugged mountain (HRM)**: This landform unit represents areas with very steep and rugged mountains, indicating high elevation and significant relief. The HRM unit is characterized by steep slopes and high elevations, with a mean elevation of approximately 1861.75 meters. The average slope gradient is around 24 degrees, indicating a challenging terrain. The topographic ruggedness index (TRI) for this unit is relatively high, with a mean TRI of 36.64. The drainage pattern in this unit is parallel, resulting from the steepslope gradient.

2. **Moderately rugged mountain (MRM):** This landform unit refers to areas with moderately steep and rugged mountains, indicating a lower elevation and relatively less pronounced relief compared to HRM. The MRM unit has a mean elevation of 1500 meters and an average slope gradient of 20.29 degrees. The drainage pattern in this unit is also parallel but with lesser drainage density compared to HRM. The drainage channels tend to bend at a 90-degree angle, suggesting a major structural control influencing their course. The mean TRI for this unit is 29.82, indicatinga moderate level of topographic heterogeneity.

3. **Moderately rugged hills (MRH)**: This landform unit comprises areas with hills that exhibit a moderate degree of steepness and ruggedness. These hills are less elevated and have a gentle relief compared to MRM. The MRH unit has a mean elevation of 836 meters and a mean TRI of approximately 28.348. The drainage pattern in this unit is dendritic, characterized by a network of branching channels.The mean slope gradient is relatively high at 19.60 degrees, contributing to the moderate ruggedness of the hills. A prominent ridge runs parallel to the strike of the hill. The Tawi riverexits from the high mountain region, known as the Tear Fault.

4. **Low rugged hills (LRH)**: This landform unit represents areas with relatively low and gently sloping hills. LRH has a smoother relief compared to MRH. The LRH unit is characterized by low elevations, with a mean of 382.67 meters, and a mean slope gradient of 14.840 degrees. The mean TRI for this unit is approximately 21.715. The drainage pattern in this unit is trellis or radial, indicating tectonic control over the formation ofthe drainage network.

5. **Intermontane basin (IB):** This landform unit refers to basins or depressions situated betweenmountain ranges. These areas are characterized by relatively flat terrain surrounded by higher elevations. The IB unit comprises valleys situated between two mountain ranges. It has a relatively flat terrain, with a mean elevation of 608 meters and a mean slope gradient of 8.514 degrees. The mean TRI for this unit is 13.17, indicating moderate topographic heterogeneity. The drainage pattern in this unit is dendritic or sub-parallel, reflecting structural control.

6. **Piedmont (PD):** This landform unit represents the foothills or transitional zone between themountains and plains. It consists of gently sloping terrain at the base of the mountains. The PD unit is characterized by a major break in slope at the foothills

of the mountains. It hasa mean elevation of 293.5 meters and a mean slope gradient of 2.649 degrees. The TRI for thisunit is very low, with a mean of approximately 2.649. The drainage pattern is sub-parallel, with streams following the slope gradient.

7. **Alluvial plains (AP):** This landform unit comprises flat and low-lying areas formed by the deposition of sediment carried by rivers. AP is characterized by fertile soil and is often found along riverbanks. The AP unit consists of flat plains with a low slope gradient of approximately 0.988 degrees. The drainage pattern in this unit is sub-dendritic, with braided channels. The mean TRI for thisunit is 2.19, indicating relatively low topographic heterogeneity.

These landform units provide a classification framework for understanding and studying the topography and geomorphology of the Tawi river basin. From this discussion, it can be concluded that the Tawi river basin exhibits diverse landform units, ranging from highly rugged mountains to alluvial plains. The topographic characteristics, slope gradients, drainage patterns, and topographic heterogeneity vary across these units, providing valuable insights into the geomorphological processes and landscape evolution of the basin.

4.2 River Planform Analysis

In order to do analysis of the river planform changes over longer time period number of processes like extraction of active channel from satellite imagery, composite images and extraction of mask from composite images need to be accomplished. These processes are completed using GEE and MATLAB software. The area of interest (AOI) considered for this study is depicted in Figure 4.11.

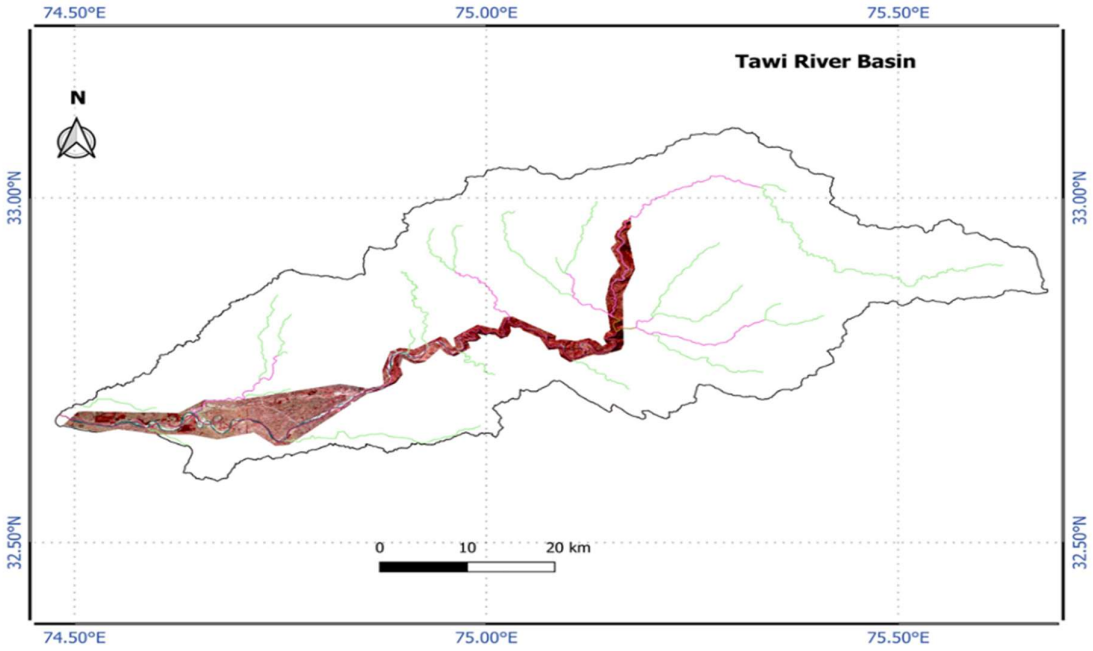

Figure 4.11. The area of interest (AOI) considered for extraction of active channels of the Tawi basin.

4.2.1 Active Channel from Landsat Imagery

In this study, Landsat imagery available in Google Earth Engine was utilized to analyze and classify the active channel, encompassing water and exposed sediment, over a span of 34 years from 1988 to 2022. The Landsat satellites employed in this analysis included Landsat 5 (LT05), Landsat 7 (LE07), and Landsat 8 (LC08). Leveraging the multispectral data captured by these satellites, with a spatial resolution of 30 meters, enabled the characterization of diverse features within the riverscape. To execute the analysis, a step-by-step approach was followed. The region of interest (ROI) was defined through the specification of a geometry or the upload of a shapefile within Google Earth Engine. This allowed for focused examination and assessment of changes in the active channel specific to the chosen area. The start and end dates were set to cover the desired 34-year timeframe from October 1st to April 30th each year. By filtering the Landsat image collection based on these dates, a comprehensive dataset was obtained, allowing for the exploration of the temporal dynamics of the active channel during the dry season. The choice of October 1st to April 30th as the study period aligns with the dry season, which is often characterized by reduced water flow and lower water levels. This period provides a clearer view of the channel morphology and facilitates the identification of channel features and patterns, as well as exposed sediment. The reduced water flow during this period

enhances the visibility and allows for a more accurate analysis of the active channel. Landsat 7 experienced a significant issue with its SLC (Scan Line Corrector) in May, 2003, which resulted in the loss of data in every alternate scan line. These missing scan lines caused diagonal gaps or stripes in the acquired images, reducing their overall quality and usability for certain applications. In the GEE code snippet, a filter was applied to exclude Landsat 7 images within the specified time range that were affected by the SLC failure. In this study, the modified normalized difference water index (MNDWI) proposed by Xu (2006) was chosen to map surface water and identify the wetted channel position. The MNDWI is computed as follows:

$$MNDWI = (G - SWIR1) / (G + SWIR1) \quad (4.1)$$

Here, G and SWIR1 represent the green and shortwave infrared bands, respectively. The resulting MNDWI values range from -1 to 1, with more positive values indicating the presence of water. This approach generated 30-meter resolution water maps by applying the constant threshold to annual temporal composite images, resulting in binary water masks.

In addition to MNDWI, the normalized difference vegetation index (NDVI), first introduced by Rouse et al. (1974), was used to produce proxy maps for live green vegetation (Figure 4E). NDVI is commonly employed for vegetation monitoring (Dzubáková et al., 2015) and is computed as follows:

$$NDVI = (NIR - R) / (NIR + R) \quad (4.2)$$

Here, NIR represents the near-infrared band, and R denotes the red band. Higher NDVI values indicate healthier and more abundant vegetation.

By utilizing both MNDWI and NDVI, the study was able to analyze surface water distribution and the presence of live green vegetation along the fluvial reach, enabling a comprehensive understanding of the dynamic interactions between water bodies and vegetation in the study area. To enhance accuracy and reliability, cloud-masking techniques were applied to exclude pixels affected by cloud cover during the analysis. Additionally, the code performed compositing of cloud-free pixels within the defined date range, generating an average image that facilitated the visualization of the active channel and its temporal transformations. The output of the analysis comprised water classification, exposed sediment classification, and a composite classification representing the active channel, which encompasses both water and

exposed sediment. These classifications were visually displayed on the map interface, offering a comprehensive understanding of the spatial distribution and temporal variations of the active channel within the ROI. (Boothroyd et al., 2021)

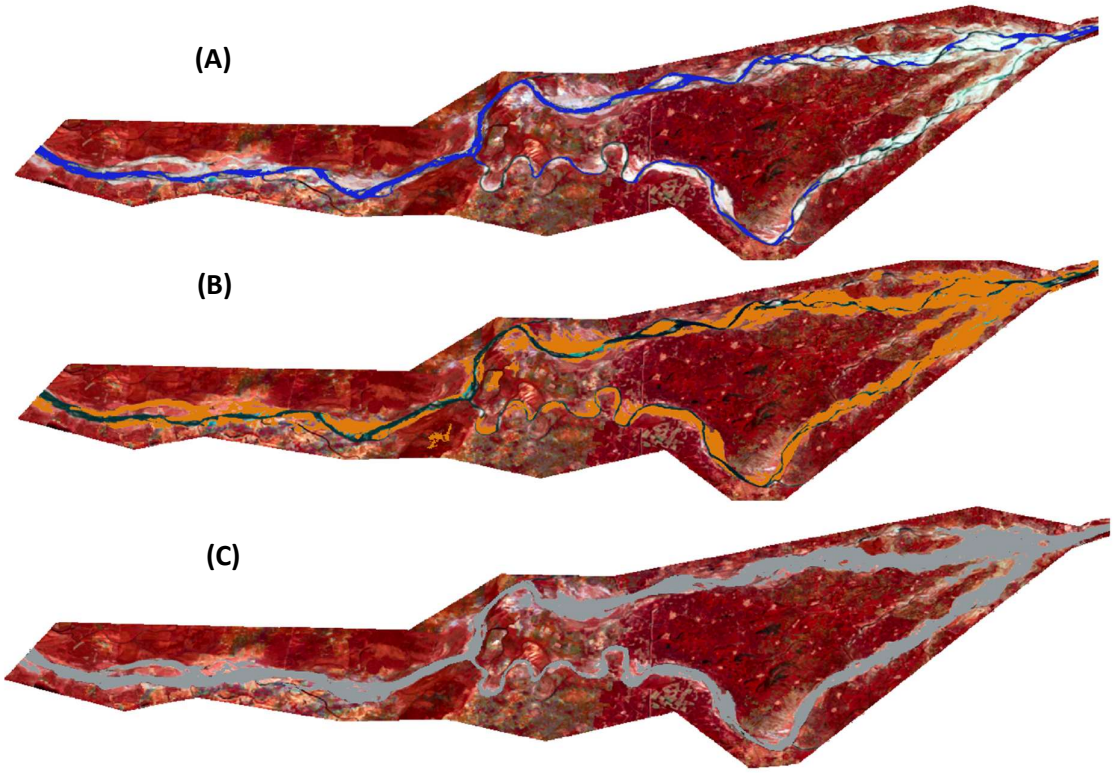

Figure 4.12. Channel Characteristics (A) Wetted Channel (blue colour), (B) Sediment Deposits (orange colour) and (C) Active Channel (Gray colour).

In addition to the analysis conducted within Google Earth Engine, the binary images of the classified active channel were downloaded and further processed using MATLAB. The use of MATLAB allowed for additional analysis and manipulation of the binary images, enabling more advanced statistical or spatial analysis techniques.

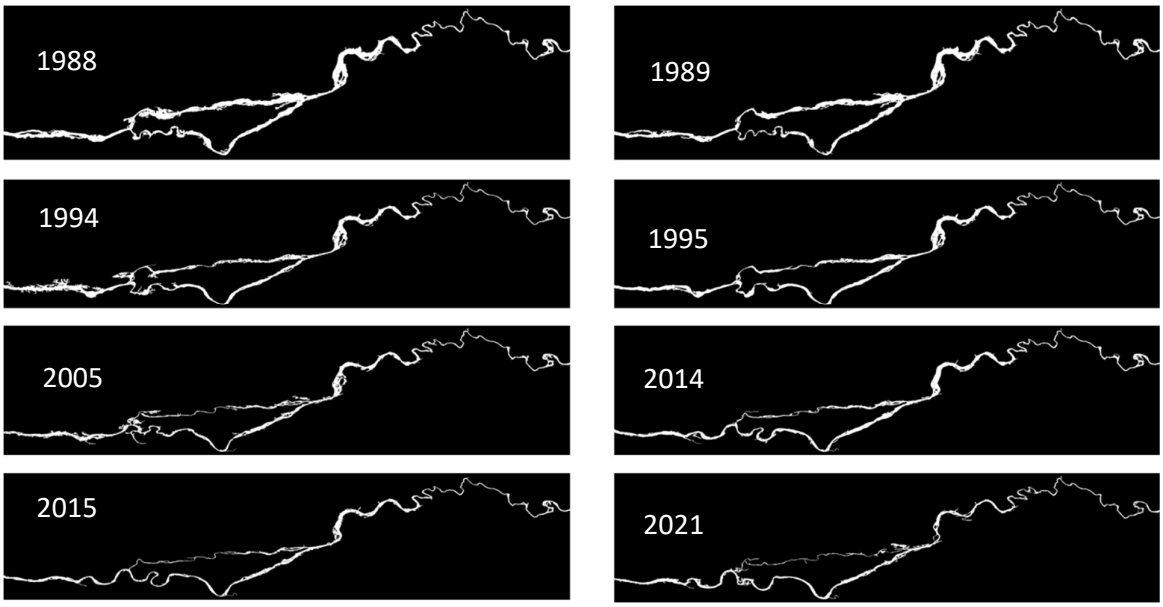

Figure 4.13. Active channel binary images downloaded from GEE.

4.2.2 Compositing Images

Prior to generating the annual composite images, noise removal was performed on the 34 individual images. This involved the elimination of disconnected pixels that did not belong to the active channel. By removing these isolated and misclassified pixels, the accuracy of the subsequent analysis was enhanced. The annual composite images were created by combining carefully selected and classified images for each year. This approach ensured that the composite images represented the most accurate and representative depiction of the river system over time. By combining the images, the temporal dynamics of the active channel were captured, allowing for a comprehensive analysis of its changes and patterns. (Schwenk et al. 2017).

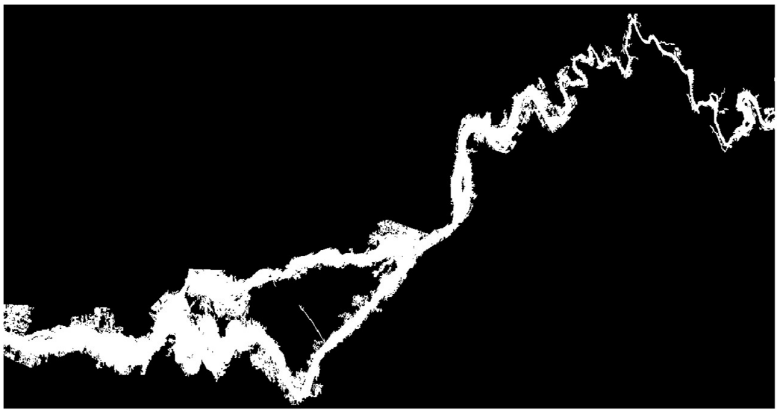

Figure 4.14. Mean Composite Image.

4.2.3 Creating Channel Masks from Composite Images

In order to create channel masks from annual composite images, a manual cleaning process is undertaken to remove all connected components not hydraulically connected to the river, such as tributaries, and cutoff remnants. Additionally, any noise resulting from errant classifications is eliminated where it intersects with the channel body. The cleaned composites are then used to generate hydraulically connected binary channel masks by selecting the largest set of connected water and sediment pixels. These masks serve as representations of the main channel and are crucial for calculating planform statistics such as migration rate, width, radius of curvature, and channel direction, often requiring a well-defined centerline to be extracted from the masks. The resulting channel masks and derived planform statistics contribute to a comprehensive understanding of river dynamics and are essential for accurate reporting and analysis.

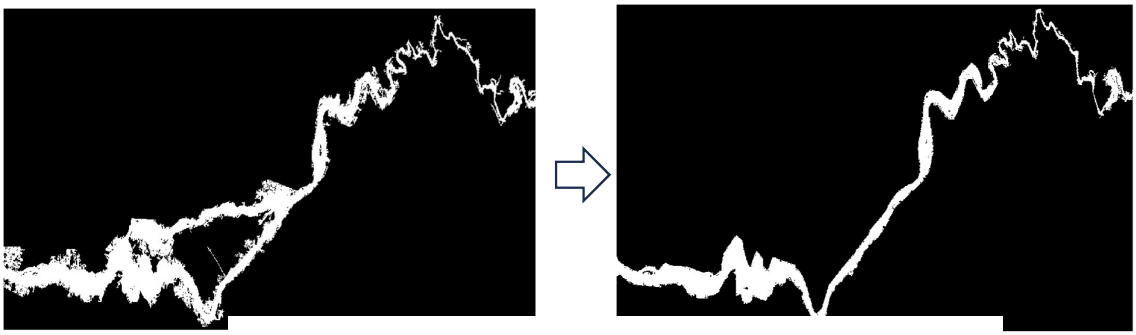

Figure 4.15. (a) Mean Composite Image and (b) Cleaned mask image.

The work on the analysis of Tawi river planform is presently under progress which will be completed in near future. Further, the task of hydraulic modelling in the Tawi basin to generate flood inundation map in the Tawi basin will be undertaken.

5.1 Centreline Change

The centerline is a crucial metric for quantifying changes in the river's course and extent over time. Figure 5.1 illustrates the centerlines of the Tawi River from 1988 to 2021, providing valuable insights into the evolution of meandering dynamics and morphological changes during this period. Notably, the Tawi River exhibits significantly greater curvature and expansion in its downstream section, with approximately 18 km of this section undergoing more pronounced changes, including expansion and meandering.

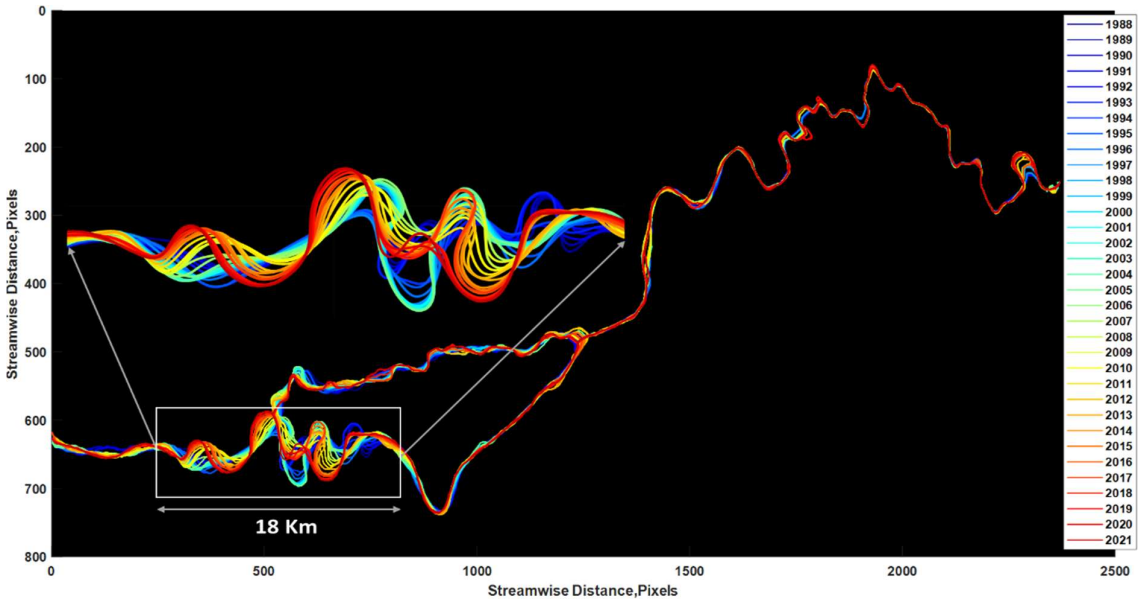

Figure 4.16. Centerline Evolution of Tawi River Reach from 1988 to 2021.

The centerline length of Tawi River's reach 1 from the figure 5.2. shows significant fluctuations over the years from 1988 to 2021. The maximum length observed was 19.61 km, while the minimum was 16.96 km. Initially, the Centerline Length remained relatively stable with minor variations, such as 17.22 km, 17.08 km, and 17.02 km, indicating a slight fluctuation around the 17 km mark. The values oscillated within a close range from 16.96 km to 17.42 km during this early period. A more significant rise begins around the midpoint of the dataset, with lengths reaching 17.42 km, 17.40 km, and a steady increase leading to values like 18.30 km, 18.50 km, and 18.38 km. The last segment of the dataset shows the most pronounced changes, with CI Lengths peaking at 18.90 km, 18.77 km, and reaching the maximum of 19.61 km.

Over the span of 34 years, the Centerline Length in reach 2 (Wadi Tawi) exhibited subtle yet significant variations. Initially, from 1988 to 1994, the Centerline Length remained relatively stable, hovering around 26.6 kilometers, as shown in figure

3a. Notable values include 26.63 kilometers in 1988 and 26.67 kilometers in 1990.

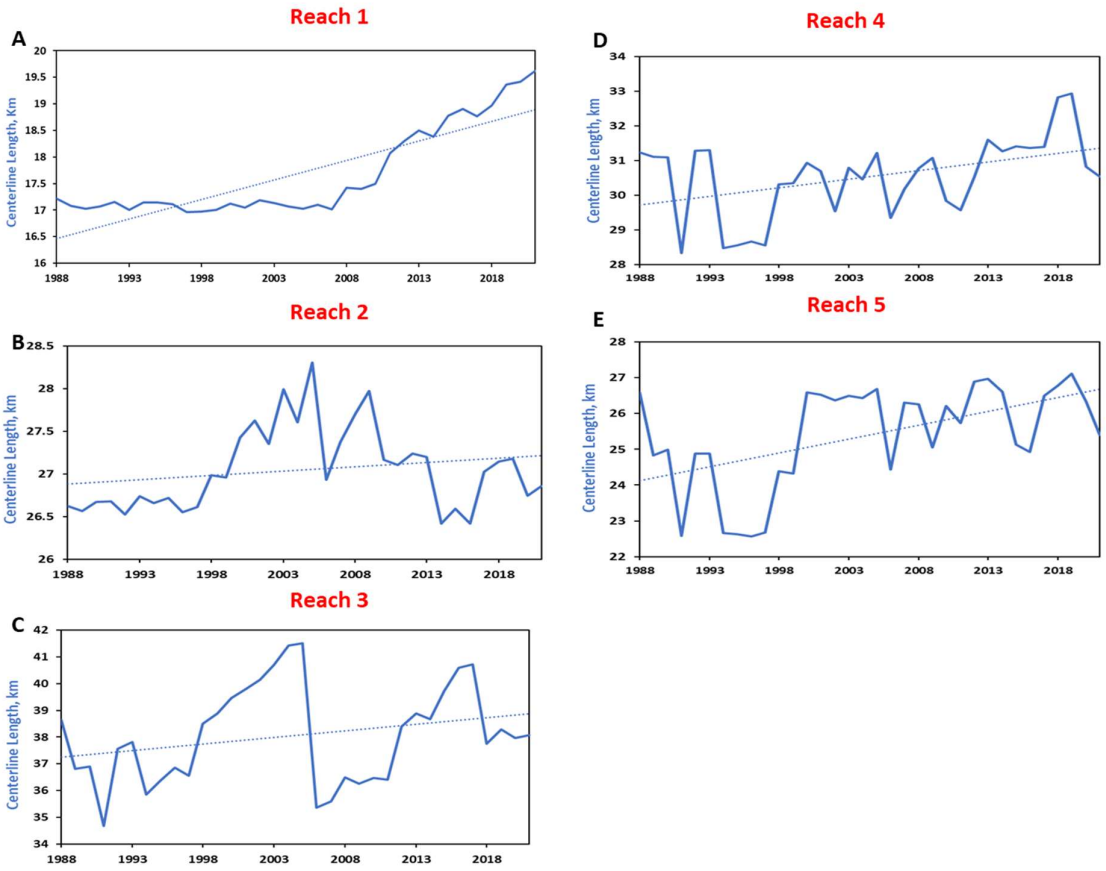

Figure 4.17. Fluctuations in river reach lengths for five reaches of the Tawi River over 34 years, showing varying stability and changes. Reach 1 and Reach 5 exhibit significant fluctuations (A-E).

Subsequently, from 1995 to 2004, more pronounced changes occurred. The Centerline Length reached a minimum of 26.55 kilometers in 1996 and then rose to 26.99 kilometers by 1998. During the early 2000s, there was an overall increasing trend, peaking at 27.42 kilometers in 2000. This expansion phase could be attributed to sediment deposition or meander migration. However, in 2005, the Length reached its highest value of 28.31 kilometers. Interestingly, the subsequent year (2006) saw a contraction to 26.93 kilometers. From 2016 to 2021, the CI Length fluctuated within a narrower range, with values ranging from 26.42 to 26.86 kilometers.

The centerline length in reach 3 (Nikki Tawi) of Tawi River exhibited subtle yet significant variations. Initially, from 1988 to 1994, the Centerline Length remained relatively stable, hovering around 36.8 kilometers. Notable values include 36.81 kilometers in 1989 and

36.67 kilometers in 1991. Subsequently, from 1995 to 2004, more pronounced changes occurred. The Cl Length reached a minimum of 35.36 kilometers in 2006 and then rose to 41.43 kilometers by 2004. During the early 2000s, there was an overall increasing trend, peaking at 41.52 kilometers in 2005. This expansion phase could be attributed to sediment deposition or meander migration. However, in 2005, the Cl Length reached its highest value of 41.52 kilometers. Interestingly, the subsequent years (2006-2015) saw a contraction, with the Cl Length decreasing to 39.73 kilometers by 2015. From 2016 to 2021, the Length fluctuated within a narrower range, with values ranging from 37.96 to 38.06 kilometers.

The centerline length in reach 4 of Tawi River has exhibited intriguing variations over the years. Initially, in 1988, it measured approximately 31.24 kilometers. Subsequent years witnessed fluctuations, with a significant drop to around 28.34 kilometers in 1991. However, from 2016 to 2019, the Centerline Length increased, reaching its peak at nearly 32.93 kilometers in 2019. By 2021, it decreased again to about 30.54 kilometers. Furthermore, the Centerline Length of Tawi River's reach 5 exhibited dynamic changes. From 1988 to 1994, the Centerline Length remained relatively stable, with minor variations around 26.59 km in 1988 and 24.98 km in 1990. Subsequently, between 1995 and 2004, more significant fluctuations occurred, reaching a minimum of 22.57 km in 1996 and rising to 26.69 km by 2005. The early 2000s saw an overall increasing trend, culminating in the highest recorded Centerline Length of 26.98 km in 2012. However, from 2016 to 2021, there was a decreasing trend, ranging from 24.92 km to 25.41 km.

5.2. Dynamics of River Width

This section presents an analysis of the average width of the Tawi River across five different reaches over a period spanning from 1988 to 2021 (Fig.5.3). The average width of a river is a critical parameter that helps in understanding river dynamics, sediment transport, and potential flood risks.

Reach 1 of the Tawi River exhibits considerable fluctuations in its average width over the study period. The width ranges from a high of 685.9 meters in 1991 to a low of 278.6 meters in 2012. The early years show significant variability, with noticeable peaks in 1991 and 1992. Post-2000, the width generally trends downward, reaching its lowest in 2012, followed by

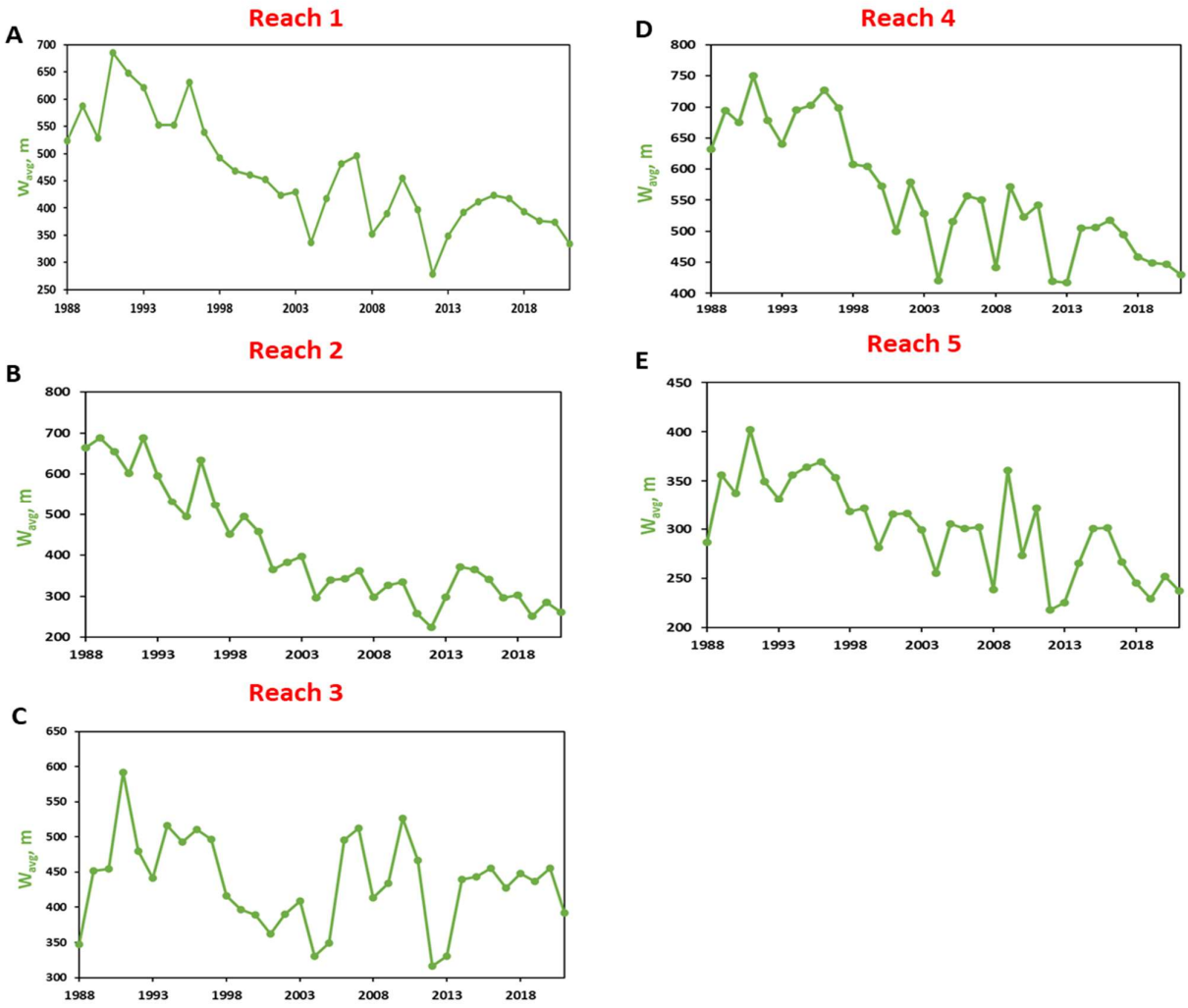

Figure 4.18. Variation of river width along different reaches of Tawi River from 1988-2021 (A-E).

minor fluctuations in subsequent years. The average width of Reach 2 (Wadi Tawi) also demonstrates variability, with a peak of 689.1 meters in 1989 and a notable low of 223.5 meters in 2012. The width in this reach shows a general decreasing trend after 1992, with occasional increases, such as in 1996 and 2014. The significant drop in 2012 mirrors the trend observed in Reach 1, indicating a possible broader environmental or climatic event affecting multiple reaches of the river.

Reach 3's (Nikki Tawi) average width ranges from a high of 591.4 meters in 1991 to a low of 258 meters in 2011. The data shows an initial period of variability, with substantial width in the early 1990s, followed by a decreasing trend. Post-2000, the width continues to fluctuate but generally trends downward, reflecting a similar pattern to Reaches 1 and 2. Reach 4 shows significant variation in its average width, peaking at 750.6 meters in 1991 and dropping to a low of 417.6 meters in 2013. The early years of the dataset exhibit large widths, particularly in the early 1990s. After the year 2000, the width shows a decreasing trend with some recovery in certain years.

Reach 5, similar to the other reaches, exhibits fluctuations in its average width, ranging from a high of 402.4 meters in 1991 to a low of 218.4 meters in 2012. The early period shows considerable variability, with a general downward trend after 1991. The width reaches its minimum in 2012, followed by modest increases and subsequent fluctuations. This reach's pattern aligns with the broader trends observed across the other reaches, indicating interconnected factors influencing the river's morphology.

5.3 Migration Rate Due to Accretion and Erosion

Figure 5.4 presents an overview of the migration rates of the Tawi River's Reaches, focusing on migration due to accretion (Mra) and erosion (Mre) measured in meters per year (m/year). Understanding the migration rates of a river is crucial for assessing its dynamic behavior, predicting future changes in its course, and implementing effective river management strategies. This analysis covers the period from 1988 to 2021, providing insights into the factors influencing river migration.

The migration rate due to accretion (Mra) in Reach 1 of the Tawi River shows significant variability over the study period. The values range from a high of 132.2 m/year in 2007 to a low of 5.7 m/year in 1990. From 1988 to 2000, the rates display substantial fluctuations, with notable peaks in 1989 (89.0 m/year) and 1999 (93.4 m/year), indicating periods of significant sediment deposition, possibly due to high sediment load carried by the river during monsoon seasons or other hydrological events. Between 2001 and 2010, the accretion rates continue to vary, reaching the highest rate of the entire study period in 2007 (132.2 m/year), suggesting an exceptionally high sediment deposition during this year. In the period from 2011 to 2021, the rates are relatively lower compared to previous years, with some fluctuations and a significant low in 2012 (8.4 m/year). This overall trend may indicate changes in sediment supply, river discharge, or human interventions such as riverbank stabilization

efforts. The migration rate due to erosion (Mre) also displays significant variability, with values ranging from a high of 166.9 m/year in 1988 to a low of 5.9 m/year in 2007. From 1988 to 2000, the erosion rates show considerable variability, with a notable high in 1988 (166.9 m/year) and a significant low in 1990 (33.2 m/year). This variability reflects the dynamic nature of the river's erosional processes, influenced by factors such as river discharge, sediment load, and bank material composition. Between 2001 and 2010, the decade exhibits both high and low erosion rates, with the highest rate observed in 2004 (100.5 m/year), indicating a period of intense riverbank erosion. This could be due to extreme weather events, changes in river flow patterns, or human activities that destabilize the riverbanks. In the period from 2011 to 2021, the erosion rates show a decreasing trend, with the lowest rate recorded in 2007 (5.9 m/year).

Figure 5.4B illustrates the migration rates of the Tawi River's Reach 2 (Wadi Tawi) due to accretion (Mra) and erosion (Mre) measured in meters per year (m/year) from 1988 to 2021. The accretion rates (Mra) fluctuate significantly, peaking at 113.4 m/year in 2009 and hitting a low of 3.7 m/year in 1995. Between 1988 and 2000, notable peaks occur in 1989 (89.3 m/year) and 1992 (74.8 m/year), indicating periods of substantial sediment deposition. The years 2001 to 2010 show varying rates, with the highest in 2009, suggesting exceptional sediment accumulation. From 2011 to 2021, the rates moderate, with a significant dip in 1995 (3.7 m/year). Erosion rates (Mre) also exhibit significant variability, reaching a maximum of 137.6 m/year in 1995 and a minimum of 3.5 m/year in 2014. Early years display considerable variation with a peak in 1995 and a low in 1989 (12.1 m/year), reflecting dynamic erosional activity. From 2001 to 2010, rates are mixed, with a notable high in 1995. The period from 2011 to 2021 generally shows a decline in erosion, indicating possible effectiveness of riverbank stabilization measures or other factors reducing erosion.

The accretion rates in Reach 3 of the Tawi River, as shown in Figure 5.4c, fluctuate widely, peaking at 141.8 m/year in 2008 and dipping to a low of 16.3 m/year in 1988. During the early years, the rates show substantial peaks, such as 1989 (36.6 m/year) and 1991 (60.0 m/year), indicating notable sediment deposition. The period from 2001 to 2010 also demonstrates high variability, with the highest rate in 2008, suggesting significant sediment accumulation. From 2011 to 2021, the rates remain varied, with a significant dip in 1997 (16.3 m/year) and peak in 2020 (61.1 m/year). Erosion rates in Reach 3 also show significant variability, reaching a maximum of 131.8 m/year in 2007 and a minimum of 3.7 m/year in 2013. Early years exhibit considerable variation, with peaks such as 1992 (108.9 m/year) and lows like 1989 (42.7 m/year), reflecting dynamic erosional activities. The period from 2001 to

2010 shows mixed rates, with a notable high in 2007 and low in 2004 (22.7 m/year). From 2011 to 2021, erosion rates decline, with the lowest in 2013, suggesting effective riverbank protection measures or other factors reducing erosional activity.

Figure 5.4D presents an overview of the migration rates of the Tawi River's Reach 4. This analysis covers the period from 1988 to 2021, highlighting significant variability. Accretion rates (Mra) ranged from a high of 105.7 m/year in 2010 to a low of 3.8 m/year in 2013, with peaks in 1992 (51.8 m/year) and 1999 (93.9 m/year) suggesting periods of significant sediment deposition. The early years, from 1988 to 2000, showed substantial fluctuations, while the period from 2001 to 2010 included both high and low rates, with the highest rate in 2010. From 2011 to 2021, accretion rates were relatively lower, with a notable dip in 2013. Erosion rates (Mre) ranged from a high of 128.9 m/year in 2008 to a low of 3.4 m/year in 2020, with early years showing considerable variability, including a peak in 1988 and a significant low in 1989. The period from 2001 to 2010 included both high and low erosion rates, with a peak in 2008, indicating periods of intense erosion. From 2011 to 2021, erosion rates showed a decreasing trend, suggesting effective riverbank protection measures or other factors reducing erosion.

In Reach 5 of the Tawi River, depicted in Figure 5.4E, the rates of accretion and erosion display a notable range of variability. Accretion rates peak at 84.2 m/year in 2020 and hit a low of 1.2 m/year in 1997. Early years show diverse rates with significant fluctuations, such as 1990 (62.6 m/year) and 1996 (19.1 m/year), indicating varied sediment deposition patterns. Between 2001 and 2010, the accretion rates also fluctuate considerably, peaking in 2009 (48.4 m/year) and reaching a low in 2006 (9.8 m/year). From 2011 to 2021, the rates continue to vary, with a notable increase in 2020 and a low in 2012 (1.2 m/year). Erosion rates similarly vary, with the highest rate of 102.2 m/year recorded in 1997 and the lowest of 0.6 m/year in 2014. Initial years show wide variability, with significant peaks such as 1988 (47.6 m/year) and lows like 1989 (2.0 m/year). During 2001 to 2010, the erosion rates remain mixed, peaking in 1997 and dipping in 2006 (9.8 m/year). From 2011 to 2021, erosion rates generally decrease, with the lowest in 2014, suggesting effective measures to control riverbank erosion or other contributing factors.

5.4. Migrated Area Due to Accretion and Erosion

From 1988 to 2021, the analysis of migrated areas due to accretion (MAa) and erosion (MAe) across different reaches reveals significant variations. In Reach 1 (Fig. 5.5A), MAa

shows considerable peaks and troughs, with the highest value of 3.9 km² in 2012 and a low of 0.3 km² in 1998. Notable sediment deposition is observed in 2001 (3.0 km²) and 2005 (2.9 km²). Conversely, MAe fluctuates widely, peaking at 5.2 km² in 1988 and dipping to 0.2 km² in 1998, with significant erosion observed in 2009 (2.8 km²) and 2016 (2.8 km²). In Reach 2 (Fig. 5.5B), MAa also demonstrates high variability, peaking at 2.7 km² in 2003 and falling to 0.2 km² in 2004. Significant periods of sediment accumulation are evident in 1991 (2.3 km²) and 2008 (2.7 km²). MAe varies significantly, with the highest value of 3.1 km² in 1997 and the lowest at 0.1 km² in 2008. Major erosion peaks occur in 2000 (2.4 km²) and 2014 (2.2 km²). For Reach 3 (Fig. 5.5C), the analysis reveals marked fluctuations in MAa and MAe. MAa peaks at 3.9 km² in 2016 and drops to 0.4 km² in 2015, indicating significant changes. Notable accretion occurs in 2012 (2.6 km²) and 2020 (2.4 km²). MAe exhibits a broad range, with the maximum of 3.6 km² in 2015 and the minimum at 0.2 km² in 2009. Significant erosion is noted in 2004 (2.8 km²) and 2018 (3.4 km²), reflecting dynamic erosion activities. In Reach 4 (Fig. 5.5D), MAa shows considerable variation, peaking at 1.7 km² in 2000 and dropping to 0.1 km² in 1996. Significant sediment deposition is observed in 1993 (1.1 km²) and 2014 (1.3 km²). MAe also varies widely, with a peak of 2.2 km² in 2014 and a low of 0.1 km² in 1996. Major erosion peaks are seen in 2010 (2.0 km²) and 2020 (1.7 km²). Finally, in Reach 5 (Fig. 5.5E), MAa and MAe exhibit significant

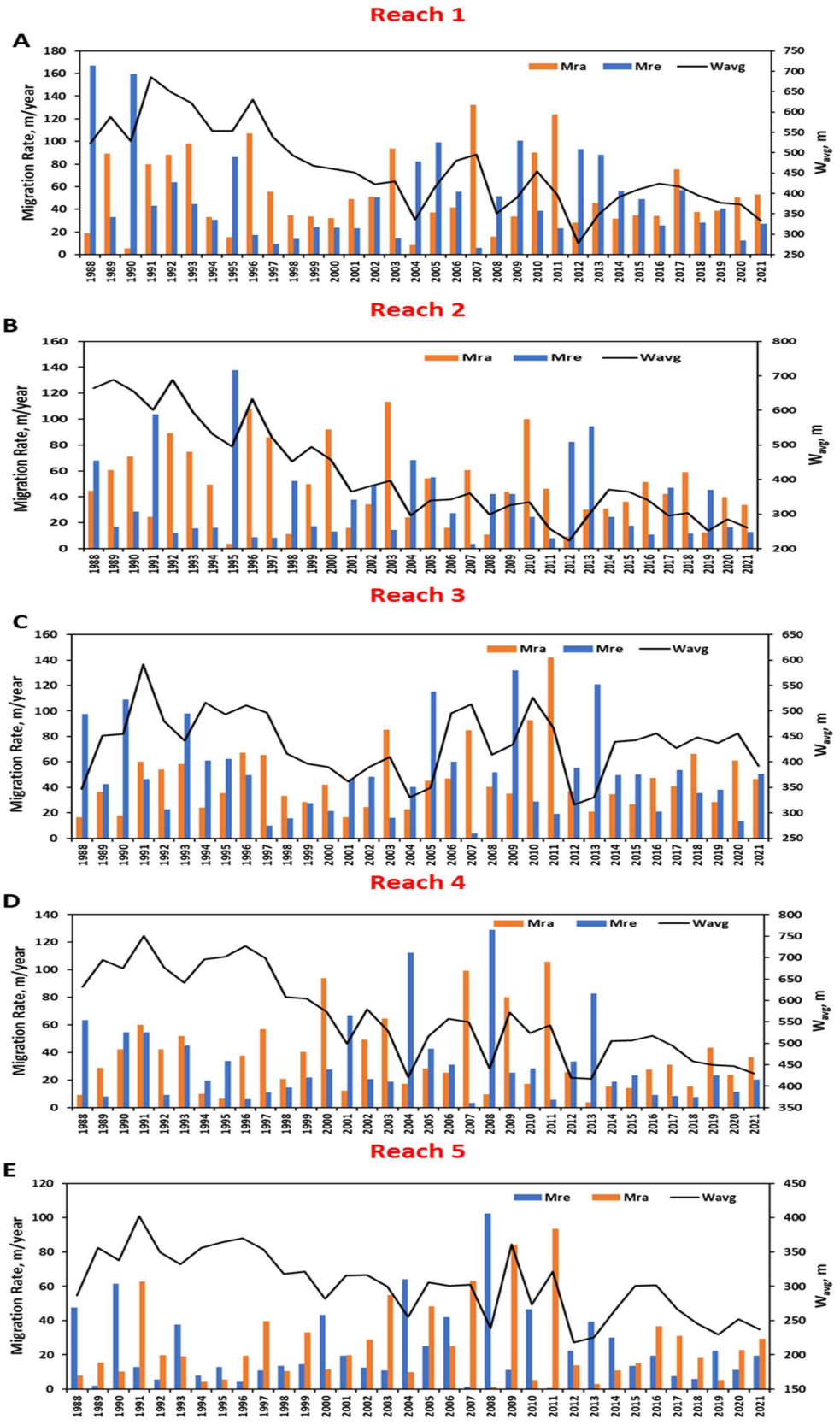

Fig. 4.19. Temporal variation of Migration Rate due to accretion (Mra) and erosion (Mre) and Average Width (Wavg) in Tawi River reaches (A-E).

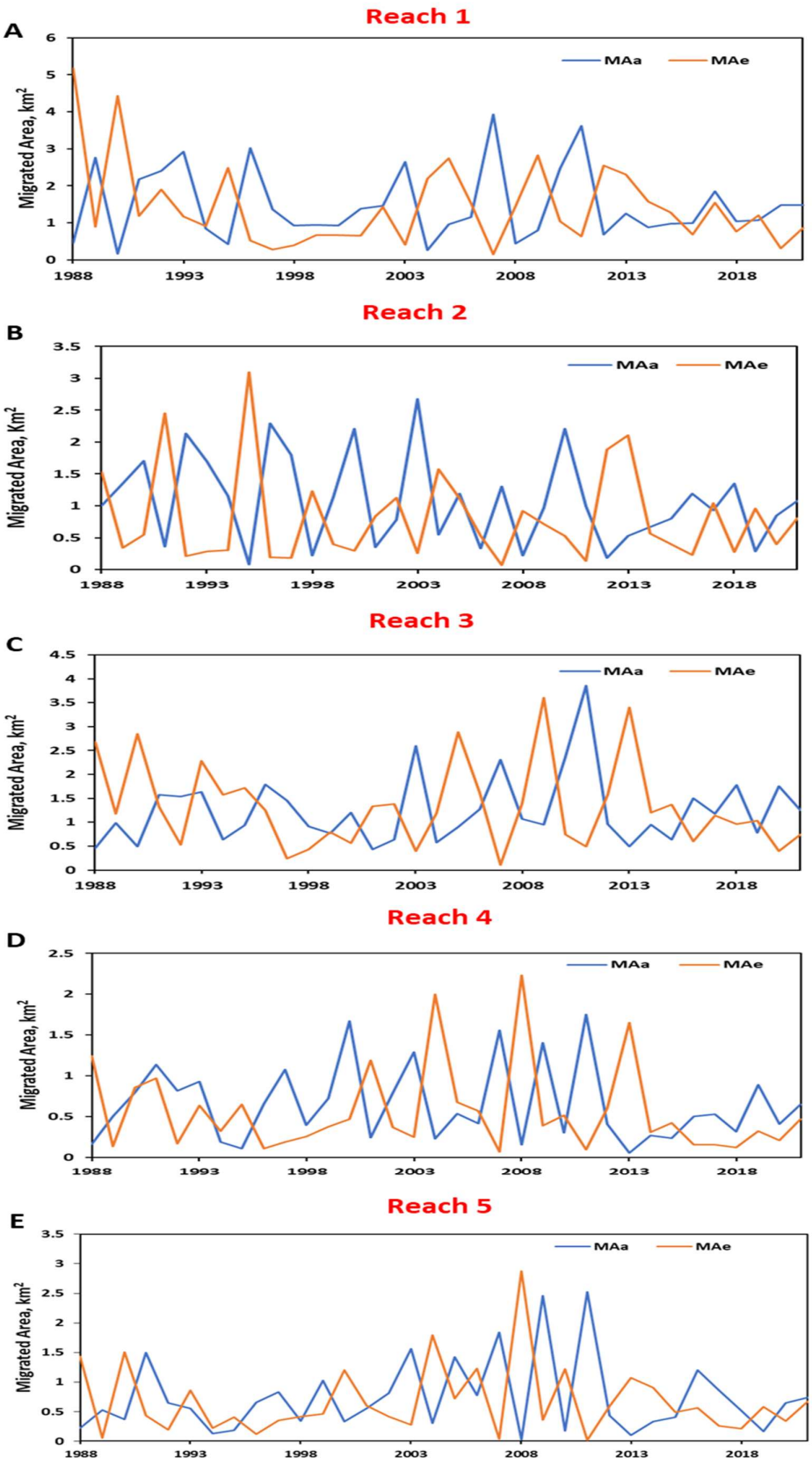

Figure 4.19. Migrated area (MAa) due to accretion (MAa) and erosion (MAe) over the years in the Tawi River reaches (A-E).

variation. MAa peaks at 2.5 km² in 2015 and drops to 0.1 km² in 2017, with notable accretion observed in 2008 (1.6 km²) and 2021 (1.4 km²). MAe reaches a maximum of 2.9 km² in 2016 and a minimum of 0.1 km² in 2005. Significant erosion occurs in 2012 (1.8 km²) and 2015 (1.2 km²), reflecting substantial changes in sediment dynamics.

5.5. Annual Percentage Migration Rates Across Multiple River Reaches

The migration rates (Mcl) for each river reach, as depicted in Figures 5.6a through 5.6e, reveal significant variability and provide valuable insights into the dynamic nature of river channel changes over time. Each reach exhibits unique patterns of migration, influenced by a range of environmental and hydrological factors. For instance, reach 1, illustrated in Figure 5.6a, shows notable peaks in Mcl values in the years 1988, 2001, and 2003, with the highest rate at 21.11% in 1988. This reach also had periods of lower migration, such as in 1994 when the Mcl was just 3.11%. These fluctuations indicate episodes of significant migration interspersed with more stable periods, reflecting the impact of varying flow regimes and sediment supply. Similarly, Reach 2, as shown in Figure 5.66b, exhibits substantial variability with the highest Mcl recorded in 2014 at 15.19%, suggesting a period of intense migration. Conversely, the lowest Mcl was observed in 1989 at 4.20%.

In Reach 3, represented in Figure 5.6c, the migration continues to demonstrate significant changes, with the highest Mcl rates in 2012 (14.66%), 2015 (12.10%), and 2016 (12.45%). The lowest Mcl was noted in 1998 at 4.18%, pointing to a period of relative stability. This reach's data suggest that the river's migration behavior is highly responsive to external factors such as flood events and sediment load, causing marked increases in migration rates during certain years. Reach 4, depicted in Figure 5.6d, also shows considerable variation in Mcl values. The highest migration rates were recorded in 2005 (12.82%) and 2009 (11.69%), whereas the lowest Mcl was in 1989 at 1.56%. Finally, reach 5, illustrated in Figure 5.6e, exhibits the highest Mcl values in 2008 (18.55%) and 2011 (13.93%), suggesting substantial migration activity. The lowest Mcl was recorded in 1989 at 1.89%. These data underscore the episodic nature of river migration in this reach, driven by a combination of high-flow events, sediment dynamics, and possibly human activities.

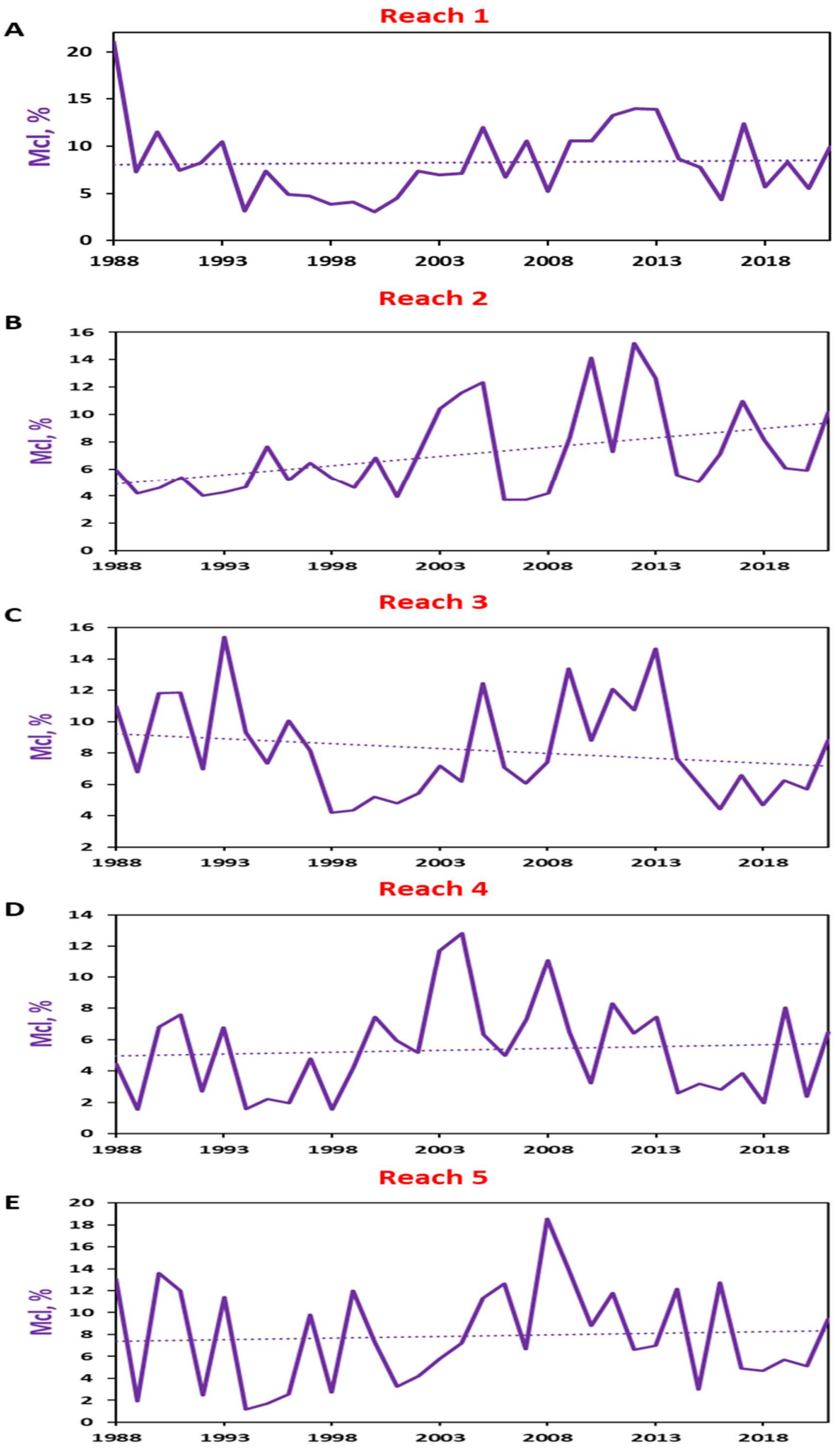
A
Reach 1
Mcl, %
0
5
10
15
20
1988
1993
1998
2003
2008
2013
2018
B
Reach 2
Mcl, %
0
2
4
6
8
10
12
14
16
1988
1993
1998
2003
2008
2013
2018
C
Reach 3
Mcl, %
2
4
6
8
10
12
14
16
1988
1993
1998
2003
2008
2013
2018
D
Reach 4
Mcl, %
0
2
4
6
8
10
12
14
1988
1993
1998
2003
2008
2013
2018
E
Reach 5
Mcl, %
0
2
4
6
8
10
12
14
16
18
20
1988
1993
1998
2003
2008
2013
2018

Figure 4.20. Percentage Migration (M_{cl}) of five river reaches over time

5.6 Sinuosity

Analyzing the sinuosity index for each river reach over the years reveals notable variations in sinuosity values, with distinct ranges and extreme values for each reach (Figure5.7). For reach 1, the sinuosity index fluctuated between a minimum value of 1.09 in 1994 and a maximum value of 1.26 in 2021, indicating significant changes in the river's meandering pattern over time. In reach 2, the sinuosity index ranged from 1.15 in 1992 to a peak of 1.22 in 2016, showing moderate variability. Reach 3 displayed a broader range, with the lowest value of 1.27 in 1991 and the highest value of 1.52 in 2017, reflecting a higher degree of meandering complexity. Reach 4 exhibited a sinuosity index range from 1.40 in 1991 to a maximum of 1.63 in 2020, suggesting significant morphological changes. Finally, reach 5 showed the most substantial sinuosity variations, with values ranging from a minimum of 1.45 in 1994 to a peak of 1.74 in 2020, indicating pronounced changes in the river's course over time.

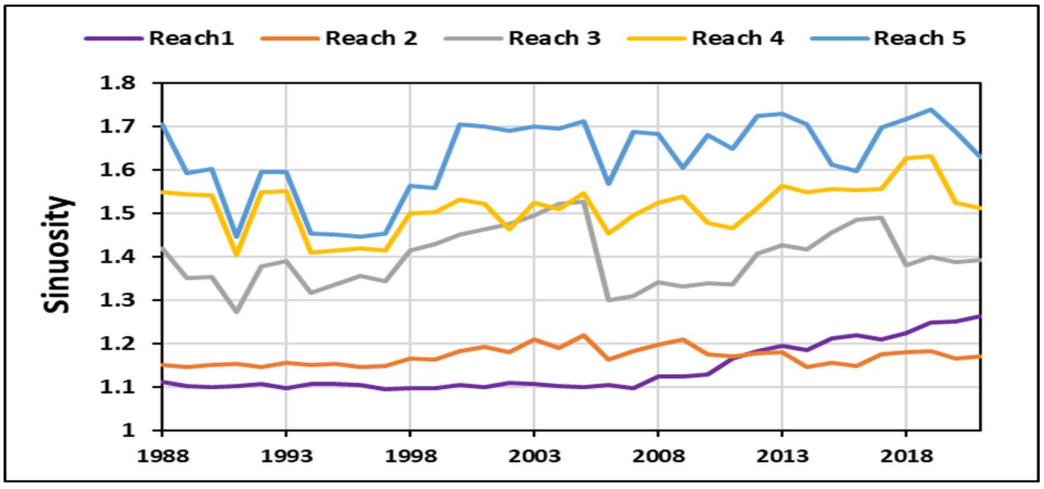

Figure 4.21. Sinuosity Index of the Tawi River Across Different Reaches (1988-2021)

CHAPTER - 5
CONCLUSIONS

The physical properties and features of a river or stream and its surroundings are referred to as fluvial morphology. It includes research on the size, cross-sectional profile, channel patterns, movement of sediment, and interactions between the river and its surroundings. Fluvial morphology must be understood for a variety of applications, such as managing flood risks. Flood hazard is the risk that a river or stream would overrun its banks and inundate nearby regions, causing property damage, fatalities, and environmental harm. Fluvial morphology, hydrology (the study of water flow and distribution), land use, climate, and human activities are some of the variables that affect flood hazards. Understanding these intricate relationships and putting policies in place to lower the risks associated with floods are necessary for effective flood hazard assessment and management.

As presented in the study, the geomorphological analysis based on various derivatives of the digital elevation model (DEM) has contributed significantly to our understanding of the Tawi river basin's diverse and dynamic landscape. The topographic roughness index (TRI) reveals the contrasting elevation changes between the landform units, underscoring the highly rugged mountains' steepness and the gentler slopes of the low rugged hills and alluvial plains. The topographic position index (TPI) helps identify the spatial distribution of ridges and depressions, shedding light on the basin's geomorphic processes and structural influences. The normalized height and hill height maps highlight the peaks and ridges, crucial for understanding the terrain's evolution. The valley depth map emphasizes the main valleys, aiding in comprehending the basin's hydrological characteristics. The elevation and slope maps effectively demarcate the various landform units and their slope gradients. The water index map provides essential information about water bodies and the active floodplain. Moreover, the stream order and drainage pattern offer insights into the basin's drainage network and its underlying controls. By integrating these findings, we gain a comprehensive picture of the Tawi river basin's complex landscape, which is crucial for sustainable land management, resource utilization, and effective hazard mitigation in the region.

Further, his study successfully employed a semi-automated workflow using Google Earth Engine (GEE) and MATLAB to analyze the active channel dynamics of the Tawi River over a 34-year period from 1988 to 2022. Leveraging Landsat imagery within GEE, we applied a series of key steps, including time and region of interest filtering, cloud masking, and temporal compositing, to generate annual image collections capturing the temporal variations of the

active channel. In MATLAB, further processing steps were undertaken to enhance the accuracy and reliability of the analysis. Noise removal techniques were implemented to eliminate disconnected pixels that did not belong to the active channel, thereby refining the channel mask. Additionally, masking out secondary channels using the mean image of composite images allowed us to focus solely on the main channel of interest. Hydraulically connected binary channel masks were created from the cleaned composite images, providing a comprehensive representation of the active channel's extent. These processes played a crucial role in refining the channel masks and providing valuable insights into the river's morphological evolution.

Furthermore, the analysis revealed significant changes in the downstream section of the river. The channel in this region has undergone substantial alterations over time, likely influenced by various factors such as geomorphic processes, human activities, and climate variations. The active channel masks generated in this study will be used further to carry out various river planform characteristics. As this study is ongoing study, thus the results as well as conclusions presented here will be slightly modified in future based on the obtained results.

REFERENCES

Abad, J. D. *et al.* (2022). Planform Dynamics and Cut-Off Processes in the Lower Ucayali River, Peruvian Amazon. *Water (Switzerland)* **14.**

Basnayaka, V., Samarasinghe, J. T., Gunathilake, M. B., Muttil, N. & Rathnayake, U. (2022). Planform Changes in the Lower Mahaweli River, Sri Lanka Using Landsat Satellite Data. *Land (Basel)* **11**.

Bhatpuria, D., Matheswaran, K., Piman, T., Tha, T. & Towashiraporn, P. (2022). Assessment of Large-Scale Seasonal River Morphological Changes in Ayeyarwady River Using Optical Remote Sensing Data. *Remote Sens (Basel)* **14**.

Boothroyd, R. *et al.* (2021) *Detecting and quantifying morphological change in tropical rivers using Google Earth Engine and image analysis techniques*.

Boothroyd, R. J., Nones, M. & Guerrero, M. (2021a). Deriving Planform Morphology and Vegetation Coverage From Remote Sensing to Support River Management Applications. *Front Environ Sci* **9**.

Boothroyd, R. J., Williams, R. D., Hoey, T. B., Barrett, B. & Prasojo, O. A. (2021b). Applications of Google Earth Engine in fluvial geomorphology for detecting river channel change. *Wiley Interdisciplinary Reviews: Water* vol. 8 Preprint at https://doi.org/10.1002/wat2.1496.

Brook, G.A. and Luft, E.R. (1987). Channel pattern changes along the lower Oconee River, Georgia, 1805/7 to 1949. Physical Geography, 8(3): 191-209.

Cook, H. River channel planforms and floodplains: a study in the Wessex landscape. *Landscape History* **39**, 5–24 (2018).

Davis WM (1909) The Mountain Ranges of the Great Basin, in Geographical Essays (pp 725-772), Boston (New York, Dover reprint 1954, originally issued 1903), Bulletin - Museum of Comparative Zoology. Harvard College 42: 129-177.

Dey, S., Basu, A., Banerjee, S.N., Jain, V., 2023. Discharge-driven rapid bank-erosion and its impact on sediment budgeting in the lower Gangetic plains. Episodes 46, 259–267. https://doi.org/10.18814/epiiugs/2022/022027

Dixon, S. J. *et al.* (2018). The planform mobility of river channel confluences: Insights from analysis of remotely sensed imagery. *Earth-Science Reviews* vol. 176 1–18 Preprint at https://doi.org/10.1016/j.earscirev.2017.09.009.

Friend, P. and Sinha, R., (1993). Braiding and meandering parameters. Geological Society, London, Special Publications, 75(1): 105-111.

Geddes, A., (1960). The alluvial morphology of the Indo-Gangetic Plain: Its mapping and geographical significance. Transactions and Papers (Institute of British Geographers) (28): 253-276.

Ground water information booklet (2013). Central Ground Water Board, Government of India Ministry of Water Resources Udhampur District, Jammu & Kashmir.

Ground water information booklet (2014). Central Ground Water Board, Government of India Ministry of Water Resources Udhampur District, Jammu & Kashmir.

Gupta, N. (2012). *Channel Planform Dynamics of the Ganga-Padma System, India*.

Gupta, N., Atkinson, P. M. & Carling, P. A. (2013). Decadal length changes in the fluvial planform of the River Ganga: Bringing a mega-river to life with Landsat archives. *Remote Sensing Letters* **4**, 1–9.

Gupta, N., Atkinson, P.M. and Carling, P.A., (2013). Decadal length changes in the fluvial planform of the river Ganga: bringing a mega-river to life with Landsat archives. Remote Sensing Letters, 4(1): 1-9.

Gutierrez, R. R., Mallma, J. A., Núñez-González, F., Link, O. & Abad, J. D. (2018). Bedforms-ATM, an open-source software to analyze the scale-based hierarchies and dimensionality of natural bed forms. *SoftwareX* **7**, 184–189.

Hasenhündl, M. & Blanckaert, K. A. (2022). Matlab script for the morphometric analysis of subaerial, subaquatic and extra-terrestrial rivers, channels and canyons. *Comput Geosci* **162**.

Khan, N.S., Roy, S.K., Mazumder, M.T.R., Talukdar, S., Mallick, J., 2022. Assessing the long-term planform dynamics of Ganges–Jamuna confluence with the aid of remote sensing and GIS. Natural Hazards 114, 883–906. https://doi.org/10.1007/s11069-022-05416-6

Kondolf, G.M., (1997). PROFILE: hungry water: effects of dams and gravel mining on river channels. Environmental management, 21(4): 533-551.

Kong, D., Latrubesse, E. M., Miao, C. & Zhou, R. (2020). Morphological response of the Lower Yellow River to the operation of Xiaolangdi Dam, China. *Geomorphology* **350**.

Kumar, V., Pal1t, A., Chakraborti, A. K. & Bhan, S. K. *Planform Analysis of Hooghly River Metamorphosis Using Multidate Satellite Data*. *Journal of the Indian Society of Remote Sensing* vol. 22 (1994).

Kummu, M., Lu, X., Rasphone, A., Sarkkula, J. and Koponen, J., (2008). Riverbank changes along the Mekong River: remote sensing detection in the Vientiane–Nong Khai area. Quaternary International, 186(1): 100-112

Larsen, E. W., A. K. Fremier, and E. H. Girvetz (2006), Modeling the effects of variable annual flow on river channel meander migration patterns, Sacramento River, California, USA, J. Am. Water Resour. Assoc., 1063–1075, doi:10.1111/j.1752-1688.2006.tb04514.x.

Li, Z. *et al.* (2021). Distribution and evolution of knickpoints along the Layue River, Eastern Himalayan Syntaxis. *J Hydrol (Amst)* **603**.

Louise, P. *et al.* River Styles and Stream Power Analysis Reveal the Diversity of Fluvial Morphology in a Philippine Tropical Catchment. doi:10.21203/rs.3.rs-125062/v1.

Matsuda, I. *River Morphology And Channel Processes*.

Petropoulos, G. P., Kalivas, D. P., Griffiths, H. M. & Dimou, P. P. Remote sensing and GIS analysis for mapping spatio-temporalchanges of erosion and deposition of two Mediterranean river deltas: The case of the Axios and Aliakmonas rivers, Greece. *International Journal of Applied Earth Observation and Geoinformation* **35**, 217–228 (2015).

Rowland, J.C., Shelef, E., Pope, P.A., Muss, J., Gangodagamage, C., Brumby, S.P., Wilson, C.J., 2016a. A morphology independent methodology for quantifying planview river change and characteristics from remotely sensed imagery. Remote Sens Environ 184, 212–228. https://doi.org/10.1016/j.rse.2016.07.005

Schwenk, J., Khandelwal, A., Fratkin, M., Kumar, V. & Foufoula-Georgiou, E. High spatiotemporal resolution of river planform dynamics from landsat: The rivMAP toolbox and results from the Ucayali river. *Earth and Space Science* **4**, 46–75 (2017).

Sebastianelli, A., Del Rosso, M. P. & Ullo, S. L. Automatic dataset builder for Machine Learning applications to satellite imagery. *SoftwareX* **15**, (2021).

Singh, P., Patil, R. G. & Singh, A. Assessment of recent changes in planform of river Ganga from Mirapur Khadar to Narora barrage, Uttar Pradesh, India. *Sustain Water Resour Manag* **5**, 575–586 (2019).

Sinha, R., Sripriyanka, K., Jain, V. & Mukul, M. Avulsion threshold and planform dynamics of the Kosi River in north Bihar (India) and Nepal: A GIS framework. *Geomorphology* **216**, 157–170 (2014).

Sinha, R., Sripriyanka, K., Jain, V. & Mukul, M. Avulsion threshold and planform dynamics of the Kosi River in north Bihar (India) and Nepal: A GIS framework. *Geomorphology* **216**, 157–170 (2014).

Sivanpillai, R., Jacobs, K. M., Mattilio, C. M. & Piskorski, E. V. Rapid flood inundation mapping by differencing water indices from pre- and post-flood Landsat images. *Front Earth Sci* **15**, (2021).

Tolentino, P. L. M. *et al.* River Styles and stream power analysis reveal the diversity of fluvial morphology in a Philippine tropical catchment. *Geoscience Letters* vol. 9 Preprint at https://doi.org/10.1186/s40562-022-00211-4 (2022).

Vercruysse, K. & Grabowski, R. C. Human impact on river planform within the context of multi-timescale river channel dynamics in a Himalayan River system. *Geomorphology* **381**, (2021).

Yang, X., Pavelsky, T. M., Allen, G. H. & Donchyts, G. RivWidthCloud: An Automated Google Earth Engine Algorithm for River Width Extraction from Remotely Sensed Imagery. *IEEE Geoscience and Remote Sensing Letters* **17**, 217–221 (2020).

Report Code: 005_GBP_IIT_FGM_DAT_01_Ver 1_Dec 2010; Active Floodplain Mapping: Defining the "River Space

Robert, A., 2014. River processes: an introduction to fluvial dynamics. Routledge.

Kondolf G.M., Piégay H. (Eds.) (2003) *Tools in fluvial geomorphology*. Wiley, Chichester, p. 1-687. DOI : 10.1002/9781118648551

Director	**:**	**Dr. M.K.Goel**
Head	**:**	**Dr. A.K. Lohani**

STUDY GROUP

Principal Investigator (PI)	**:**	**Dr. Ravindra V. Kale, Scientist D, SWHD**
Team (Co-PIs)	**:**	**Dr. A. K. Lohani, Scientist G and Head SWHD**
		Er. J. P. Patra, Scientist D, SWHD
		Er. Drona Khurana, SRA, WHRC, Jammu